

RESEARCH TECHNICAL REPORT  
*SMART Sprinkler Protection  
for Highly Challenging Fires –  
Phase 1: System Design and  
Function Evaluation*





# **SMART Sprinkler Protection for Highly Challenging Fires – Phase 1: System Design and Function Evaluation**

Prepared by

Yibing Xin  
Kyle Burchesky  
Jaap de Vries  
Harold Magistrale  
Xiangyang Zhou  
Stephen D'Aniello

April 2016

FM Global  
1151 Boston-Providence Turnpike  
Norwood, MA 02062

PROJECT ID 0003048211

## Disclaimer

---

The research presented in this report, including any findings and conclusions, is for informational purposes only. Any references to specific products, manufacturers, or contractors do not constitute a recommendation, evaluation or endorsement by Factory Mutual Insurance Company (FM Global) of such products, manufacturers or contractors. FM Global makes no warranty, express or implied, with respect to any product or process referenced in this report. FM Global assumes no liability by or through the use of any information in this report.

## Executive Summary

---

Modern technology has resulted in very efficient warehouse storage, such as high on-end storage of roll paper and automatic storage and retrieval system (ASRS). Traditional sprinklers encounter tremendous challenges in protecting fires in these storage configurations. Traditional sprinkler protection relies on sensible elements with relatively high temperature rating and slow thermal response to detect and react to the fire. The combination of high storage and resultant fast fire spread requires new protection methods for the highly challenging fires (HCFs) beyond the protection recommendations of traditional sprinklers.

The overall objective of this program is to demonstrate a new sprinkler system that can provide adequate protection for HCFs. The objectives of this program included (1) to design and test the system at the component level, and (2) is to perform integrated system tests to examine its effectiveness in fire protection. The present report documents the progress associated with the first objective.

The system design starts with the objectives of detecting, locating and suppressing a fire as early and as locally as possible. The combination of early detection and local response is essential to maximize the protection effect and to reduce the system cost. In this work, we refer to the technology to achieve these goals as Simultaneous Monitoring, Assessment and Response Technology (SMART). Such a sprinkler protection system is defined as a SMART sprinkler. Based on the design objectives and the characteristics of HCFs, smoke and temperature based sensors were selected to achieve fire detection; a thermal centroid based calculation was adopted to determine the fire location; and a dynamic control procedure was utilized to activate the sprinklers.

In order to evaluate these system functions, a series of experiments was designed and conducted in the Small Burn Lab at the FM Global Research Campus, West Glocester, RI. Fire detection tests were carried out with various fire sizes, fire locations and sprinkler spacing; sprinkler activation tests were conducted using liquid pan fires with different ignition locations; and preliminary fire suppression tests were performed using cartoned unexpanded plastic commodities under different sprinkler activation criteria, ignition sources and locations and sprinkler discharge densities.

The experimental results show that the use of multi-sensor detection technology, *e.g.*, the combination of smoke and temperature signals can help the SMART sprinklers respond faster, avoid false alarms and improve fire locating accuracy. The fire location can be determined with reasonable accuracy using the thermal centroid based calculation. The sprinkler activation can be achieved by the control unit through triggering individual sprinklers locally and dynamically, based on the results of fire detection and fire location. Fire suppression, even fire extinguishment, can be achieved with adequate sprinkler discharge densities. In summary, the results from fire detection, sprinkler activation and preliminary suppression tests have shown that the newly developed system meets design objectives for fire protection purposes.

The second report [1] on this work will present evaluation of the SMART sprinkler system in a series of full-scale fire tests using standard commodities in rack storage configurations. The full-scale rack-storage fire tests using standard commodities are selected because of the long-time experience accumulated on

testing sprinklers for this type of fire hazard, and the abundant data available to compare the performance of SMART and traditional sprinklers.

## Abstract

---

An experimental study was conducted to demonstrate the concept of a new protection system – a SMART sprinkler system. The present work focuses on the system design and function evaluation at the component level. The objective is to demonstrate that the SMART sprinkler system can provide adequate protection to highly challenging fires. The new protection system has several key functions including multi-sensor detection, real-time fire location calculation, dynamic sprinkler activation and wireless communication coordinating the system components. A series of fire detection, sprinkler activation and fire suppression tests were carried out to evaluate these system functions. Results show that 1) a combination of smoke and temperature sensors can detect the fire at a very early stage and provide sufficient data to locate the fire; 2) a thermal centroid based algorithm can determine the fire location with reasonable accuracy; and 3) the sprinkler activation concentrating water discharge in the vicinity of the fire can suppress and even extinguish the fire under certain experimental conditions. These results confirm that the design objectives have been achieved. The experimental data also provide crucial information to assess system performance in full-scale tests.

## Acknowledgements

---

The authors would like express their gratitude to Ms. Kristin Jamison for providing full-scale test data; to Mr. Jason Tucker, Mr. Mark Bardol and Mr. Dereck Mencarini for conducting all tests; to Mr. Scott Ulricksen and Mr. Christopher LaButti for assistance on instrumentation; to Mr. Jeff Chaffee for reviewing the test plan.

---

# Table of Contents

---

Executive Summary.....	i
Abstract.....	iii
Acknowledgements.....	iv
1. Introduction .....	1
1.1 Background .....	1
1.2 Previous work on HCF protection .....	1
1.3 Objectives.....	2
1.4 Organization of this report.....	3
2. System design .....	4
2.1 Fire detection .....	4
2.2 Fire event assessment.....	5
2.3 Fire location .....	6
2.4 Sprinkler activation .....	7
2.5 System communication.....	9
3. Experimental method .....	11
3.1 Experimental setup .....	11
3.1.1 Fire detection tests .....	11
3.1.2 Sprinkler activation tests .....	14
3.1.3 Fire suppression tests .....	15
3.2 System communication and data acquisition .....	16
3.3 Experimental conditions .....	17
4. Results and discussions.....	20
4.1 Characterization of source fires .....	20
4.1.1 Propane fires on a sand burner .....	20
4.1.2 Heptane fires on a circular pan.....	20
4.1.3 CUP rack-storage fires.....	22
4.2 Fire detection tests with 0.76 m (2.5 ft) spacing .....	22
4.2.1 Impact of HRR on smoke detector response time .....	22
4.2.2 Impact of HRR on fire location calculation .....	24
4.2.3 Impact of ignition location .....	26
4.3 Fire detection tests with 2.44 m (8 ft) spacing .....	28
4.3.1 Impact of HRR on smoke detector response time .....	28
4.3.2 Impact of HRR on thermal centroid calculation.....	29

4.3.3	Impact of ignition locations .....	32
4.4	Sprinkler activation tests .....	34
4.5	Preliminary suppression tests .....	36
4.5.1	Fire development in 2x2, 1-tier rack storage.....	37
4.5.2	Development of CUP fires in 2x2, 2-tier rack storage.....	40
4.5.3	Development of CUP fires in 2x2, 3-tier rack storage.....	41
5.	Conclusions and future work .....	46
5.1	Summary and conclusions of current work .....	46
5.2	Future work.....	46
	Nomenclature .....	48
	References .....	49
	Appendix A. Fire detection test data.....	51
A.1	Test data with 0.76 m (2.5 ft) sprinkler spacing .....	51
A.2	Fire detection tests with 2.44 m (8 ft) sprinkler spacing .....	63
	Appendix B. Sprinkler activation test data .....	70
	Appendix C. Fire suppression test data .....	74
C.1	Test 47.....	74
C.2	Test 48.....	75
C.3	Test 49.....	77
C.4	Test 50.....	78
C.5	Test 51.....	80
C.6	Test 52.....	81
C.6.1	First run.....	81
C.6.2	Second run .....	83
C.7	Test 53.....	84

## List of Figures

1-1: Roll paper in high on-end storage configurations.....	1
1-2: Fire growth rates of different roll paper types [3].....	2
2-1: Basic functions of a SMART sprinkler system. ....	4
2-2: Thermal centroid deviation relative to ignition location. ....	6
2-3: Determination of number of sprinklers to be activated. ....	9
2-4: Wireless transceiver connected to smoke and heat detectors. ....	10
3-1: Schematic of experimental setup under the movable ceiling in the SBL. ....	12
3-2: Detector, sensor and sprinkler installation on a SMART sprinkler (unit: cm).....	13
3-3: Sprinkler layout and ignition locations under the movable ceiling (unit: m). ....	14
3-4: Solenoid valve and sprinkler connection in sprinkler activation tests.....	15
3-5: Experimental setup of fire suppression tests in 2x2, 3-tier rack storage (unit: m). ....	16
3-6: SMART sprinkler system connection and communication. ....	17
4-1: Chemical HRRs of 0.91-m dia. propane fires.....	20
4-2: Chemical HRR of 0.30-m heptane pan fire (Calibration Test #2). ....	21
4-3: Chemical HRR of 0.91-m heptane pan fire (Calibration Test #4). ....	21
4-4: Initial fire growth of CUP fires in 2x4, 3-tier rack storage [8]. ....	22
4-5: Response times of smoke detectors in Test 3 (HRR = 160kW, ignition among 4 sprinklers). ....	23
4-6: Response times of smoke detectors in Test 4 (HRR = 320kW, ignition among 4 sprinklers). ....	24
4-7: Normalized thermal centroid deviations with HRR = 80 kW. ....	25
4-8: Normalized thermal centroid deviations with HRR = 160 kW. ....	25
4-9: Normalized thermal centroid deviations with HRR = 320 kW. ....	26
4-10: Normalized thermal centroid deviations with different ignition locations. ....	27
4-11: Temperature rise at the ceiling in Test 24 at 300 s – no smoke detector activation (HRR = 80kW, ignition among 4 sprinklers). ....	28
4-12: Smoke detector response times in Test 25 (HRR = 160kW, ignition among 4 sprinklers).....	29
4-13: Temperature rise in Test 25 at the time of first smoke detector activation (HRR = 160kW, ignition among 4 sprinklers). ....	29
4-14: Smoke detector response times in Test 26 (HRR = 320kW, ignition among 4 sprinklers).....	30
4-15: Temperature rise in Test 26 at the time of first smoke detector activation (HRR = 320kW, ignition among 4 sprinklers). ....	30
4-16: Normalized thermal centroid deviations calculated using different data sets in Test 24. ....	31
4-17: Normalized thermal centroid deviations with 2.44 m spacing and HRR = 80 kW. ....	31
4-18: Normalized thermal centroid deviations with 2.44 m spacing and HRR = 160 kW. ....	32
4-19: Normalized thermal centroid deviations with 2.44 m spacing and HRR = 320 kW. ....	32
4-20: Normalized thermal centroid deviations with 2.44 m spacing and under-one ignition.....	33
4-21: Normalized thermal centroid deviations with 2.44 m spacing and between-two ignition. ....	33
4-22: Normalized thermal centroid deviations with 2.44 m spacing and among-four ignition.....	34

4-23: Sprinkler activation with under 1 ignition in Test 41 (L) and 44 (R). .....	35
4-24: Sprinkler activation with between 2 ignition in Test 42 (L) and 45 (R).....	35
4-25: Sprinkler activation with under 4 ignition in Test 43 (L) and 46 (R). .....	36
4-26: Fire development in Test 47 (K80 sprinkler, 4.9 mm/min).....	37
4-27: Sprinkler activation with under 4 ignition in Test 47.....	38
4-28: Water pressure and flow rate in Test 47 (K80 sprinkler, 15.3 mm/min).....	38
4-29: Fire development in Test 48 (K80 sprinkler, 15.3 mm/min).....	39
4-30: Fire development in Test 49 (K80 sprinkler, 15.3 mm/min).....	40
4-31: Fire development in Test 50 (K80 sprinkler, 15.3 mm/min).....	41
4-32: Fire development in Test 51 (K80 sprinkler, 15.3 mm/min).....	42
4-33: Fire development in Test 52 (no water delivered). .....	43
4-34: Fire development in Test 53 (K200 sprinkler, 26.9 mm/min).....	44
4-35: Sprinkler activation with between-2 ignition in Test 53.....	45
A-1: Temperature rise at the ceiling in Test 2. ....	51
A-2: Normalized thermal centroid deviations in Test 2 (no detector activated in 300 s).....	51
A-3: Temperature rise at the ceiling in Test 3. ....	52
A-4: Normalized thermal centroid deviations and smoke detector response times in Test 3.....	52
A-5: Temperature rise at the ceiling in Test 4. ....	52
A-6: Normalized thermal centroid deviations and smoke detector response times in Test 4.....	52
A-7: Temperature rise at the ceiling in Test 5. ....	53
A-8: Normalized thermal centroid deviations in Test 5 (no detector activated in 300 s).....	53
A-9: Temperature rise at the ceiling in Test 6. ....	53
A-10: Normalized thermal centroid deviations and smoke detector response times in Test 6.....	53
A-11: Temperature rise at the ceiling in Test 7. ....	54
A-12: Normalized thermal centroid deviations and smoke detector response times in Test 7.....	54
A-13: Temperature rise at the ceiling in Test 8. ....	54
A-14: Normalized thermal centroid deviations in Test 8 (no detector activated in 300 s).....	54
A-15: Temperature rise at the ceiling in Test 9. ....	55
A-16: Normalized thermal centroid deviations and smoke detector response times in Test 9.....	55
A-17: Temperature rise at the ceiling in Test 10. ....	55
A-18: Normalized thermal centroid deviations and smoke detector response times in Test 10.....	55
A-19: Temperature rise at the ceiling in Test 11. ....	56
A-20: Normalized thermal centroid deviations and smoke detector response times in Test 11.....	56
A-21: Temperature rise at the ceiling in Test 12. ....	56
A-22: Normalized thermal centroid deviations and smoke detector response times in Test 12.....	56
A-23: Temperature rise at the ceiling in Test 13. ....	57
A-24: Normalized thermal centroid deviations and smoke detector response times in Test 13.....	57
A-25: Temperature rise at the ceiling in Test 14. ....	57
A-26: Normalized thermal centroid deviations and smoke detector response times in Test 14.....	57
A-27: Temperature rise at the ceiling in Test 15. ....	58

A-28: Normalized thermal centroid deviations and smoke detector response times in Test 15.....	58
A-29: Temperature rise at the ceiling in Test 16. ....	58
A-30: Normalized thermal centroid deviations and smoke detector response times in Test 16.....	58
A-31: Temperature rise at the ceiling in Test 17. ....	59
A-32: Normalized thermal centroid deviations and smoke detector response times in Test 17.....	59
A-33: Temperature rise at the ceiling in Test 18. ....	59
A-34: Normalized thermal centroid deviations and smoke detector response times in Test 18.....	59
A-35: Temperature rise at the ceiling in Test 19. ....	60
A-36: Normalized thermal centroid deviations and smoke detector response times in Test 19.....	60
A-37: Temperature rise at the ceiling in Test 20. ....	60
A-38: Normalized thermal centroid deviation in Test 20 (no detector activated in 300 s).....	60
A-39: Temperature rise at the ceiling in Test 21. ....	61
A-40: Normalized thermal centroid deviations and smoke detector response times in Test 21.....	61
A-41: Temperature rise at the ceiling in Test 22. ....	61
A-42: Normalized thermal centroid deviations in Test 22 (no detector activated in 300 s). ....	61
A-43: Temperature rise at the ceiling in Test 23. ....	62
A-44: Normalized thermal centroid deviations and smoke detector response times in Test 23.....	62
A-45: Thermal centroid deviations in Test 24 (no detector activated in 300 s). ....	63
A-46: Thermal centroid deviations in Test 25. ....	63
A-47: Smoke detector response times and temperature rise at the ceiling in Test 25.....	63
A-48: Thermal centroid deviations in Test 26. ....	64
A-49: Smoke detector response times and temperature rise at the ceiling in Test 26.....	64
A-50: Thermal centroid deviations in Test 27 (no detector activated in 300 s). ....	64
A-51: Thermal centroid deviations in Test 28. ....	64
A-52: Smoke detector response times and temperature rise at the ceiling in Test 28.....	65
A-53: Thermal centroid deviations in Test 29. ....	65
A-54: Smoke detector response times and temperature rise at the ceiling in Test 29.....	65
A-55: Thermal centroid deviations in Test 30 (no detector activated in 300 s). ....	65
A-56: Thermal centroid deviations in Test 31. ....	66
A-57: Smoke detector response times and temperature rise at the ceiling in Test 31.....	66
A-58: Thermal centroid deviations in Test 32. ....	66
A-59: Smoke detector response times and temperature rise at the ceiling in Test 32.....	66
A-60: Thermal centroid deviations in Test 33. ....	67
A-61: Smoke detector response times and temperature rise at the ceiling in Test 33.....	67
A-62: Thermal centroid deviations in Test 34. ....	67
A-63: Smoke detector response times and temperature rise at the ceiling in Test 34.....	67
A-64: Thermal centroid deviations in Test 35. ....	68
A-65: Smoke detector response times and temperature rise at the ceiling in Test 35.....	68
A-66: Thermal centroid deviations in Test 36. ....	68
A-67: Smoke detector response times and temperature rise at the ceiling in Test 36.....	68

A-68: Thermal centroid deviations in Test 37. ....	69
A-69: Smoke detector response times and temperature rise at the ceiling in Test 37.....	69
A-70: Thermal centroid deviations in Test 38. ....	69
A-71: Smoke detector response times and temperature rise at the ceiling in Test 38.....	69
B-1: Normalized thermal centroid deviations and water discharge rate in Test 40. ....	70
B-2: Smoke detector response times and temperature rise at the ceiling in Test 40.....	70
B-3: Normalized thermal centroid deviations and water discharge rate in Test 41. ....	70
B-4: Smoke detector response times and temperature rise at the ceiling in Test 41.....	71
B-5: Normalized thermal centroid deviations and water discharge rate in Test 42. ....	71
B-6: Smoke detector response times and temperature rise at the ceiling in Test 42.....	71
B-7: Normalized thermal centroid deviations and water discharge rate in Test 43. ....	72
B-8: Smoke detector response times and temperature rise at the ceiling in Test 43.....	72
B-9: Normalized thermal centroid deviations and water discharge rate in Test 44. ....	72
B-10: Smoke detector response times and temperature rise at the ceiling in Test 44.....	72
B-11: Normalized thermal centroid deviations and water discharge rate in Test 45. ....	73
B-12: Smoke detector response times and temperature rise at the ceiling in Test 45.....	73
B-13: Normalized thermal centroid deviations and water discharge rate in Test 46. ....	73
B-14: Smoke detector response times and temperature rise at the ceiling in Test 46.....	73
C-1: Normalized thermal centroid deviations and water discharge rate in Test 47. ....	74
C-2: Smoke detector response times and temperature rise at the ceiling in Test 47.....	74
C-3: Temperature rise at the ceiling near ignition location (R = 1.72 m) in Test 47. ....	75
C-4: Normalized thermal centroid deviations and water discharge rate in Test 48. ....	75
C-5: Smoke detector response times and temperature rise at the ceiling in Test 48.....	76
C-6: Temperature rise at the ceiling near ignition location (R = 1.72 m) in Test 48. ....	76
C-7: Normalized thermal centroid deviations and water discharge rate in Test 49. ....	77
C-8: Smoke detector response times and temperature rise in Test 49. ....	77
C-9: Temperature rise at the ceiling near ignition location (R = 1.72 m) in Test 49. ....	78
C-10: Normalized thermal centroid deviations and water discharge rate in Test 50. ....	78
C-11: Smoke detector response times and temperature rise at the ceiling in Test 50.....	79
C-12: Temperature rise at the ceiling near ignition location (R = 1.72 m) in Test 50. ....	79
C-13: Normalized thermal centroid deviations and water discharge rate in Test 51. ....	80
C-14: Smoke detector response times and temperature rise at the ceiling in Test 51.....	80
C-15: Temperature rise at the ceiling near ignition location (R = 1.72 m) in Test 51. ....	81
C-16: Thermal centroid deviations in Test 52-1. ....	81
C-17: Smoke detector response times and temperature rise at the ceiling in Test 52-1. ....	82
C-18: Temperature rise at the ceiling near ignition location (R = 1.72 m) in Test 52-1. ....	82
C-19: Normalized thermal centroid deviations and water discharge rate in Test 52-2.....	83
C-20: Smoke detector response times and temperature rise at the ceiling in Test 52-2. ....	83
C-21: Temperature rise at the ceiling near ignition location (R = 1.72 m) in Test 52-2. ....	84
C-22: Normalized thermal centroid deviations and water discharge rate in Test 53. ....	84

C-23: Smoke detector response times and temperature rise at the ceiling in Test 53..... 85  
C-24: Temperature rise at the ceiling near ignition location (R = 1.72 m) in Test 53. .... 85

## List of Tables

---

3-1: Experimental conditions of fire detection tests with a 0.76 m sprinkler spacing. ....	18
3-2: Experimental conditions of fire detection tests with a 2.44 m sprinkler spacing. ....	18
3-3: Experimental conditions of sprinkler activation tests with a 2.44 m sprinkler spacing. ....	19
3-4: Experimental conditions of fire suppression tests with a 2.44 m sprinkler spacing.....	19
4-1: Heptane pan fire calibration tests. ....	21
4-2: Summary of sprinkler activation tests .....	36

# 1. Introduction

---

## 1.1 Background

Modern warehouse storage has become increasingly challenging for fire protection systems due to recent developments in automated handling technology. This often results in Highly Challenging Fires (HCFs) for which there exists no current protection recommendations. One example of HCFs is roll paper with high packing densities that can be stored on end in very high stacks, *e.g.*, > 12 m (40 ft). These rolls can be transferred in a storage facility using vacuum lifters or mechanical grippers attached to ceiling cranes. The ceiling cranes and the handlers often require a vertical clearance of 6 m – 9 m (20 ft – 30 ft) for operation. Figure 1-1 shows roll paper in high storage configurations and the handling equipment used to transfer the rolls. As a result, the challenges to fire protection include both high storages and high ceiling clearances. Another example is provided by Automatic Storage and Retrieval Systems (ASRS) using open-top containers, where water transport is largely blocked even for in-rack sprinkler protection. In this work, the high storage of roll paper will be used as an example for demonstration purposes.



Figure 1-1: Roll paper in high on-end storage configurations (photo courtesy of Terex MHPS Corp).

## 1.2 Previous work on HCF protection

Using the roll paper storage as an example, current fire protection recommendations are limited to 12 m and 18 m (40 ft and 60 ft), under a building height of 26 m (85 ft) or less [2]. These protection options were developed through full-scale tests conducted over the past three decades by FM Global. The protection problem is particularly difficult when in-rack sprinklers are not an option for very high on-end roll paper storage. For the high on-end storage, the fire growth can be fast, resulting in a large fire size in a short period of time. Figure 1-2 shows fire growth rates of various roll paper types measured as the variation of chemical heat release rate (HRR) per unit time [3]. In addition, the high ceiling clearance can

further delay sprinkler response. The relatively fast fire growth and slow sprinkler response are the main limits on fire protection options using currently available sprinkler systems. Therefore, the key to improve the sprinkler performance and to reduce potential fire and water damage is to activate the sprinklers as early as possible. To counteract the fast fire growth rate, a sprinkler may need to be activated ahead of the fire spread so that the combustible commodities can be adequately pre-wetted.

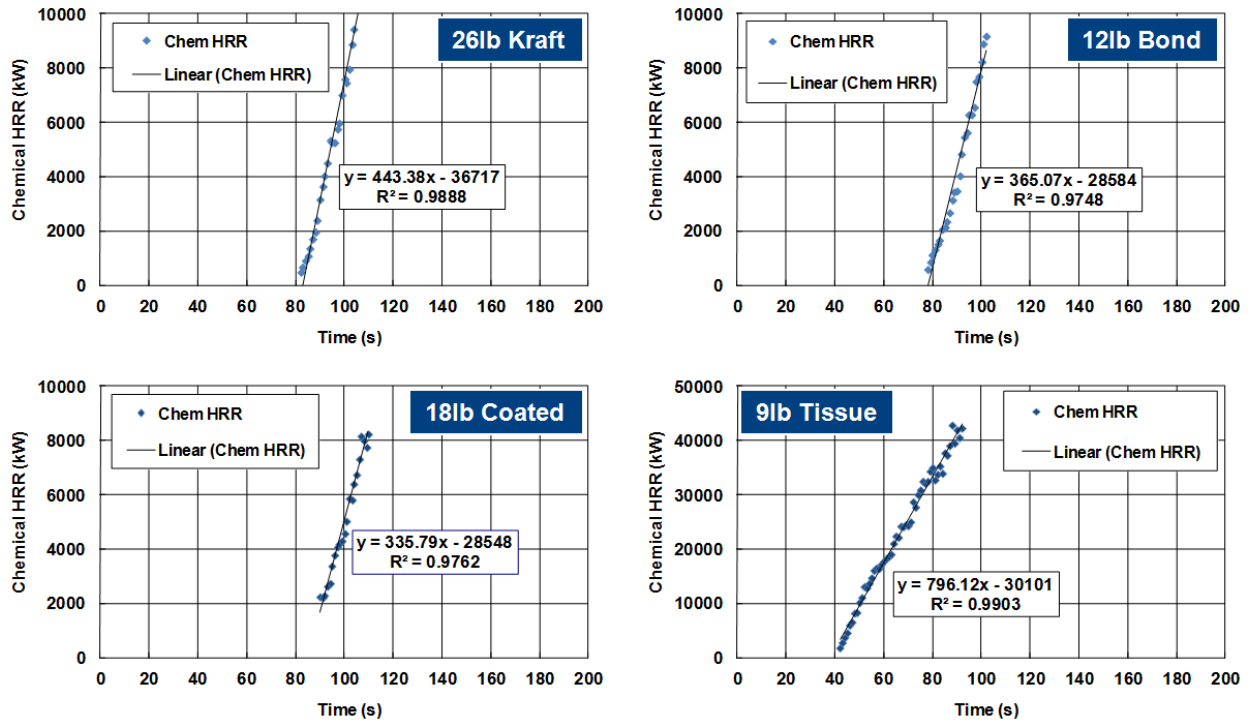


Figure 1-2: Fire growth rates of different roll paper types [3].

### 1.3 Objectives

To address the protection of HCFs, a new protection concept was proposed in 2012 and a prototype system was designed and tested in 2013-2015. The overall objective of this program is to demonstrate a new sprinkler system that can provide adequate protection for HCFs in storage configurations. The first objective was to design and test the system at a component level. The second objective was to perform integrated system tests to examine its effectiveness in fire protection. The present report documents the results associated with the first objective.

The overall objective of this work is to complete component-level development and testing for the new sprinkler system. Specific tasks include the measurement of fire growth rates and critical delivered fluxes at reduced scales, and the evaluation of system functions including fire detection, fire location and sprinkler activation under various experimental conditions. In addition, preliminary suppression experiments are also included to assess the feasibility of achieving fire suppression or extinguishment. The latter is important for HCFs because fire fighters may not be able to enter the storage facility due to safety concerns. Therefore, it is desirable for the new protection system to have the capability of extinguishing the fire.

## 1.4 Organization of this report

To achieve the objectives listed above, a prototype sprinkler system was designed and fabricated. This development is discussed in Chapter 2, including means to achieve fire detection, sprinkler activation and fire suppression. Chapter 3 describes the experimental method employed to evaluate system functions, including test configurations, instrumentation and test matrix. The results of a series of fire detection, sprinkler activation and fire suppression tests are reported in Chapter 4, together with discussion of the system performance. In the last part of this report, Chapter 5, a summary of the work completed is provided, along with a discussion of full-scale fire tests documented in a separate report [1] to evaluate the new system in more realistic fire protection scenarios.

## 2. System design

The system design starts with the objectives of detecting, locating and suppressing a fire as early and as locally as possible. In this work, we refer to the technology to achieve this objective as Simultaneous Monitoring, Assessment and Response Technology (SMART). Such a sprinkler protection system is defined in this work as a SMART sprinkler. The SMART sprinkler system needs to include hardware and software components to achieve fire detection, fire location, sprinkler activation and fire suppression. The basic system design is summarized in Figure 2-1. Details of the system components are described in the following Sections 2.1 – 2.5.

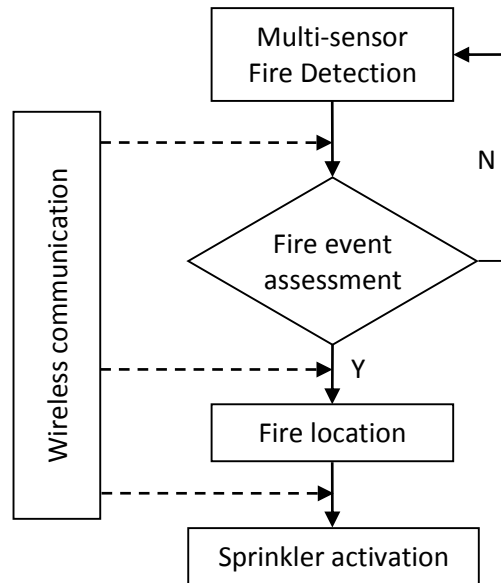


Figure 2-1: Basic functions of a SMART sprinkler system.

### 2.1 Fire detection

Fire detection can be achieved by using different types of detection methods, which identify various fire phenomena including combustion product generation (smoke or gas), convective heat transfer and flame radiation. These detection methods are implemented as smoke detectors, heat detectors and flame (optical) detectors [4]. Fire detection can also be achieved by using more than one type of detector, which is defined as multi-sensor detection technology.

Typical smoke detectors use either photoelectric or ionization sensors. Photoelectric sensors monitor light scattered or obscured by smoke particles onto an optical detector to trigger an alarm. An ionization smoke detector ionizes air in a sensing chamber to allow the passage of a small electric current between charged electrodes. If any smoke particles enter the chamber, the ions will attach to the particles resulting in lower conductivity to carry the current, which triggers the detector. In general, ionization and photoelectric detectors are more sensitive to the flaming and the smoldering stage of the fire, respectively. The smoke detector response time depends on both the predetermined threshold in the

sensor and the transport time for combustion products to reach the sensor. The detection time within the sensor, either photoelectric or ionization, is often negligible compared to the transport time.

Heat detection relies on a temperature sensor to determine a fire event, at a fixed temperature threshold, a rate-of-rise, or a combination of both. Fire sprinklers can also be considered a type of heat detector since the sensible element of a sprinkler breaks when its temperature reaches the rated value. Similar to the smoke detector, the response time of a heat detector is dependent on the transport time and the detection threshold of the fixed temperature and/or the rate-of-rise. However, due to thermal inertia of the heat sensor, there is often a thermal lag in heat detectors compared to smoke detectors.

A flame (optical) detector uses an optical sensor to detect flame radiation. The optical sensor can work in the infrared, visible and/or ultraviolet range of the spectrum. The main advantage of optical flame detectors is their independence of detection on fire-induced convective transport time. As a result, the response time for optical detectors is almost instantaneous as long as the flame radiation level exceeds the sensor threshold. However, the optical detector requires a line-of-sight path to the fire so that it can “see” the flame radiation. This restriction can present a big challenge to the use of optical detectors, since the field of view of fires in very high storage is often very limited.

Given the detection mechanisms and the response characteristics of different sensors, both smoke and heat detectors were selected in the present work to evaluate the feasibility of triggering the sprinkler system. The use of two different types of detectors, *i.e.*, multi-sensor detection, is aimed at reducing false alarms, which may cause unwanted water damage. Flame (optical) detectors are excluded from the present work mainly due to the limited view factor within very high storage as discussed above. If the storage array is sufficiently open, a combination of flame and smoke detectors may provide faster response than combined smoke and heat detectors.

## 2.2 Fire event assessment

The detected signals from smoke and heat sensors need to be assessed to determine if a fire event has occurred. The smoke and heat sensors generate continuous time-dependent signals. For a single detector, a threshold can be imposed to judge the fire event. For multiple sensors, this can be done either using cross correlations [5] or simple logic operations. Since the focus of the present work is to demonstrate the feasibility of the new system, *i.e.*, proof-of-concept, a simple logic operation is implemented for fire event assessment

$$Fire\ event = [(\Delta I/I) > (\Delta I/I)_{min}] AND [(\Delta T) > (\Delta T)_{min}], \quad 2-1$$

where  $\Delta I/I$  is the obscurity of the smoke alarm;  $\Delta T$  is the temperature rise above the ambient; and the subscript *min* denotes the threshold value. For fire protection using sprinklers, a fire event is confirmed positive when both conditions in Equation 2-1 are satisfied simultaneously for at least one SMART sprinkler unit. However, in the fire detection and sprinkler activation tests, only the smoke alarm condition was required to simplify the evaluation of specific system functions, which will be discussed in detail in Chapters 3 and 4.

## 2.3 Fire location

Once a fire event is confirmed, the next step is to locate the source fire. This is crucial to the determination of the number and pattern of sprinklers that need to be activated for fire suppression. In the present work, the smoke detectors are smoke alarms that provide only an event signal. Therefore, thermocouples (TCs) at the ceiling are used to determine the fire location. The algorithm determining the fire location is based on a calculated thermal centroid at the ceiling level. For a given time the ceiling TC data are first normalized by the maximum and minimum values; then those normalized temperatures above 90% of the peripheral values of the test site are included in the centroid calculation; finally the thermal centroid coordinates are computed by

$$x_i = \sum_i x_i T_i^* / \sum_i T_i^* , \quad 2-2$$

$$y_i = \sum_i y_i T_i^* / \sum_i T_i^* , \quad 2-3$$

where  $x_i$  and  $y_i$  are coordinates of the  $i$ th TC, and  $T_i^*$  is the normalized temperature using the maximum and minimum values. The use of the 90% cut-off threshold is aimed at improving accuracy to determine the centroid by eliminating the biasing effect of values differing by very small amounts from ambient temperature.

In the present work, different algorithms were tested to compute the x-y coordinates of the thermal centroid, which are treated as the fire location in two-dimensional plan view. One method is to simply use all TC values to compute the centroid, since only relatively few TCs are installed under the ceiling in the experiments described in Chapter 3. A second method is to only include the TCs located within a predetermined distance from the maximum temperature point, under the assumption that the maximum temperature should occur in the vicinity of the fire center. The point of the latter method is also to improve the accuracy of the centroid calculation by eliminating the impact of relatively trivial values. Comparison of these methods will be also discussed in Chapter 3.

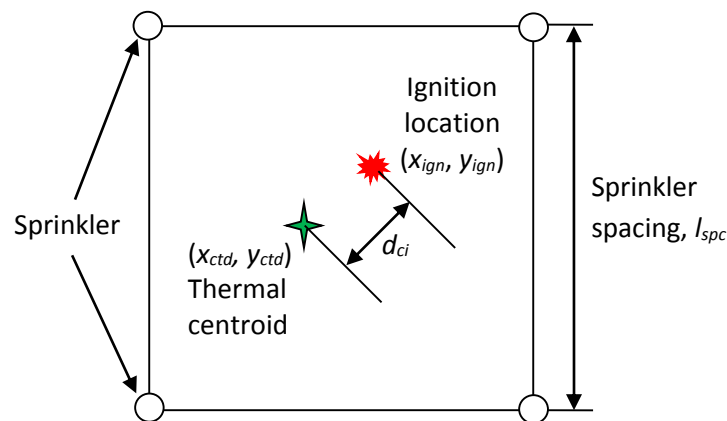


Figure 2-2: Thermal centroid deviation relative to ignition location.

To quantify the accuracy of the calculated fire location, the distance between the thermal centroid location and the ignition location is defined as thermal centroid deviation,  $d_{ci}$ . Figure 2-2 shows the relative positions of a calculated thermal centroid location and the ignition location in a sprinkler layout with a spacing of  $l_{spc}$ . The thermal centroid deviation,  $d_{ci}$ , can be computed as

$$d_{ci} = \left[ (x_{ctd} - x_{ign})^2 + (y_{ctd} - y_{ign})^2 \right]^{1/2}, \quad 2-4$$

where the coordinates of the centroid location are  $(x_{ctd}, y_{ctd})$  and those of the ignition location are  $(x_{ign}, y_{ign})$ .

The purpose of computing the thermal centroid deviation,  $d_{ci}$ , is to determine how accurately the thermal centroid location can approximate the actual fire location, so that its impact on sprinkler activation can be determined and used for sprinkler activation. For this purpose, the thermal centroid deviation is compared to the sprinkler spacing,  $l_{spc}$ . If the thermal centroid location is a good approximation of the fire location, the value of  $d_{ci}$  should be much smaller than the sprinkler spacing,  $l_{spc}$ . But if  $d_{ci}$  is larger than  $l_{spc}$ , an extra ring of sprinklers may need to be activated in addition to those only under the consideration of fire propagation. Therefore, a nondimensional quantity,  $R_{dl}$ , is defined as

$$R_{dl} = d_{ci}/l_{spc}. \quad 2-5$$

The quantity  $R_{dl}$  is referred to as the normalized thermal centroid deviation in this work, which represents the distance from the thermal centroid to the ignition location normalized by the sprinkler spacing. This quantity will be used in Chapters 3 and 4 to describe the accuracy of fire location calculation.

## 2.4 Sprinkler activation

Sprinkler activation is the final step in all functions of the SMART sprinkler system. There are two basic questions that need to be answered to determine the sprinkler activation: what is the coverage area and what is the adequate design water density? The answer to these questions determines the number of sprinklers to be activated and the total water flow rate for the system design.

For a given fuel, the adequate water flux is primarily a function of the protection objective to control, suppress or extinguish the fire. The minimum level of protection is to control the fire, *i.e.*, to prevent further fire propagation subsequent to the sprinkler activation. As the water flux increases beyond the fire-control level, fire suppression and even fire extinguishment can be achieved. Note that, upon water discharge, there is often a delay in controlling the fire due to water operating pressure fluctuation and water transport to the burning region. The latter is the main challenge for high storage fires, as water has to be from the top to the bottom of the fuel array.

The first option to overcome this delay time is to increase the applied water flux. For very high storage of HCFs, the water transport time can be estimated as

$$t = h_s/u_w, \quad 2-6$$

where  $h_s$  is the fuel storage height and  $u_w$  is the mean water flow speed on the fuel surface. Based on a previous study [6], the water flow speed scales as

$$u_w \sim (\dot{m}'_w)^{2/3}, \quad 2-7$$

where  $\dot{m}'_w$  is the water flow rate per unit length in the lateral direction. Previous commodity classification studies [7] [8] suggest that the critical delivered flux (CDF) may scale approximately with storage height as a linear function,

$$\dot{m}'_w \sim h_s. \quad 2-8$$

Combining these equations yields

$$t \sim (h_s)^{1/3}. \quad 2-9$$

Equation 2-9 suggests that the water transport time increases by a factor of  $h_s^{1/3}$ , after taking into account the increase of CDF with storage height. In order to counteract the impact of this delay, the applied water flux needs to be increased as

$$\dot{m}'_w \sim (h_s)^{3/2}. \quad 2-10$$

Equation 2-10 suggests that to maintain the water transport time constant, the applied water flux needs to be increased as the 3/2 power of the storage height. This is a more conservative requirement than the linear relationship in Equation 2-8, which is based on empirical results from previous commodity classification work [7] [8].

Another option to overcome the water transport delay is to activate sprinklers ahead of the fire propagation, *i.e.*, to pre-wet the fuel surface. This is one of the main strategies in SMART sprinkler protection. Therefore, the range of sprinklers to be activated is not only a function of the fire size and fire growth rate, but also a function of the fuel storage height. The specific range of sprinklers for activation can be determined by considering the water transport delay time and the fire propagation speed.

For the present work, the sprinkler activation algorithm is determined by considering the basic ignition fire scenarios shown in Figure 2-3. Analysis of past full-scale tests shows that the SMART sprinklers should activate at a very early stage of fire development. That is, for vertical fire spread the flame height should be no more than half of the fuel storage height; and for lateral fire spread, the flame front should be within the length of one fuel stack. Based on this analysis, the activation of the first ring sprinklers around the fire location should be sufficient to prevent further fire spread. From Figure 2-3, the number of first ring sprinklers that need to be activated is between four and six for the three basic ignition scenarios. To keep the sprinkler activation algorithm simple and conservative, it was decided that the nearest six sprinklers from the calculated fire location (thermal centroid) should be activated.

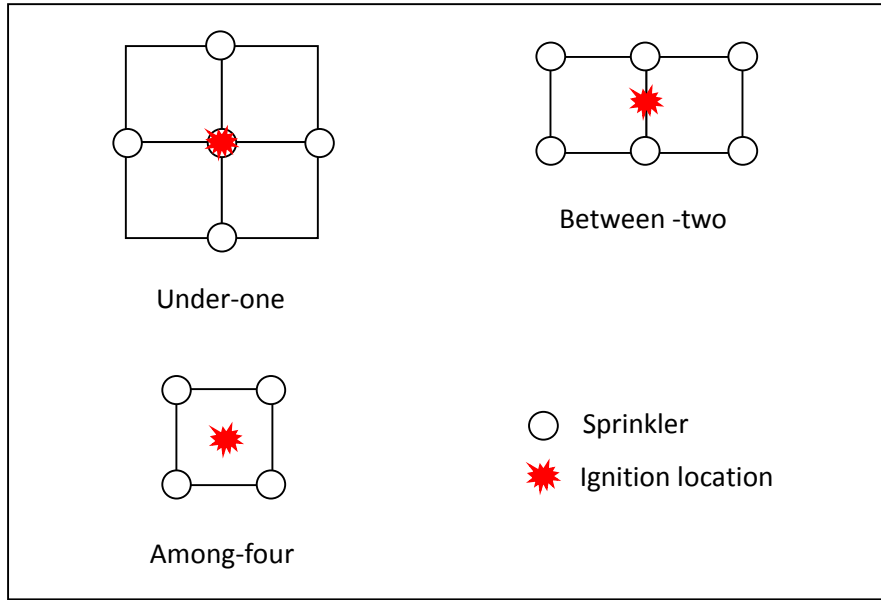


Figure 2-3: Determination of number of sprinklers to be activated.

## 2.5 System communication

The communication among system components is crucial to achieve all the functions described in Sections 2.1-2.4. In a traditional sprinkler system, there is only one type of communication between fire detection and sprinkler activation within each sprinkler unit, *i.e.*, the breakage of the sensible element upon reaching its rated temperature. Since the sprinkler activation is not coordinated among sprinklers, water sprays from sprinklers opened earlier can impinge onto neighboring sprinklers and result in sprinkler skipping [9]. For SMART sprinklers, the skipping issue can be effectively eliminated by activating a group of sprinklers simultaneously when a fire event is confirmed and the fire location is determined. The communication needs to be designed so that the fire event assessment, fire location calculation and sprinkler activation pattern can be accomplished as shown in Figure 2-1 to achieve the overall protection objective.

In the present work, each SMART sprinkler unit is equipped with a transceiver that is linked to the fire detectors via wired connections. Meanwhile, each transceiver also communicates wirelessly to a central control unit. Figure 2-4 shows an example of the wireless transceiver connected to the smoke and heat detectors and installed for an individual SMART sprinkler. Note that only commercially available sensors and transceivers were used in the present work for the purposes of feasibility study. The central control unit consists of a computer and a master node transceiver that communicates to each sprinkler. The fire event assessment, fire location calculation and sprinkler activation determination are all performed at the central control unit, while the sprinkler activation is executed via an electromagnetic (solenoid) valve at each individual sprinkler unit. The data collected by the master node is processed by the computer to accomplish the aforementioned functions. The evaluation of these system functions requires dedicated experiments, which will be described in detail in Chapter 3.



Figure 2-4: Wireless transceiver connected to smoke and heat detectors.

It should be pointed out that the aforementioned design is based on one HCF scenario of high storage of roll paper. The SMART sprinkler system design may be adapted to other HCFs, such as a combination of in-rack detectors and ceiling-only sprinklers for very high rack storage, a combination of image-based detectors and ceiling-only sprinklers for very high clearance applications and a combination of in-rack detectors and surrounding water mist nozzles for ASRS using open-top containers. If ignitable liquid is of concern, a foam system can be used in place of the sprinkler or water mist system. In addition, the combination of multi-detectors as well as co-located or separated detector/sprinkler arrangements can also be used, as long as the common objective of suppressing fires as early and locally as possible is achieved in a cost-effective manner.

## 3. Experimental method

---

In order to evaluate the system functions, three types of experiments are considered in this study:

- Fire detection tests. The objectives of the fire detection test are to evaluate the response times of various detectors and to assess the algorithm used to compute the fire location. Two detector spacings were tested to simulate different fire scenarios of HCFs.
- Sprinkler activation tests. The objective of the sprinkler activation test is to examine the control algorithm for simultaneously activating a group of sprinklers upon the detection of a fire event. The number of sprinklers activated and the locations of these sprinklers will be the focus of the sprinkler activation tests.
- Fire suppression tests. These tests are included to conduct a preliminary assessment of the suppression effectiveness using the SMART sprinkler. The results were used to provide a design basis for full-scale tests.

### 3.1 Experimental setup

#### 3.1.1 Fire detection tests

Two fire scenarios were considered in the detection experiments. The first fire scenario considers very high storage with a ceiling height of 25.6 m (84 ft). Given that the maximum height of the movable ceiling in the Small Burn Laboratory (SBL) is 7.9 m (26 ft), a scaling ratio of 1/4 based on Froude number modeling [10, 11] is used in the test design.

It is assumed in this work that the ceiling height of a high-storage warehouse is 25.6 m (84 ft). The movable ceiling in the SBL, therefore, is positioned at 6.4 m (21 ft) above the source fire. In order to simulate a flat warehouse ceiling, the four edges of the movable ceiling are kept open without installation of any smoke draft curtain. Similarly, the detector installation spacing, which should be 3.05 m × 3.05 m (10 ft × 10 ft) at a 25.6 m (84 ft) ceiling level, becomes 0.76 m × 0.76 m (2.5 ft × 2.5 ft) using the 1/4 scaling ratio. By the use of the scale-down geometry, in conjunction with scaled fire sizes, the locations of the fire detectors being triggered can be preserved. In addition, it is also expected that the time sequence of detector response can be preserved. Note that, even though the physical dimensions are scaled, the detection times may vary since the detector characteristics such as threshold and response time constant are not scaled. Figure 3-1 shows the schematic of the test setup under the movable ceiling in the SBL.

It should also be pointed out that the scaled-down test, although designed according to Froude number modeling, has a relatively small spacing [0.76 m (2.5 ft)] between the sprinklers. Given that the flame may fluctuate around the burner axis and the ceiling clearance [6.4 m (21 ft)] is relatively high, it is expected that the uncertainties associated with the fire location calculation can be quite large, leading to a more conservative estimation of sprinkler coverage area.

The second fire scenario considers relatively low storage. In this case, the test was set up using the same ceiling clearance, but with a larger sprinkler spacing of 2.44 m (8 ft). Note that the selection of 2.44 m (8 ft) is due to the limited ceiling area in the SBL and the need to install a reasonable grid of SMART sprinklers. The two cases with different spacing are expected to reveal the range of uncertainties associated with the fire location calculation.

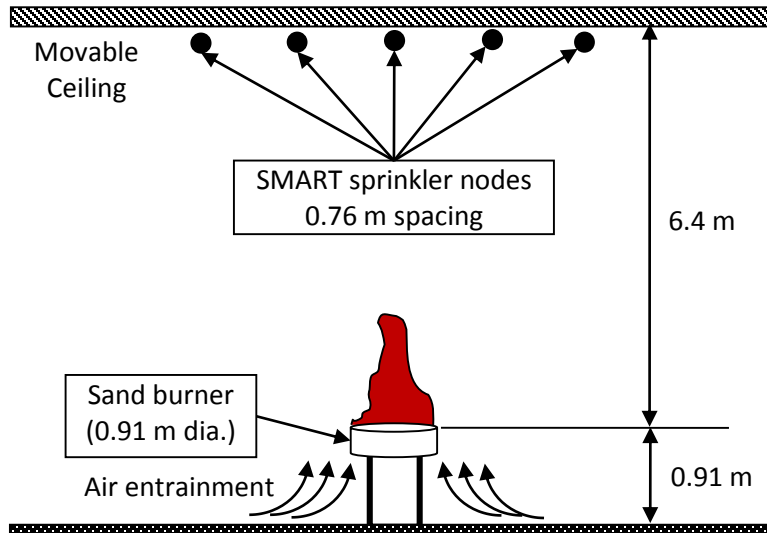


Figure 3-1: Schematic of experimental setup under the movable ceiling in the SBL.

In either test scenario, the source fire is established on a circular sand burner. Based on Froude number modeling, a 10 MW fire, which represents the upper end of HRR in full-scale tests, should scale down by a factor of  $(1/4)^{5/2}$  resulting in an approximate HRR of 320 kW. Since the SMART sprinkler may activate faster than traditional sprinklers, three fire sizes are included in this work: 320 kW, 160 kW and 80 kW. This should be sufficient to cover the range of fire sizes expected upon sprinkler activation in HCFs. It should be pointed out that the scaling laws used here were mainly developed using pool fire and gas flame data [10, 11], which may be different from the high storage fires especially in the location of the virtual origin. More thorough analysis can certainly help improve the scaling laws, however, that pursuit was deemed beyond the scope of this work.

Observations from full-scale tests also indicated that the lateral dimension of the fire upon the first sprinkler activation is approximately 3 m - 4.6 m (10 ft - 15 ft). Therefore, a circular sand burner of 0.91 m (3 ft) in diameter was used to establish the source fire based on the scaling ratio. To ensure symmetry of the fire, *i.e.*, no significant flame leaning, the sand burner was elevated so that the fuel exit surface was 0.91 m (3 ft) above the lab floor.

The smoke yield from solid fuels also affects detection. According to Tewarson [12], the range of smoke yield for typical cardboard and wood is  $0.01 - 0.015 \text{ g}_{\text{smoke}}/\text{g}_{\text{fuel}}$ , while plastics usually have higher smoke yields. To simulate the smoke yield conservatively, propane gas with a smoke yield of  $0.024 \text{ g}_{\text{smoke}}/\text{g}_{\text{fuel}}$  [12] was used to generate the steady-state fires on the sand burner.

Twelve SMART sprinkler units were installed under the movable ceiling. The detailed layout of the sprinkler unit is shown in Figure 3-2. Each sprinkler unit consists of a heat detector, a smoke detector, a thermocouple (TC), an XBEE transceiver with a thermistor plugged in and an open sprinkler installed nearby. The TC beads and the inlets of the smoke and heat detectors were all 7.6 cm - 8.2 cm (3 in. - 3.25 in.) from the ceiling in the vertical direction. The sprinkler layout under the ceiling is shown in Figure 3-3. A node ID (NID) was assigned to each unit and used by the central control unit to identify each sprinkler unit. The sprinkler spacing was uniform in all directions. The four ignition locations selected in this work are also marked in Figure 3-3.

The test procedure was identical for the two fire scenarios with 0.76-m (2.5-ft) and 2.44-m (8-ft) sprinkler spacing. Each test started approximately 60 s prior to ignition to collect ambient data. Then the propane flow was switched on and the sander burner was ignited using a torch flame at the center of the sand burner. Measurements were recorded through both a wired data acquisition system and the wireless communication to the master node of the central control unit. Each test was terminated either shortly after smoke alarms were triggered and before ceiling temperatures exceeded the limits of SMART sprinkler components, or when no alarm was triggered in the 5 minutes following ignition.

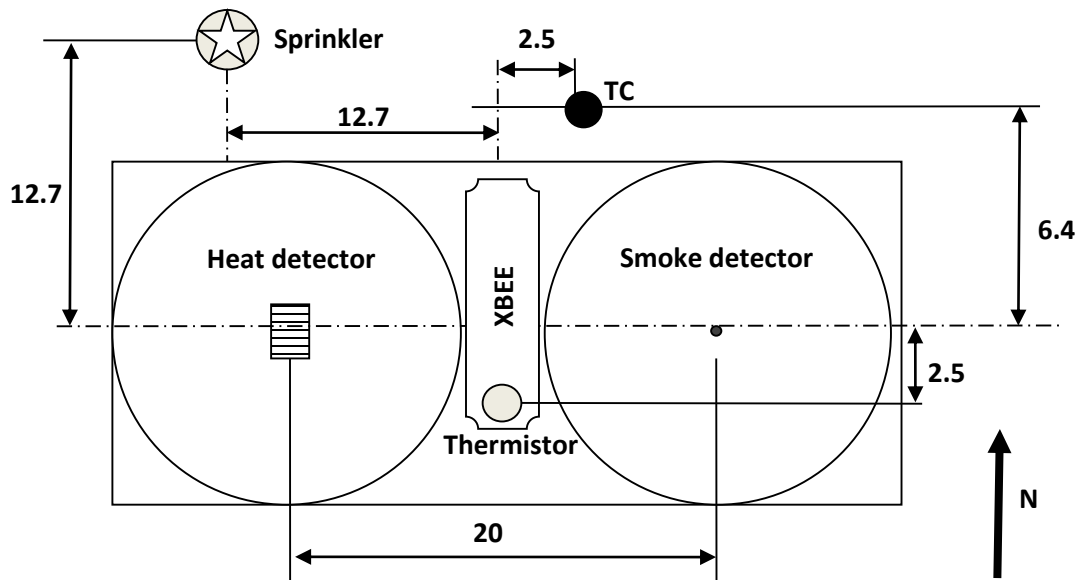


Figure 3-2: Detector, sensor and sprinkler installation on a SMART sprinkler (unit: cm).

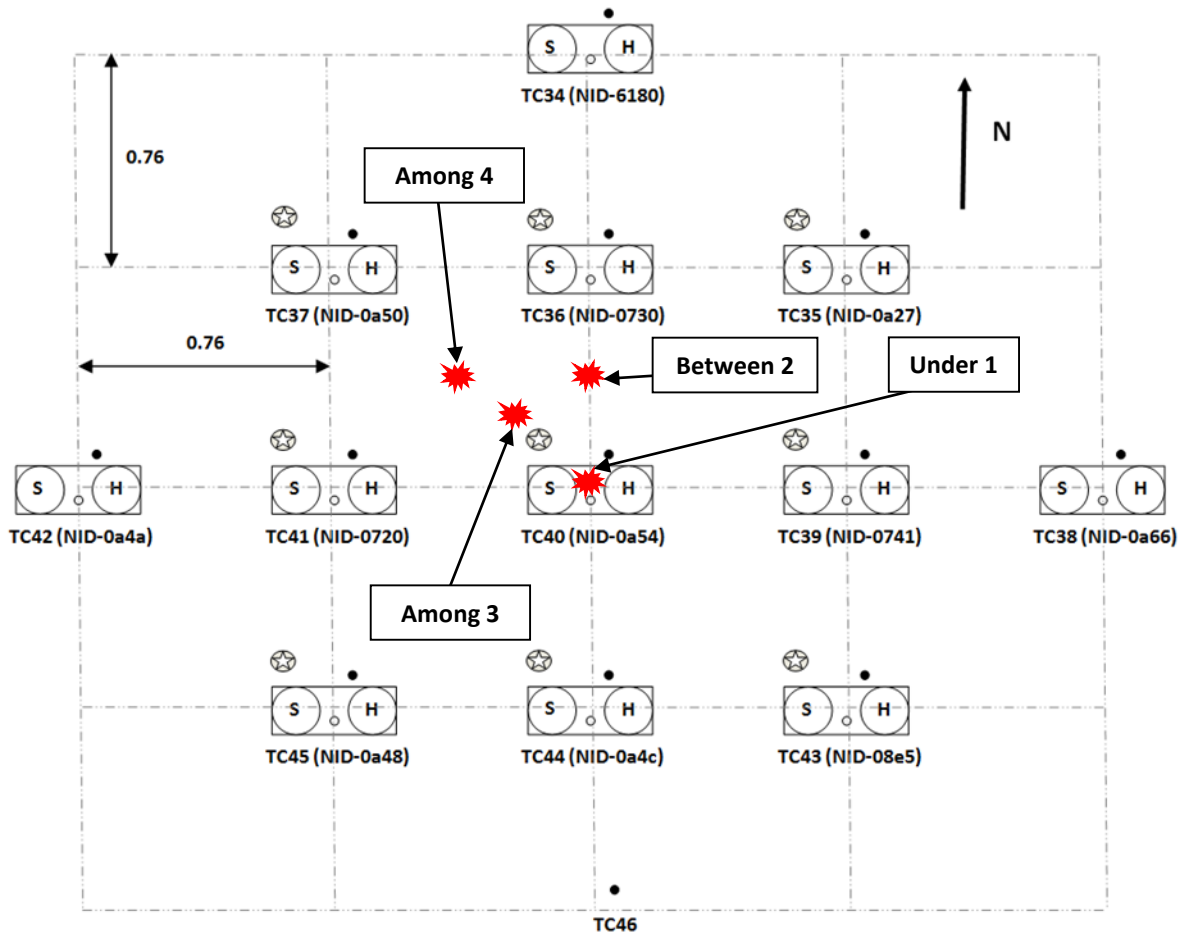


Figure 3-3: Sprinkler layout and ignition locations under the movable ceiling (unit: m).

### 3.1.2 Sprinkler activation tests

The experimental setup for the sprinkler activation tests was the same as that used in the fire detection tests (cf. Figure 3-1), except that a heptane pan fire replaced the sand burner. The use of a heptane fire avoids wetting the sand burner during water discharge. Since heptane produces more soot than propane, the source fire established on a small circular pan (0.3 m or 12 in. diameter) was sufficient to trigger the smoke alarm. The circular pan was filled with a 2.5 cm (1 in.) thick layer of heptane on top of a 7.6 cm (3 in.) layer of water. The fire was ignited at the center of the fuel surface using a torch flame. Similar to the detection test, the pan fire was positioned 0.91 m (3 ft) above the lab floor; the movable ceiling was positioned at 6.4 m (21 ft) above the pan fire; and the sprinkler spacing on the ceiling remained at 2.44 m (8 ft). The layout of sprinkler and ignition locations was the same as in Figure 3-3.

In addition to the detectors and transceivers described earlier, solenoid valves were installed on nine sprinklers for the sprinkler activation tests (cf. Figure 3-3). The water supply and control is shown in Figure 3-4. The solenoid valve is installed between the water supply pipe and the open sprinkler. The trigger signal of the solenoid valve is provided by a relay connected to the transceiver of each sprinkler

unit. Note that the use of solenoid valve in this work is merely intended to demonstrate the SMART sprinkler concept. In engineering practice, the SMART sprinklers should be activated via other cost-effective means such as an electric heater and explosive actuator.

Each sprinkler activation test started with ignition of the pan fire. Smoke alarms were selected as the only signal to trigger the sprinkler activation. Each test was terminated when the sprinkler activation pattern was visually confirmed. The water flow rate to the sprinklers was also recorded as an additional means to verify the number of sprinkler activations. The results of the sprinkler activation tests were the basis for designing the fire suppression experiments.

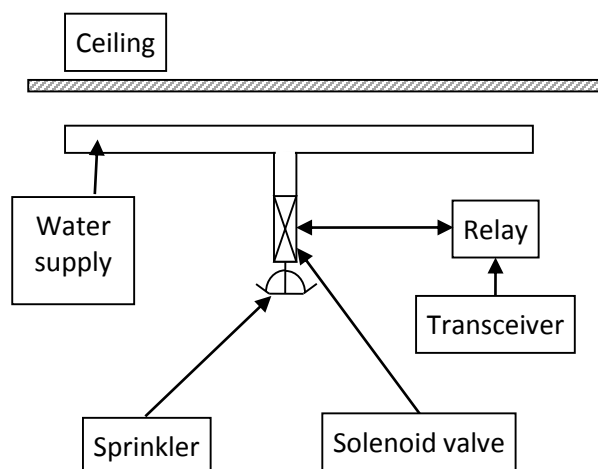


Figure 3-4: Solenoid valve and sprinkler connection in sprinkler activation tests.

### 3.1.3 Fire suppression tests

Fire suppression tests were designed to conduct a preliminary assessment of the SMART sprinkler in protecting combustible commodities. The commodity selected for the suppression tests was the cartoned unexpanded plastic (CUP) commodity representing a medium level of fire hazard [8]. The fuel array was a standard rack storage configuration with 15 cm (6 in.) flues in both longitudinal and transversal directions. Figure 3-5 shows the schematic of a 2x2, 3-tier CUP test. All suppression tests used the same floor plan of four commodity stacks in a 2x2 matrix. The fuel storage height varied from one tier to three tiers with an increasing degree of fire hazards. Each tier of CUP rack storage has a nominal height of 1.5 m (5 ft).

The fuel array was set up under the movable ceiling in the SBL. The ceiling was positioned at 3 m (10 ft) above the top surface of the fuel array. As a preliminary suppression study, the ignition location was fixed in this work at the center of the fuel array on the floor level, as shown in the plan view in Figure 3-5.

Two pendent sprinklers with a K-factor of 80 lpm/bar<sup>1/2</sup> (5.6 gpm/psi<sup>1/2</sup>) and 200 lpm/bar<sup>1/2</sup> (14 gpm/psi<sup>1/2</sup>) were selected for fire suppression tests based on estimated water densities. Note that the small orifice sprinkler (K = 80 lpm/bar<sup>1/2</sup>), which is typically not recommended in engineering practice, was used in this work for testing purposes only due to the minimum required water operating pressures

under low water densities. Ignition was carried out using either four half-igniters, or a 15 cm (6 in.) square alcohol pan fire, placed at the center of the bottom tier on the floor level. The alcohol pan fire was used to replace the standard igniters which often produce excessive smoke capable of triggering the sprinkler system without involving the test commodity.

Each suppression test started with fire ignition at the center of the fuel array. The estimated fire size upon fire detection and sprinkler activation was less than 0.5 MW based on detection test results. Once the sprinklers were activated, observation of fire size in terms of flame height and lateral flame spread were made to determine the termination of the test. Due to safety concerns, any indication that the fire was uncontrolled resulted in immediate termination of the test with manual firefighting to extinguish the fire.

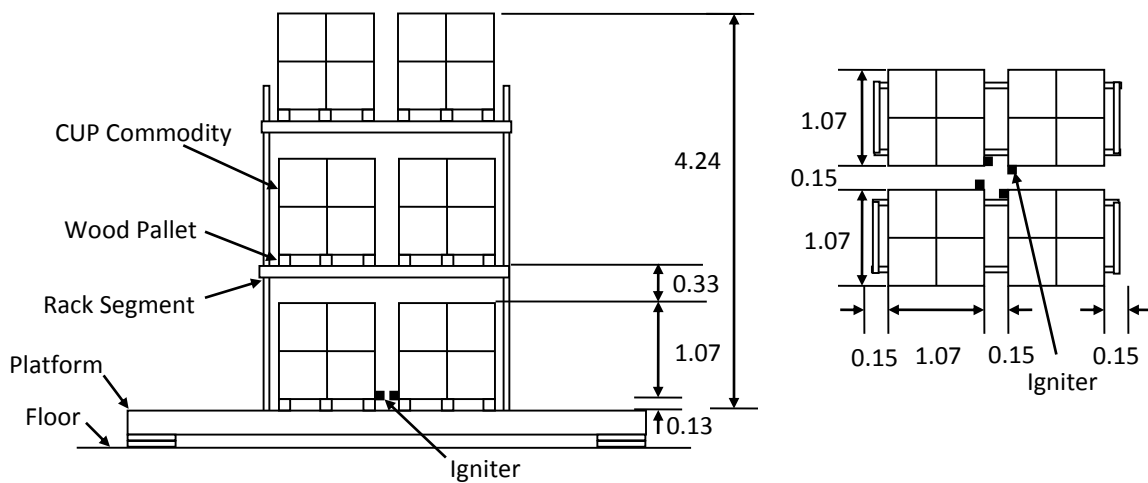


Figure 3-5: Experimental setup of fire suppression tests in 2x2, 3-tier rack storage (unit: m).

### 3.2 System communication and data acquisition

As discussed in Section 2.5, the SMART sprinkler system involves both wired and wireless connections and communications. Figure 3-6 shows the links among various components of the system. The core for communication in each sprinkler unit is an XBEE transceiver (wireless module) connected to a heat alarm [ $T = 57.2\text{ }^{\circ}\text{C}$  ( $135\text{ }^{\circ}\text{F}$ )], a smoke alarm (AC/DC powered, ionization type), a temperature sensor (Thermistor) and a ceiling TC (Type "T") via a linear TC module. The TC module amplifies the linearized voltage signal generated by the TC. The heat and smoke alarms are powered by 120V AC and provide a triggering (interconnect) signal of  $9\pm 2\text{ V DC}$ . The heat alarm was triggered when the temperature rose above  $57.2\text{ }^{\circ}\text{C}$  ( $135\text{ }^{\circ}\text{F}$ ). The smoke alarm was an ionization detector with a normal sensitivity of 1.6 - 3.0 %/m (0.50 - 0.92 %/ft) obscuration. The output signals from the two alarms were wired to the XBEE module as well as the data acquisition system of the FM Global Research Campus. The temperature sensor (Thermistor) was plugged into the XBEE module directly. The thermistor also provided continuous temperature signals to the XBEE. All XBEEs were configured wirelessly to communicate to the master node on the central control unit, which serves as another data collection device in addition to the data acquisition system of the FM Global Research Campus. The SMART sprinklers formed a

wireless network that communicated information to the master node at a rate of 1 Hz, while the wired data acquisition read data at 10 Hz.

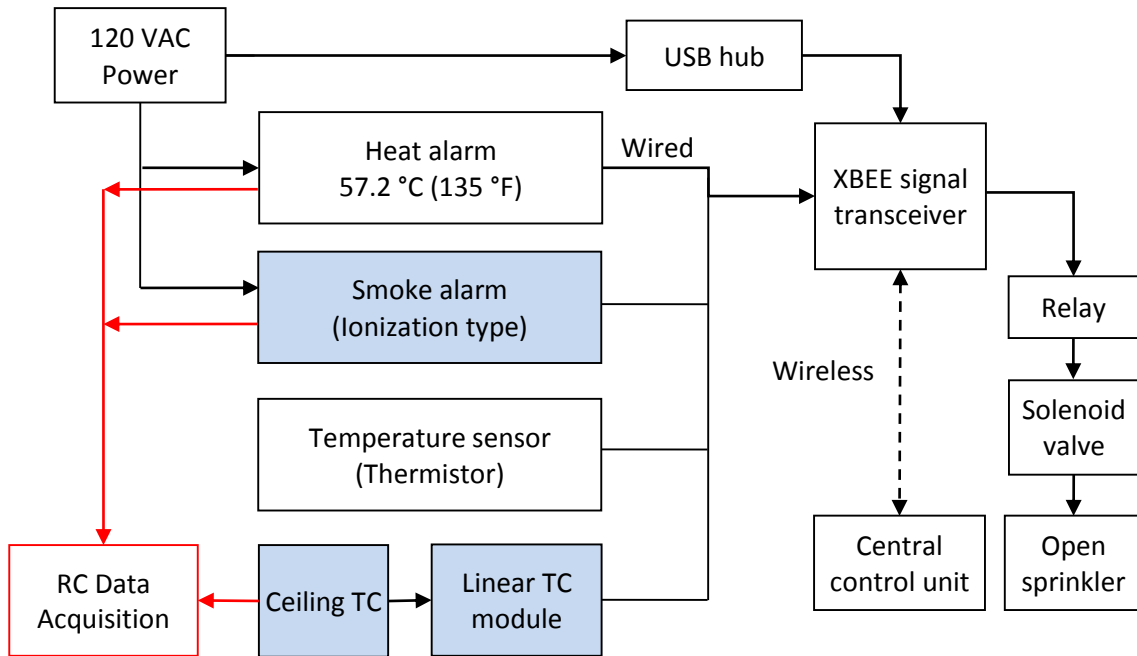


Figure 3-6: SMART sprinkler system connection and communication.

### 3.3 Experimental conditions

Experimental conditions for fire detection tests are listed in Table 3-1 and Table 3-2 for 0.76 m (2.5 ft) and 2.44 m (8 ft) sprinkler spacing, respectively. In Tests 1-23 (Table 3-1), the sprinkler spacing was 0.76 m (2.5 ft). Among these tests, the first case was a trial test where no data were recorded. The subsequent nine tests (Tests 2-10) were conducted with a fixed ignition location (under 4) with respect to the sprinkler grid as shown in Figure 3-3. The objective of these tests was to observe the impact of HRR on fire detection. Tests 11-20 were conducted to investigate the impact of fire location on response times. The remaining tests in Table 3-1 were carried out to repeat some previous cases where wireless data transmission failed during a test. When this phenomenon was identified before ignition, the test was immediately halted and the freezing XBEE transceiver was power-cycled to restore the communication.

Similarly, all tests conducted with a 2.44 m (8 ft) sprinkler spacing are listed in Table 3-2, with Tests 24-32 aimed at investigating the HRR impact and Tests 33-38 for ignition location impact on the detection response time.

Table 3-3 lists the experimental conditions for the sprinkler activation tests. As described in the table note, Test 39 was a trial case where no data were recorded. Tests 40-46 were conducted using the same source fire, but with various ignition locations with respect to the sprinkler grid. The focus of these tests was to observe the sprinkler activation number and pattern.

Table 3-4 describes the experimental conditions for the preliminary fire suppression tests. Note that, among these tests, the igniters, ignition locations, sprinkler types and activation criteria were adjusted from one test to another. Considerations behind these changes are described in detail in the next chapter on experimental results.

Note that the wireless communication was frozen in several tests as shown in Table 3-1 ~ 3-4. This suggests relatively weak signals from the XBEE to the control unit in fire testing environment. In future work new XBEE models with stronger signals will be used to improve the wireless communication.

Table 3-1: Experimental conditions of fire detection tests with a 0.76 m sprinkler spacing.

Test #	Chemical HRR	Fire location	Test #	Chemical HRR	Fire location
	kW	(-)		kW	(-)
1 <sup>a</sup>	80	Among four	12	160	Under one
2	80	Among four	11	160	Between two
3	160	Among four	13	160	Among Three
4	320	Among four	14	160	Under one
5	80	Among four	15	160	Between two
6	160	Among four	16 <sup>d</sup>	160	Among Three
7	320	Among four	17	160	Under one
8	80	Among four	18	160	Between two
9 <sup>b</sup>	160	Among four	19	160	Among Three
10 <sup>c</sup>	320	Among four	20 <sup>e</sup>	80	Among four
Note: all tests were conducted using a 0.91-m sand burner fueled by propane under a 6.4-m ceiling clearance.			21	320	Among four
			22 <sup>f</sup>	80	Among four
			23 <sup>g</sup>	160	Among Three
<sup>a</sup> Test 1: a trial case where data were not recorded; <sup>b</sup> Test 9: wireless data frozen at 200 s; <sup>c</sup> Test 10: wireless data frozen at 314 s; <sup>d</sup> Test 16: some wireless channels dropped during test; <sup>e</sup> Test 20: wireless data frozen at 337 s; <sup>f</sup> Test 22: wireless data frozen at 307 s; <sup>g</sup> Test 23: repeat of Test 16.					

Table 3-2: Experimental conditions of fire detection tests with a 2.44 m sprinkler spacing.

Test #	Chemical HRR	Fire location	Test #	Chemical HRR	Fire location
	kW	(-)		kW	(-)
24	80	Among four	33	160	Between two
25	160	Among four	34	160	Under one
26	320	Among four	35	160	Between two
27	80	Among four	36	160	Under one
28	160	Among four	37	160	Between two
29	320	Among four	38	160	Under one
30	80	Among four	Note: all tests were conducted using a 0.91-m sand burner fueled by propane under a 6.4-m ceiling clearance.		
31	160	Among four			
32	320	Among four			

Table 3-3: Experimental conditions of sprinkler activation tests with a 2.44 m sprinkler spacing.

Test #	Fire location	Test #	Fire location
39 <sup>a</sup>	Between two	43	Among four
40	Between two	44	Under one
41	Under one	45	Between two
42	Between two	46	Among four

Note: all tests were conducted using a 0.3-m heptane pool fire under a 6.4-m ceiling clearance with predetermined six sprinklers for activation. The fire size is approximately 36 kW.

<sup>a</sup> Test 39: a trial case where no data were recorded.

Table 3-4: Experimental conditions of fire suppression tests with a 2.44 m sprinkler spacing.

Test #	Fuel array	Ignition location	Sprinkler protection	Trigger Condition	Igniter
47	1x2, 1-tier	Among four	K80, Pendent, 1.1 bar	Smoke Alarm	Two half-igniters
48	1x2, 1-tier	Among four	K80, Pendent, 2.4 bar	Smoke Alarm	Two half-igniters
49	1x2, 1-tier	Among four	K80, Pendent, 2.4 bar	Smoke Alarm	Alcohol Pan 15 x 15 cm <sup>2</sup>
50	1x2, 2-tier	Among four	K80, Pendent, 2.4 bar	Smoke Alarm & $\Delta T=10K$	Alcohol Pan 15 x 15 cm <sup>2</sup>
51	2x2, 3-tier	Among four	K80, Pendent, 2.4 bar	Smoke Alarm & $\Delta T=5K$	Alcohol Pan 15 x 15 cm <sup>2</sup>
52 <sup>a</sup>	2x2, 3-tier	Among four	K200, Pendent, 1.7 bar	Smoke Alarm & $\Delta T=5K$	Alcohol Pan 15 x 15 cm <sup>2</sup>
53	2x2, 3-tier	Between Two	K200, Pendent, 1.7 bar	Smoke Alarm & $\Delta T=5K$	Alcohol Pan 15 x 15 cm <sup>2</sup>

<sup>a</sup> A technical error occurred in the first test, resulting in no water supply to the sprinklers; in the second attempt, the wireless data transfer froze after ignition, and had to be restarted after the trigger of the smoke alarm.

## 4. Results and discussions

### 4.1 Characterization of source fires

Prior to each test series, the source fires were characterized using the calorimeters in the SBL. The key quantity for characterizing the fire is the chemical HRR, which was measured using CO-CO<sub>2</sub> generation and O<sub>2</sub> consumption based methods. The results are presented in the next three sections.

#### 4.1.1 Propane fires on a sand burner

The chemical HRRs of the propane fires are plotted in Figure 4-1. Note that the test numbers used as labels in Figure 4-1 refer to the calibration tests only and are not relevant to the fire detection, sprinkler activation and fire suppression tests discussed elsewhere. Each fire size was repeated twice. The three sets of curves show that at steady state the chemical HRRs are 80, 160 and 320 kW, and highly repeatable. There are clearly ramp-up times in Figure 4-1 indicating that the real source fires reach the design HRRs in a finite amount of time, instead of a step function. It appears that the ramp-up time is inversely proportional to the HRR, mainly due to the time difference to fill the sand burner by the design fuel flow rate.

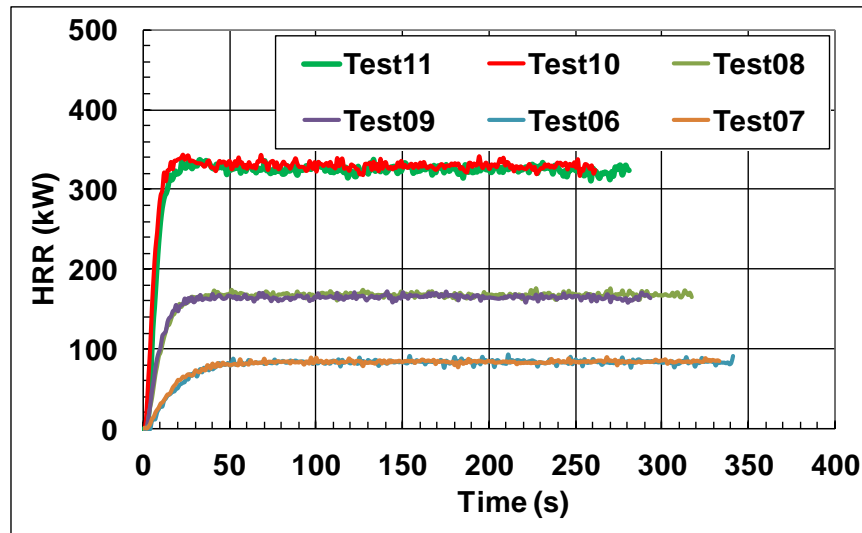


Figure 4-1: Chemical HRRs of 0.91-m dia. propane fires.

#### 4.1.2 Heptane fires on a circular pan

Five calibration tests were conducted to characterize the chemical HRRs of heptane fires. Table 4-1 lists the experimental conditions. Representative results are shown in Figures 4-2 and 4-3, where the HRRs were computed using both CO-CO<sub>2</sub> generation and O<sub>2</sub> consumption based methods. From the HRRs and ceiling temperature estimation, it appears that the 0.91-m (3-ft) dia. pan fire is too large to be used under the SBL movable ceiling, given that the electronic components such as the XBEE and the smoke detectors cannot tolerate more than 38 °C. Therefore, all sprinkler activation tests were conducted using the 0.30-m (1-ft) heptane pan fire, with an average chemical HRR of 36 kW under steady state.

Table 4-1: Heptane pan fire calibration tests.

Test #	Pool fire diameter (m)	Ambient conditions	
		T <sub>amb</sub> (°C)	RH <sub>amb</sub> (%)
1	0.30	73	13
2	0.30	71	24
3	0.30	68	13
4	0.91	73	10
5	0.30	71	7

Note: all tests were conducted under the 1-MW calorimeter with exhaust flow rate of 5.66 m<sup>3</sup>/s. The depth of the heptane fuel in all tests was 2.54 cm.

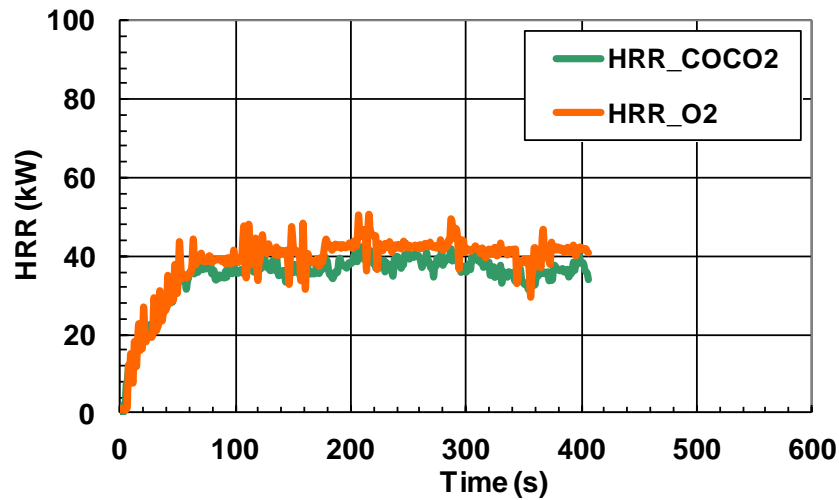


Figure 4-2: Chemical HRR of 0.30-m heptane pan fire (Calibration Test #2).

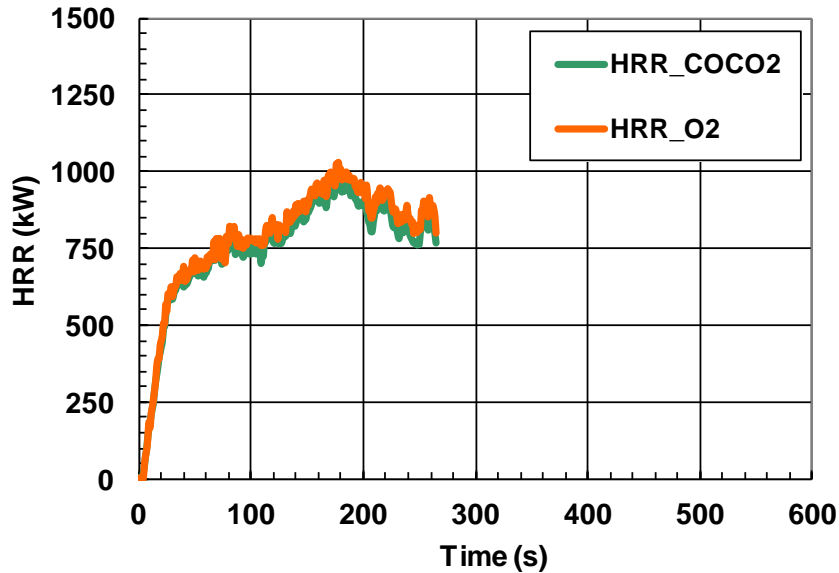


Figure 4-3: Chemical HRR of 0.91-m heptane pan fire (Calibration Test #4).

### 4.1.3 CUP rack-storage fires

The HRRs of CUP fires were not characterized in this work, due to the lack of instrumentation under the SBL movable ceiling. However, numerous tests have been carried out in previous work for CUP in similar fuel geometry [8]. To account for the time difference in the early stage of fire development, these HRR curves were shifted so they aligned at 2 MW. The tests appear to generate repeatable results for HRRs with the moisture content (MC) controlled between 4% and 8%.

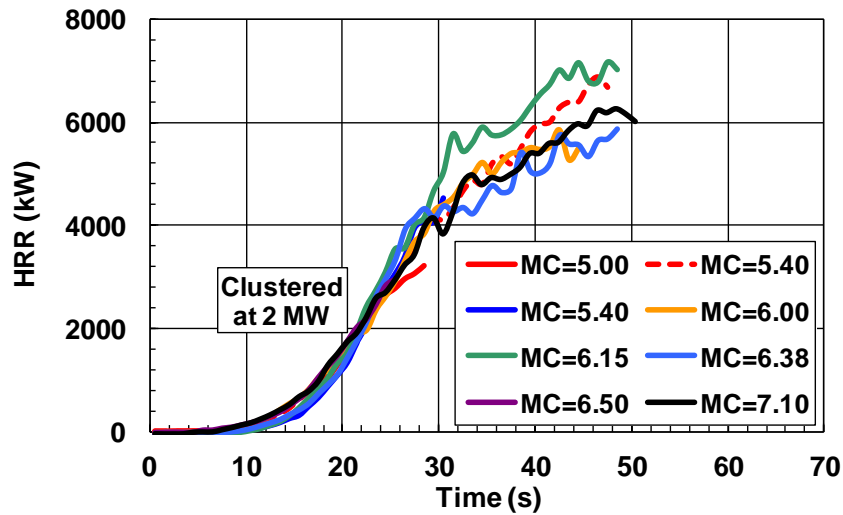


Figure 4-4: Initial fire growth of CUP fires in 2x4, 3-tier rack storage [8].

## 4.2 Fire detection tests with 0.76 m (2.5 ft) spacing

In the fire detection tests, the measured quantities were the ceiling temperatures and the response times from smoke and heat detectors as well as sprinklers. Note that, in the first series of detection tests, sprinklers with sensible elements were installed to compare the response times from different sensors. Under all test conditions investigated in this work, the smoke alarm always responded faster than any other sensors when activation occurred. Therefore, the results of response time discussed in this and the next sections all refer to the smoke detector. In addition, the fire locations were all calculated using the ceiling temperature rise measured by the TC in each SMART sprinkler unit. These two types of results are expected to provide the information on how fast the system can respond to a fire event and how accurately the system can locate the fire.

### 4.2.1 Impact of HRR on smoke detector response time

In the first test conducted (Test 2, HRR = 80 kW), no smoke alarm was triggered within 300 s. The response times ( $t_{act}$ ) of the smoke detectors in Tests 3 - 4 are shown in Figures 4-5 and 4-6, respectively. The response time for each detector is represented by a column while the twelve detectors are listed as a function of radial distance from the ignition location. For the 320 kW fire (Figure 4-6), all smoke alarms responded within less than 10 s. The smoke detector response times for the 160 kW fire (Figures 4-5) were between the other two cases. Clearly the system responds faster as the HRR increases. This can be explained by analyzing the smoke concentrations at the detector locations.

If the smoke yield,  $y_s$ , is assumed to be constant for the given fuel, then the smoke generation rate,  $\dot{m}_{smk}$ , is proportional to the chemical HRR,  $\dot{Q}_{chem}$ ,

$$\dot{m}_{smk} = y_s \dot{m}_f \sim y_s \dot{Q}_{chem} / \Delta h_c \quad 4-1$$

where  $\dot{m}_f$  is the mass burning rate and  $\Delta h_c$  is the heat of combustion. Since the smoke generated by the fuel will be diluted by air entrainment as the plume rises, the smoke concentration can be estimated approximately as

$$C_{smk} \sim \dot{m}_{smk} / (\dot{m}_{ent} + \dot{m}_f) \quad 4-2$$

In Equation 4-2, the air entrainment rate,  $\dot{m}_{ent}$ , is assumed to be much larger than the mass burning rate for typical fuels [13]. Also according to Heskestad [13], the air entrainment rate in a fire plume is determined by the convective HRR,  $\dot{Q}_{conv}$ , and downstream distance,  $z$ , from the fire virtual origin,  $z_0$ ,

$$\dot{m}_{ent} \sim \dot{Q}_{conv}^{1/3} (z - z_0)^{5/3} = [\dot{Q}_{chem} (1 - X_R)]^{1/3} (z - z_0)^{5/3} \quad 4-3$$

If we also assume that the radiation loss fraction,  $X_R$ , from the fire is constant, then the estimated smoke concentration can be expressed as

$$C_{smk} \sim \dot{m}_{smk} / \dot{m}_{ent} \sim \dot{Q}_{chem}^{2/3} / (z - z_0)^{5/3} \quad 4-4$$

From Equation 4-4, the smoke concentration increases with the HRR, since the virtual origin,  $z_0$ , is only a weak function of  $\dot{Q}_{chem}$ . This analysis explains the change in smoke detector response times in Figures 4-5 and 4-6 and in Test 2 where no smoke detectors responded in 300 s with HRR = 80 kW.

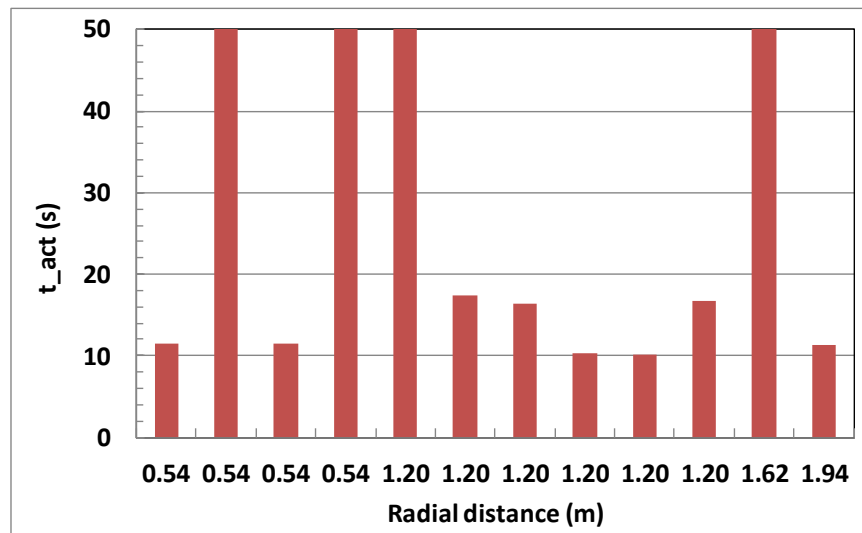


Figure 4-5: Response times of smoke detectors in Test 3 (HRR = 160kW, ignition among 4 sprinklers).

Note that there are large variations in smoke detector response times in Test 3 (HRR = 160 kW, Figure 4-5) compared to those in Test 4 (HRR = 320 kW, Figure 4-6), which may be attributed to the differences

of the smoke concentrations at the ceiling. With a relatively low HRR in Test 3, the smoke concentrations at some detector locations may be close to the detection threshold, which can result in very long response time. In Test 4, in contrast, the smoke concentrations at the ceiling can well exceed the detection threshold due to the relatively large HRR. As a result, the difference among detector response times becomes very small, with all detectors being triggered almost at the same time. In addition, each detector has its own response characteristics including the threshold value and the response time constant. The variations in response time among different smoke detectors also reflect the differences of the detector characteristics.

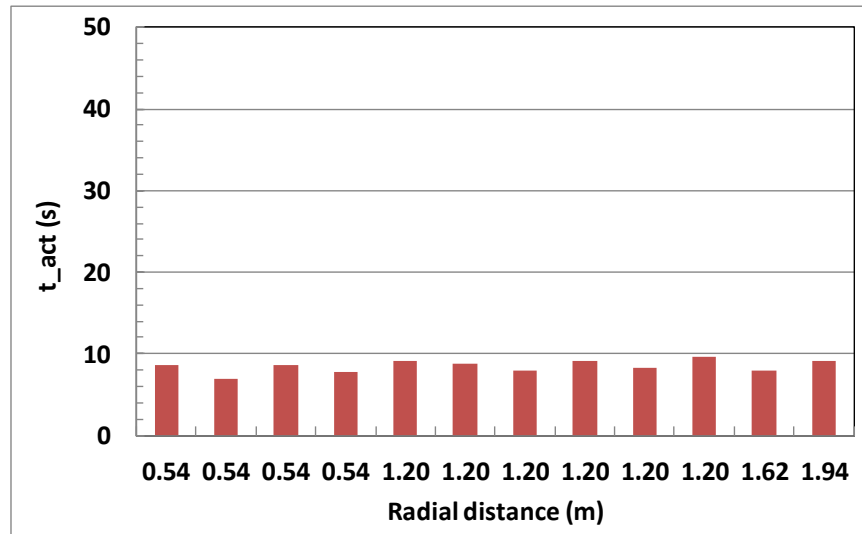


Figure 4-6: Response times of smoke detectors in Test 4 (HRR = 320kW, ignition among 4 sprinklers).

#### 4.2.2 Impact of HRR on fire location calculation

The normalized thermal centroid deviations are plotted in Figures 4-7, 4-8 and 4-9 with three different HRRs. As defined in Chapter 2, the normalized thermal centroid deviation stands for the distance between the calculated thermal centroid location and the ignition location in plan view. In each figure there are three curves representing repeated tests under the same HRR. In Figures 4-8 and 4-9, each curve is marked with a symbol denoting the response time of the first triggered smoke detector. The curves in Figure 4-7 are not marked since there was no detector response in 300 s after ignition. All the results in Figures 4-7, 4-8 and 4-9 were collected with ignition location among four sprinklers.

It can be seen from these figures that the normalized thermal centroid deviation generally decreases shortly after ignition and then reaches steady state. This reflects the transient HRR variations as shown in Figure 4-1. From Figures 4-8 and 4-9, the thermal centroid deviations can be 0.3 – 0.8 times the sprinkler spacing when the first smoke detector respond (as marked with symbols). Note that the relative large thermal centroid deviations upon first detector response all appear in Figure 4-9 before the fire reaches steady state. This suggests that the use of smoke alarm alone for fire event assessment may result in higher uncertainty in fire location calculation, since the thermal field at the ceiling has not been well established. Further examination of this point and the use of multi-sensor detection will be discussed later in connection with the fire suppression tests.

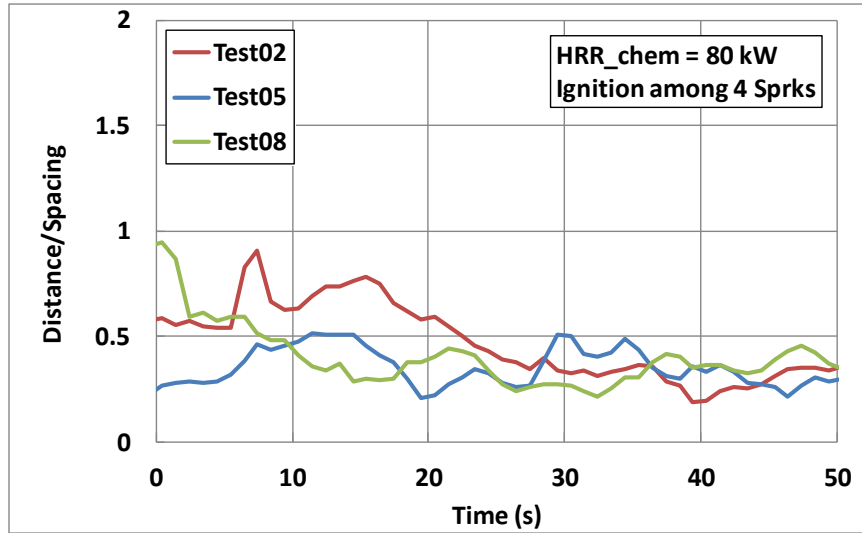


Figure 4-7: Normalized thermal centroid deviations with HRR = 80 kW.

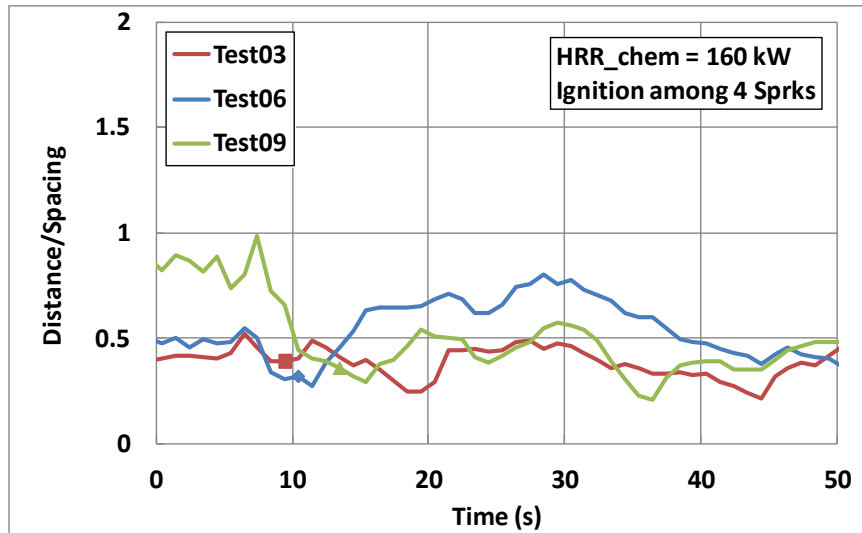


Figure 4-8: Normalized thermal centroid deviations with HRR = 160 kW.

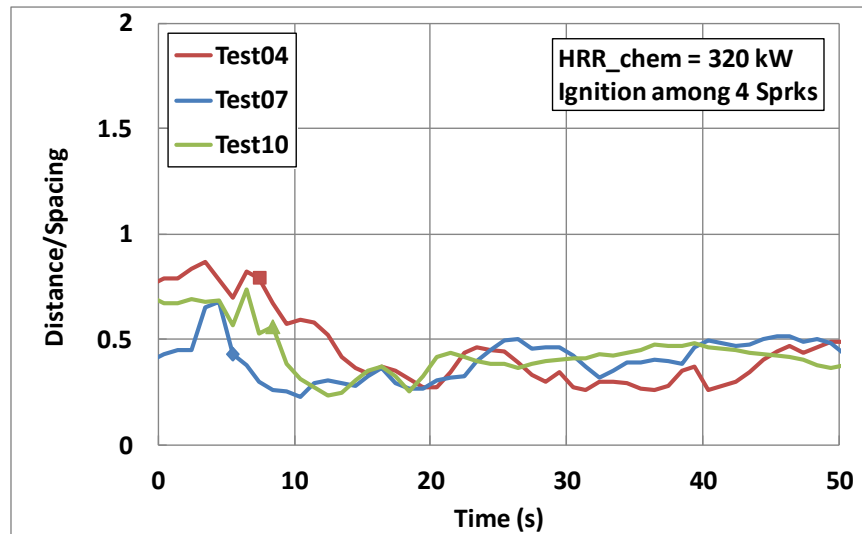


Figure 4-9: Normalized thermal centroid deviations with HRR = 320 kW.

### 4.2.3 Impact of ignition location

The effect of ignition location is examined using test cases with the same chemical HRR of 160 kW. Figure 4-10 shows the results in terms of thermal centroid deviations normalized by the 0.76 m (2.5 ft) spacing. The four panels in Figure 4-10 represent the four ignition locations as labeled in Figure 3-3. In each panel, there are three curves showing repeated tests under the same experimental conditions. The response time of the first triggered smoke detector is marked with a symbol in each curve.

Comparison of the repeated tests suggests that there are significant uncertainties in the calculated fire locations from the actual locations. On average, the cases with ignition under one sprinkler appear to provide better accuracy for fire location than other ignition locations, with the distance between the calculated and actual fire location less than 0.25 times of the sprinkler spacing. All other ignition scenarios show that the calculated fire location can be within 0.5 times the sprinkler spacing. The overall results suggest that there is probably no need to activate an extra ring of sprinklers in addition to those selected on the basis of fire propagation considerations.

Also note that the response times of the smoke detectors, as marked by symbols in Figure 4-10, exhibited significant variations among repeated tests. Therefore, the impact of ignition location cannot be identified from the comparison of the data in these detection tests with 0.76 m (2.5 ft) sprinkler spacing.

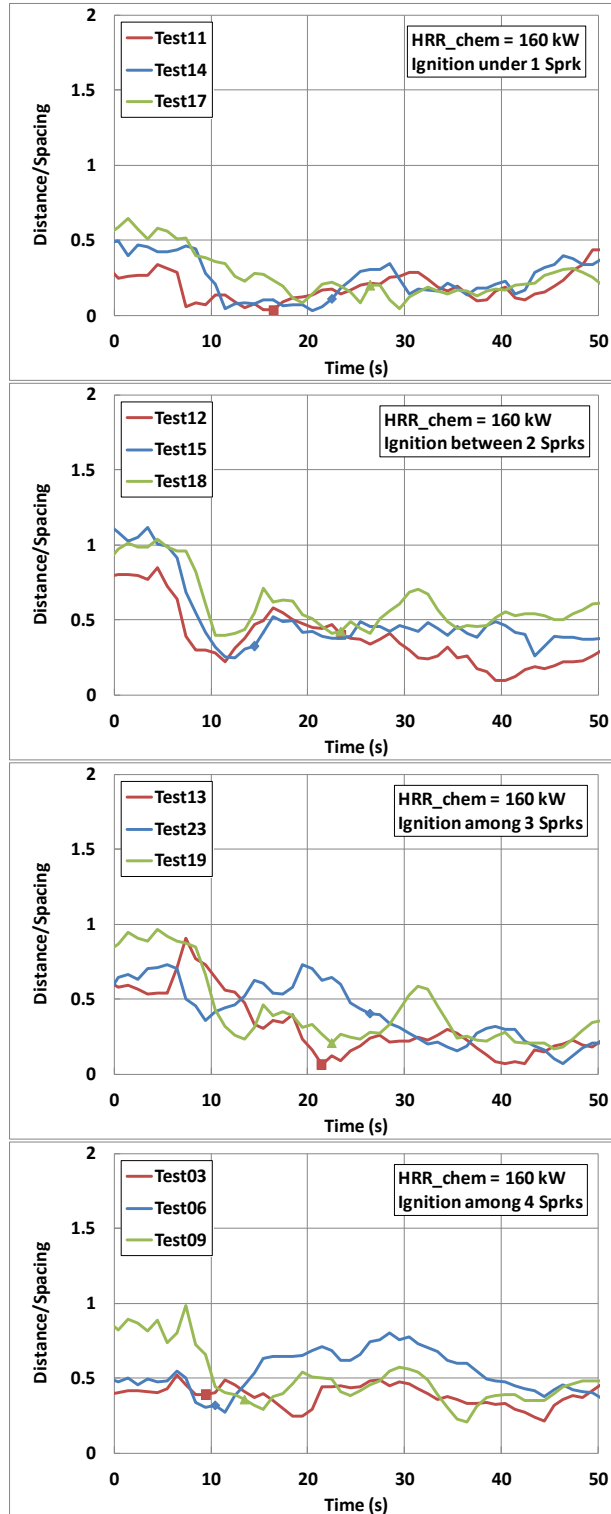


Figure 4-10: Normalized thermal centroid deviations with different ignition locations.

### 4.3 Fire detection tests with 2.44 m (8 ft) spacing

#### 4.3.1 Impact of HRR on smoke detector response time

Tests 24-26 are the first three fire detection tests conducted with a 2.44 m (8 ft) sprinkler spacing. Among these tests, only the HRR was changed while all other experimental conditions were kept identical (Table 3-1). Figures 4-11 - 4-15 show the measured smoke detector response times ( $t_{act}$ ) and corresponding temperature rises at the ceiling ( $\Delta T_{act}$ ) for Tests 24-26. In Test 24, no alarm was triggered in 300 seconds after ignition; therefore, only the temperature rise at 300 s is shown in Figure 4-11. Similar to previous tests with 0.76 m (2.5 ft) spacing, the smoke detector response time decreases with increasing fire size, due to shorter convective transport times and higher smoke concentrations at detection locations.

In Figures 4-11, 4-13 and 4-15, it is observed that the magnitude of the temperature rise is similar in the range of 15-20 K upon the first smoke alarm triggering, although the smoke detector response time for the larger fire is much shorter. It also appears that the temperature rise for sensors near the ignition location, for example, at 1.72 m (5.64 ft), is higher than those further away, which provides the basis to approximate the fire location using the thermal centroid based method. Also note that the temperature rise in Figure 4-11 appears to decrease more consistently with increasing radial distance than those in Figures 4-13 and 4-15. This is largely due to the fact that the ceiling layer was better established in 300 s after ignition as shown in Figure 4-11, compared to the other two tests shown in Figures 4-13 and 4-15.

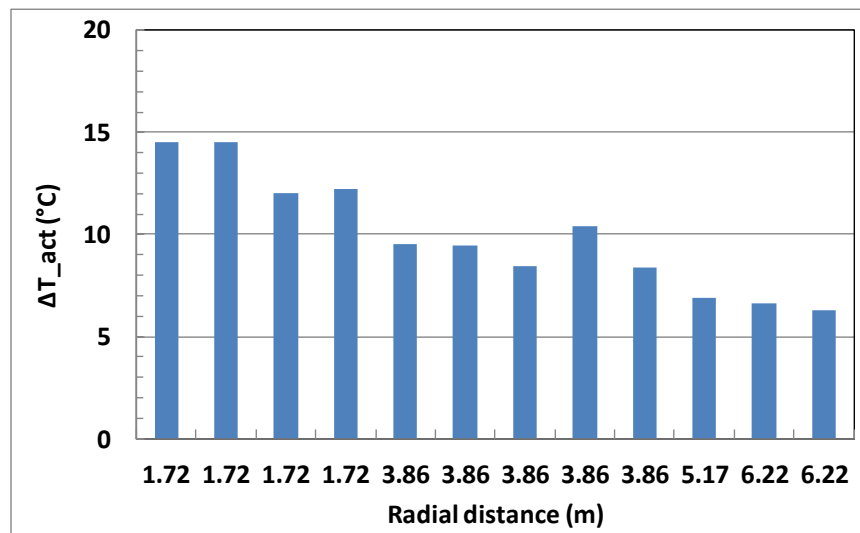


Figure 4-11: Temperature rise at the ceiling in Test 24 at 300 s – no smoke detector activation (HRR = 80kW, ignition among 4 sprinklers).

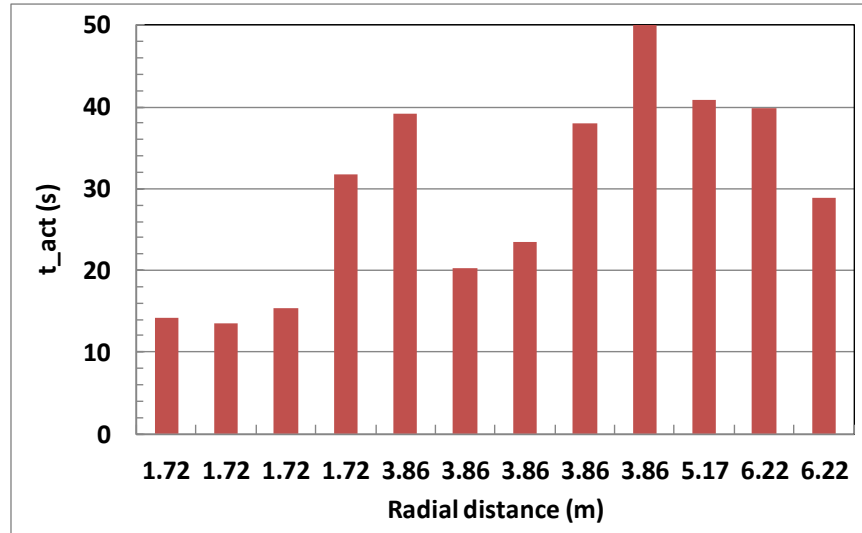


Figure 4-12: Smoke detector response times in Test 25 (HRR = 160kW, ignition among 4 sprinklers).

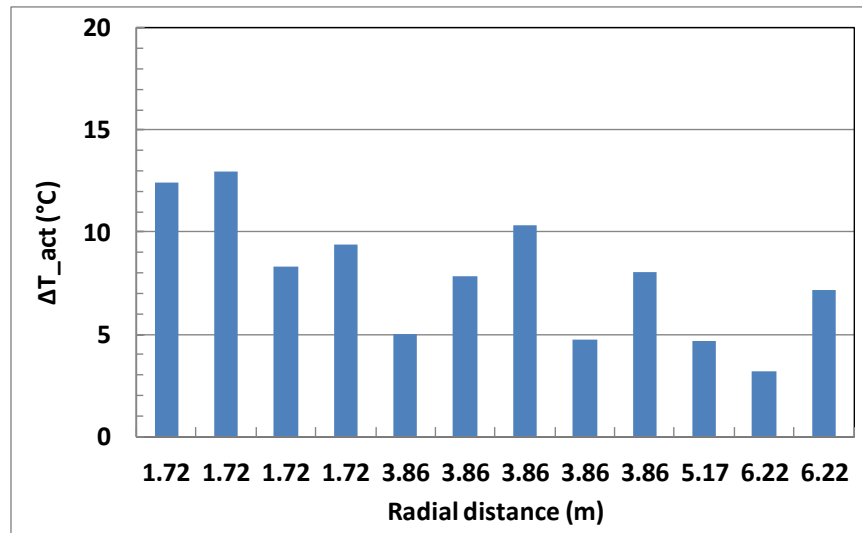


Figure 4-13: Temperature rise in Test 25 at the time of first smoke detector activation (HRR = 160kW, ignition among 4 sprinklers).

#### 4.3.2 Impact of HRR on thermal centroid calculation

As discussed in Chapter 3, the thermal centroid locations (X-Y coordinates) can be calculated based on different methods and TC data sets. Figure 4-16 shows the thermal centroid deviations combining different methods and data sets. The curve labeled “WiredAll” is the calculated result using TC data from all sprinkler locations obtained by the wired data acquisition system; the curve labeled “Wired1.5S” is calculated using wired TC data only within 1.5 times of sprinkler spacing from the maximum temperature location; the curve labeled “Wireless1.5S” is similar to the “Wired1.5S” curve except for the use of wireless TC data; and the curve labeled “TruCalcAll” is the result using all wired TC data in an internal code TarResponse Utility based on fire plume correlations.

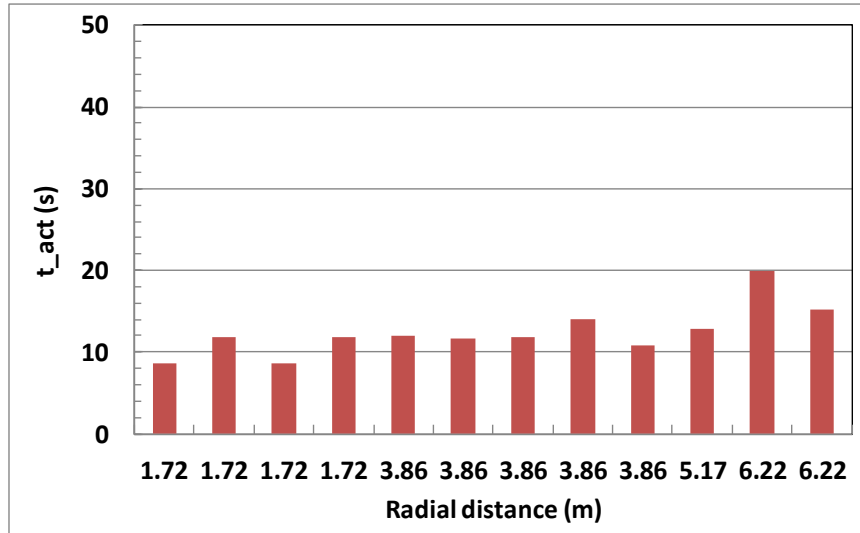


Figure 4-14: Smoke detector response times in Test 26 (HRR = 320kW, ignition among 4 sprinklers).

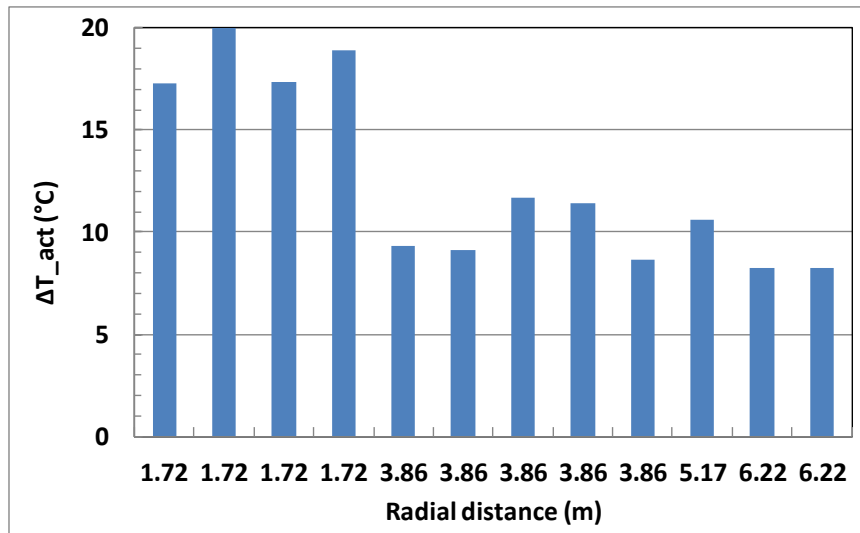


Figure 4-15: Temperature rise in Test 26 at the time of first smoke detector activation (HRR = 320kW, ignition among 4 sprinklers).

The comparison in Figure 4-16 shows that the differences among the calculated results are not significant, especially when compared to the fluctuations of each data series under steady state. Note that the normalized thermal centroid deviations using all wired TC data appear to be slightly better than other results using only data within 1.5 times of the sprinkler spacing. Therefore, subsequent comparisons of HRR and ignition impacts are based on the calculations using all wired TC data.

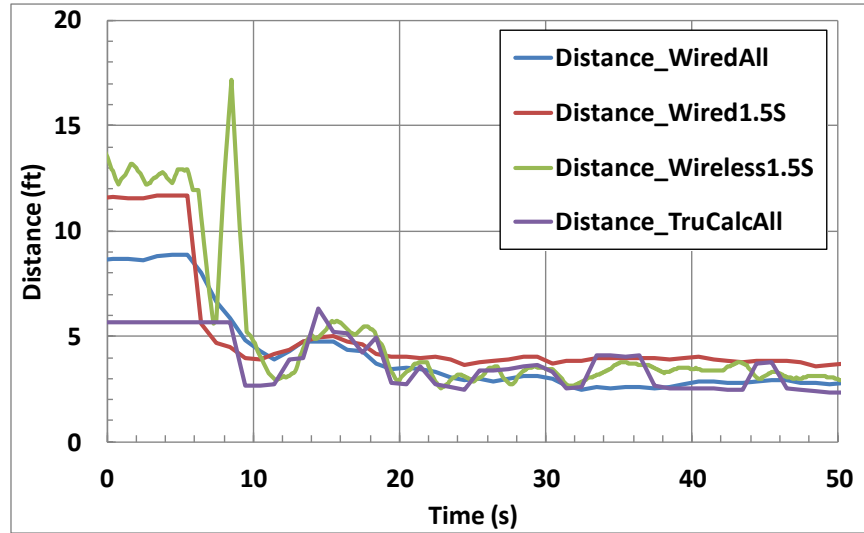


Figure 4-16: Normalized thermal centroid deviations calculated using different data sets in Test 24.

Figures 4-17, 4-18 and 4-19 show the normalized thermal centroid deviations under different HRRs. As defined in Chapter 2, the normalized thermal centroid deviation is the distance from the calculated thermal centroid to the ignition location normalized by the sprinkler spacing. In each figure, there are three curves representing three repeated tests under the same experimental conditions. Also in Figure 4-18 and 4-19, the first alarm response time for each test is denoted by a symbol on the curve. There is no response time symbols in Figure 4-17 because there was no alarm triggered in 300 s in these cases with HRR = 80 kW. From the marked symbols in Figures 4-18 and 4-19, it can be seen that the smoke detector response times become shorter with increasing HRRs from 160 kW to 320 kW. The reason for this trend is the same as analyzed in the Section 4.2.1: the local smoke concentration increases and the convective transport time decreases as the HRR becomes larger. The results also suggest that for the same fire size and fire spread rate, sootier flames may trigger the SMART sprinkler system faster.

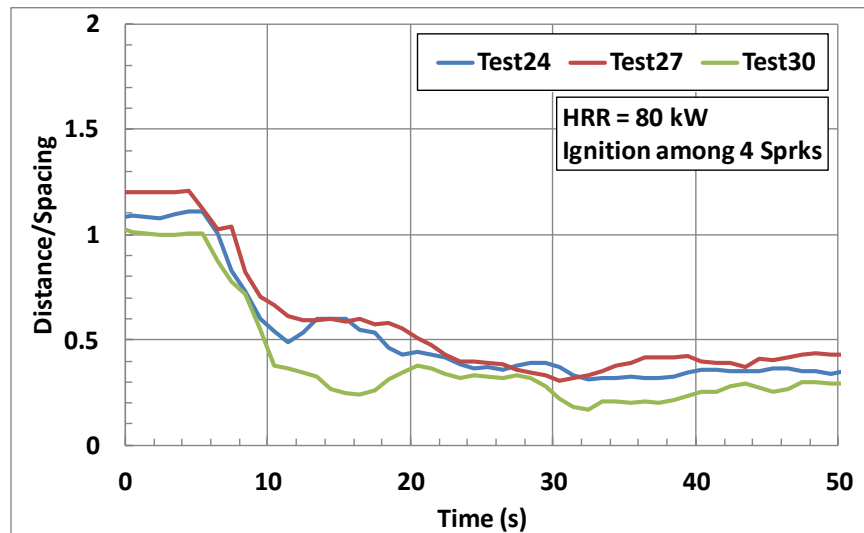


Figure 4-17: Normalized thermal centroid deviations with 2.44 m spacing and HRR = 80 kW.

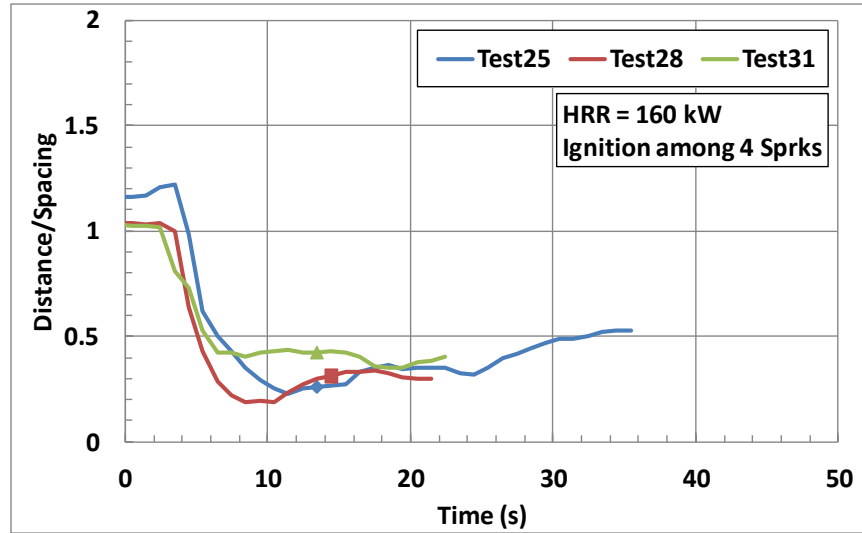


Figure 4-18: Normalized thermal centroid deviations with 2.44 m spacing and HRR = 160 kW.

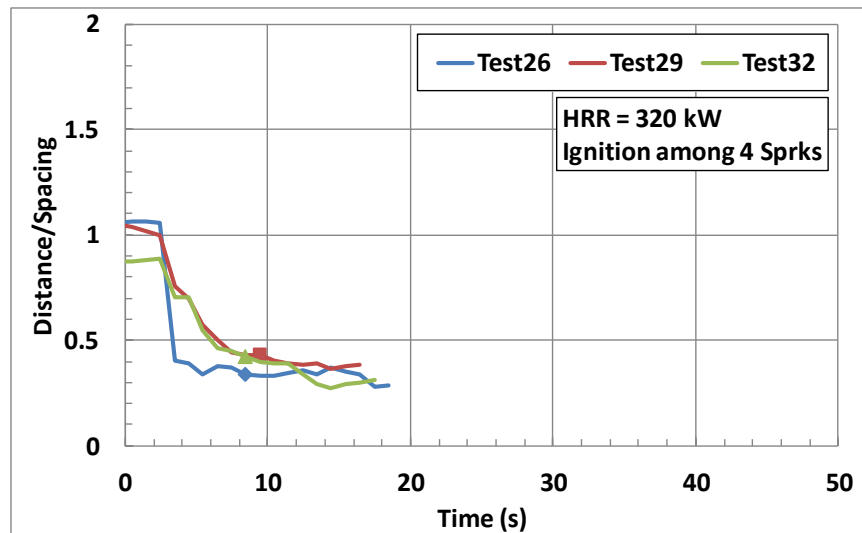


Figure 4-19: Normalized thermal centroid deviations with 2.44 m spacing and HRR = 320 kW.

In contrast to the clear impact on smoke detector response time, the HRR does not appear to affect the accuracy of the thermal centroid calculations significantly. After ignition, all thermal centroid deviations move toward the ignition location, resulting in the decrease of the distance/spacing ratio in Figures 4-17, 4-18 and 4-19. Upon the triggering of the smoke alarm (cf. Figures 4-18 and 4-19), the thermal centroid deviations are within 30-40% of the sprinkler spacing. Note that these results are lower than those in Figures 4-8 and 4-9, and thus also provide reassurance that no extra sprinklers need to be activated in addition to those selected on the basis of fire propagation considerations.

### 4.3.3 Impact of ignition locations

Figures 4-20, 4-21 and 4-22 show the variation of the normalized thermal centroid deviations with time under different ignition locations. In all these figures, the chemical HRR is 160 kW; in each figure, there are three curves representing three repeated tests under the same experimental conditions; and in each

curve, the first smoke alarm response time is denoted by a symbol. It can be seen that the smoke detector response times among different ignition locations range from 12 to 22 seconds, while the uncertainties associated with the response time for repeated tests under the same experimental conditions range from 2 to 7 seconds. Therefore, the ignition location does not appear to have a significant impact on the system response time, given the current ceiling clearance of 6.4 m (21 ft) and the HRR of 160 kW.

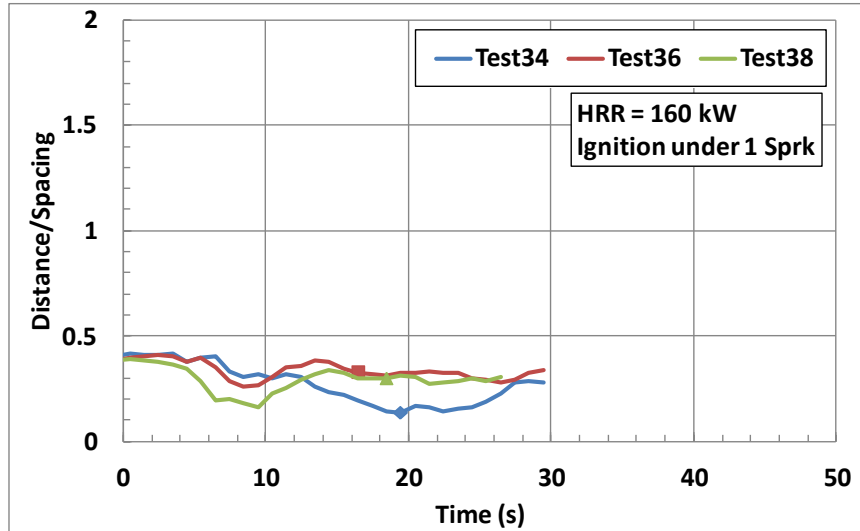


Figure 4-20: Normalized thermal centroid deviations with 2.44 m spacing and under-one ignition.

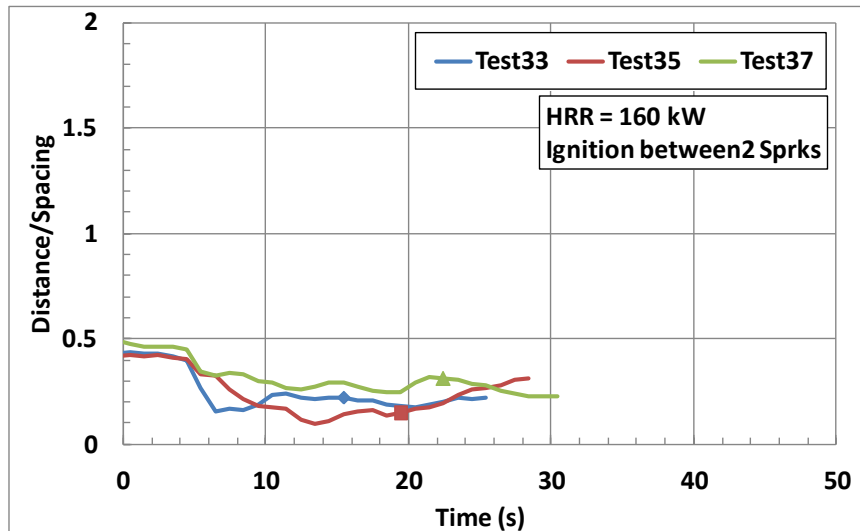


Figure 4-21: Normalized thermal centroid deviations with 2.44 m spacing and between-two ignition.

The thermal centroid deviations for all tests are consistently below 0.5 times the sprinkler spacing (2.44 m or 8 ft), less than those with smaller spacing (0.76 m or 2.5 ft) discussed in the previous section (see Figures 4-7, 4-8 and 4-9). This again shows that, under these experimental conditions, no extra ring of

sprinklers needs to be activated, in addition to those selected on the basis of fire propagation considerations.

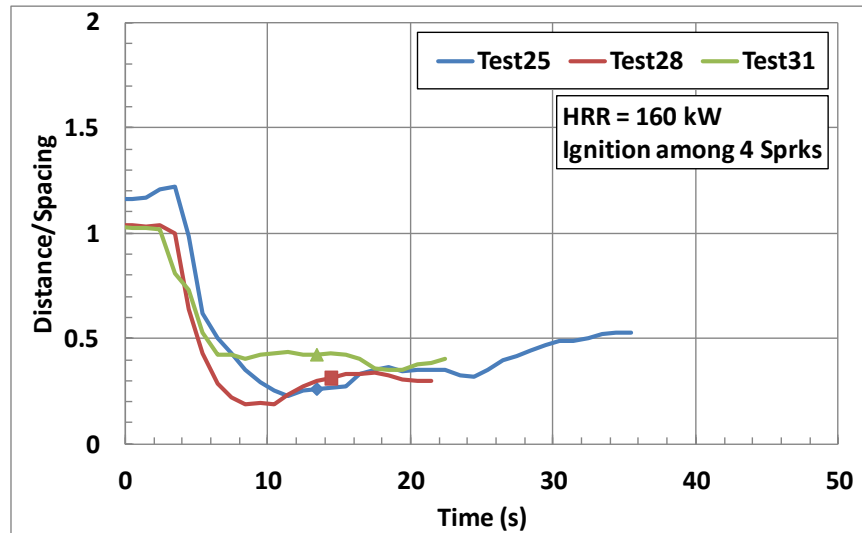


Figure 4-22: Normalized thermal centroid deviations with 2.44 m spacing and among-four ignition.

#### 4.4 Sprinkler activation tests

All sprinkler activation tests were carried out with a 2.44 m (8 ft) sprinkler spacing. Table 4-2 summarizes the test results, including the first sprinkler activation time ( $t_{act}$ ), the temperature rise at the first activated sprinkler ( $\Delta T_{act}$ ), the number of sprinkler activated and the normalized thermal centroid deviation (Distance/Spacing). As discussed in Chapter 3, the sprinkler activation condition for all these tests was the first triggering of a smoke alarm, which caused the activation of the nearest six sprinklers from the calculated thermal centroid location. Under a 6.4 m (21 ft) ceiling clearance, the sprinkler response times to the 36 kW pan fire varied from 17.4 s to 23.2 s. The temperature rises near the detectors upon sprinkler activation were all below 5 K. The calculated thermal centroid deviation varied between 0.03 and 0.77 times the sprinkler spacing. In all tests, the six sprinklers close to the calculated centroid were activated simultaneously by the central control unit.

Figures 4-23, 4-24 and 4-25 show snapshots of the control unit screen displaying the activation pattern. In these figures, each square is labeled with a node ID representing a SMART sprinkler location. The node ID was used by the control unit to communicate with each individual sprinkler. The two-decimal value in the middle of each sprinkler node is the measured temperature ( $^{\circ}\text{C}$ ) by the ceiling TCs. When a smoke alarm is triggered, the label "SMOKE!" is shown beneath the TC data in that sprinkler location. When a sprinkler is activated, the corresponding sprinkler location (square) is colored in blue. A white-dotted circle is also used in the figures to represent the calculated thermal centroid location. For example, in Test 41 (left panel of Figure 4-23), the calculated thermal centroid was between Sprinkler Nodes 0a54 and 0730, where the temperature was 21.03  $^{\circ}\text{C}$  and six sprinklers (blue squares) were activated around the thermal centroid location. Note that in each screen snapshot the sprinkler pattern varies due to the specified activation algorithm, *i.e.*, the nearest six sprinklers from the thermal centroid location.



Figure 4-23: Sprinkler activation with under 1 ignition in Test 41 (L) and 44 (R).



Figure 4-24: Sprinkler activation with between 2 ignition in Test 42 (L) and 45 (R).

Figures 4-23, 4-24 and 4-25, together with Table 4-2, show that the designed sprinkler activation algorithm worked well. Furthermore, the system is capable of responding to very small fires, *i.e.*, 36 kW heptane pan fire, by the use of a smoke detector. However, the variation of calculated fire locations appears to be quite large compared to those using propane fires of 160 kW and 320 kW (see Section

4.3). Based on test observations, the fire plume established on a relatively small pan fire (0.3 m diameter) resulted in significant fluctuations around the ignition location, which contributed to the uncertainties in the calculated thermal centroid deviations, *e.g.*, the distance/spacing ratio can be as large as 0.77 as shown in Table 4-2. Potential improvement on this problem could involve the use of a higher detection threshold to create a stronger thermal plume before activating the sprinklers. This possibility will be examined in the suppression tests discussed in Section 4.5.



Figure 4-25: Sprinkler activation with under 4 ignition in Test 43 (L) and 46 (R).

Table 4-2: Summary of sprinkler activation tests

Test #	Fire location	t <sub>act</sub> (s)	ΔT <sub>act</sub> (K)	No. Sprinkler Activated	Distance/Spacing
41	Under one	19.38	1.64	6	0.50
44	Under one	19.80	1.25	6	0.03
42	Between two	17.41	2.63	6	0.24
45	Between two	23.20	0.29	6	0.31
43	Among four	18.37	4.80	6	0.77
46	Among four	21.68	3.26	6	0.66

## 4.5 Preliminary suppression tests

Similar to the sprinkler activation tests, all fire suppression tests were carried out under the movable ceiling in the SBL with a 6.4 m (21 ft) ceiling clearance and a 2.44 m (8 ft) sprinkler spacing. Due to the limited space and ventilation rate in the testing site, the tests were conducted systematically with an increasing level of fire hazard. That is, the test series started with CUP commodities in a 2x2, 1-tier rack

storage configuration, and then gradually increased to 2-tier and 3-tier rack storage configurations. The applied sprinkler design densities were also adjusted accordingly.

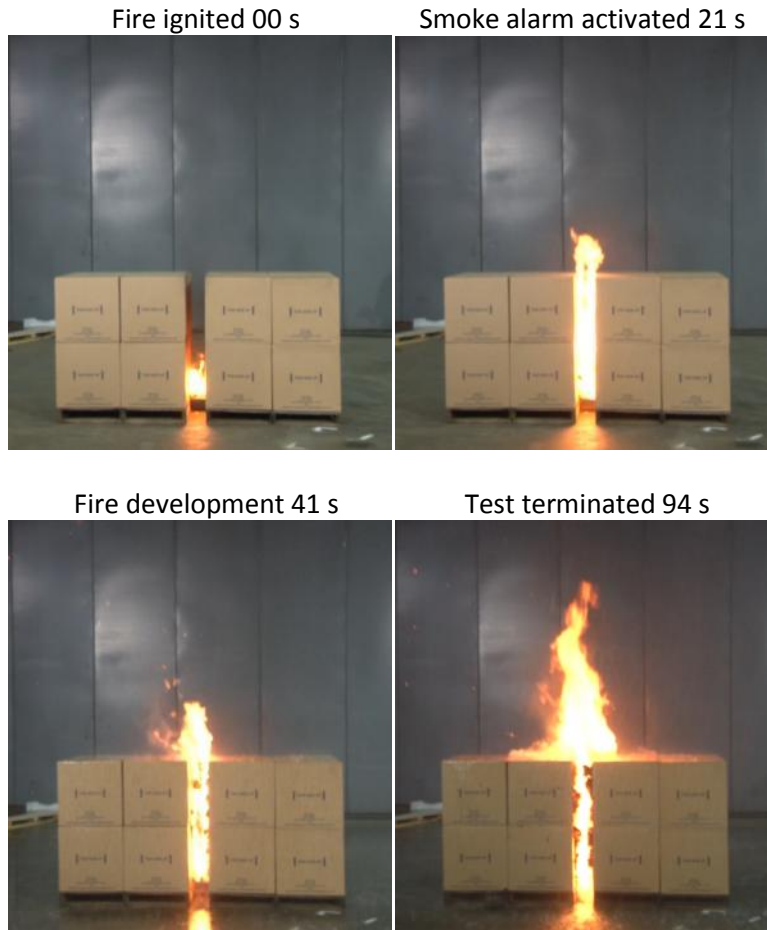


Figure 4-26: Fire development in Test 47 (K80 sprinkler, 4.9 mm/min).

#### 4.5.1 Fire development in 2x2, 1-tier rack storage

In the first suppression test (Test 47), the fire started with ignition at the center of the fuel array. Ignition was achieved using four half-standard igniters placed on the floor against the corner of each pallet load. A smoke alarm was triggered at 21 s after ignition (see upper right panel in Figure 4-26), which was the only criterion used for sprinkler activation. At this time, the estimated chemical HRR was approximately 30 kW based on the flame volume with a constant conversion factor of 1100 kW/m<sup>3</sup> [14]. Six sprinklers were activated simultaneously, as shown in Figure 4-27 where the white-dotted circle stands for the calculated fire location, the blue colored square represents the activated sprinkler and the label “SMOKE!” denotes a triggered smoke alarm. Figure 4-28 shows the water operating pressure and total flow rate discharged from the sprinkler system. As indicated in Figure 4-28, the water flow rate was not stabilized until 54 s after sprinkler activation or 75 s after ignition. The estimated sprinkler water application density, therefore, increased gradually from 3.4 mm/min (0.08 gpm/ft<sup>2</sup>) to 4.9 mm/min (0.12

gpm/ft<sup>2</sup>). Upon test termination at 94 s after ignition, the fire was still growing due to an inadequate water flux applied to the commodity.

		(South Up)		
	Node: 08e5 16.90	Node: 0a4c 20.52 SMOKE!	Node: 0a48 22.58 SMOKE!	
Node: 0a66 16.39	Node: 0741 18.45	Node: 0a54 21.68 SMOKE!	Node: 0934 22.06 SMOKE!	Node: 0a4a 18.19
	Node: 0a27 18.71	Node: 0730 20.00	Node: 0a50 20.65 SMOKE!	
		Node: 6180 17.03		

Figure 4-27: Sprinkler activation with under 4 ignition in Test 47.

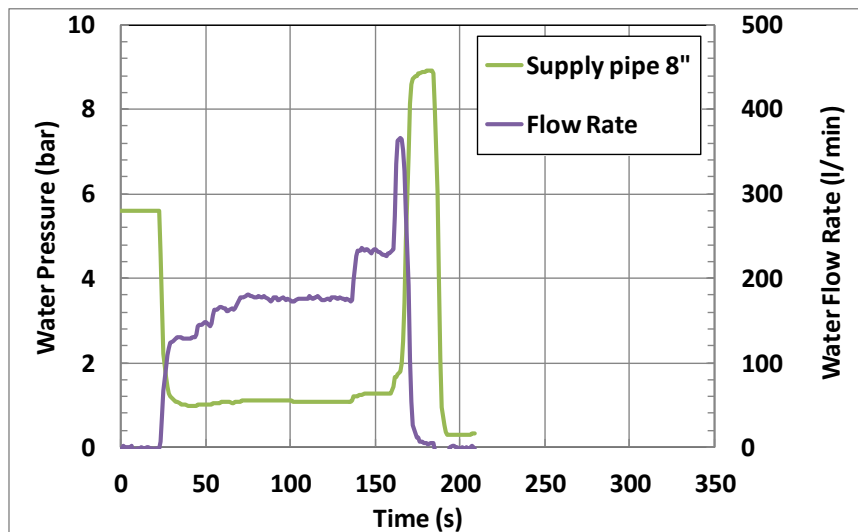


Figure 4-28: Water pressure and flow rate in Test 47 (K80 sprinkler, 15.3 mm/min).

In the second test (Test 48), the sprinkler design density was increased to 15.3 mm/min (0.38 gpm/ft<sup>2</sup>). As shown in Figure 4-29, the smoke alarm was triggered 16 seconds after ignition and six sprinklers were activated at the same time. Note that upon sprinkler activation the fire was only attributed to the igniters without propagating further along the fuel surfaces. Under the increased water density, the fire never grew beyond the ignition location. The test was terminated at 215 s after ignition. Due to the significant difference in the first two tests, the third test was conducted with a modified ignition fire.

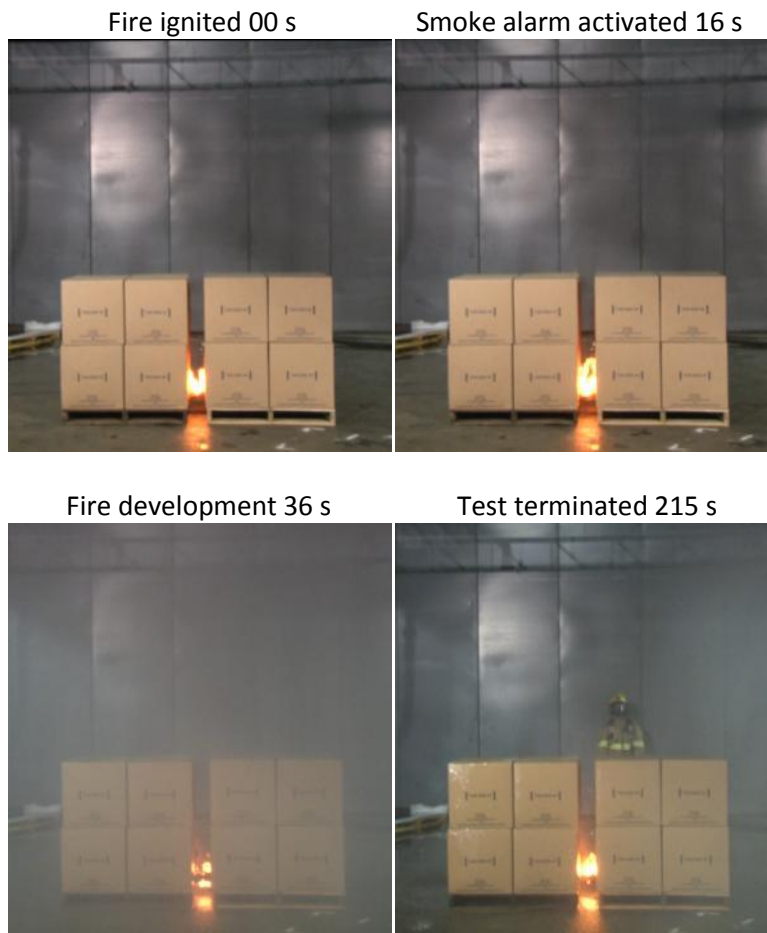


Figure 4-29: Fire development in Test 48 (K80 sprinkler, 15.3 mm/min).

In Test 49, a 15-cm (6-in.) square pan was placed at the center of the flue space in the test array (2x2, 1-tier). A layer of alcohol (2.54 cm thick) was used as fuel in the pan fire, aimed at avoiding sprinkler activation merely due to smoke produced by the standard igniters. As shown in Figure 4-30, the smoke alarm was triggered at 93 s after ignition, when the estimated fire size was about 20 kW. Note that the prolonged incipient period of fire growth is largely due to the intermittent contact of the pan fire with the commodity surface. Shortly after sprinkler activation, the fire was extinguished under a water density of 15.3 mm/min (0.38 gpm/ft<sup>2</sup>).

#### 4.5.2 Development of CUP fires in 2x2, 2-tier rack storage

In Test 50, the fuel array was increased to 2-tiers high. In addition, the sprinkler activation criteria were changed to include both a smoke alarm and a fixed temperature rise of 10 K above the ambient value in the lab. The added  $\Delta T$  criterion was aimed at allowing fire development beyond the vicinity of the igniters, and also aimed at improving the accuracy of the fire location calculation with an increased fire size. The applied water density was maintained at 15.3 mm/min (0.38 gpm/ft<sup>2</sup>). Figure 4-31 shows the fire development at different times after ignition. The fire size upon sprinkler activation increased to approximately 50 kW using the flame volume based estimation (upper right panel of Figure 4-31). The test was terminated at 165 s after ignition due to excessive smoke in the test site.

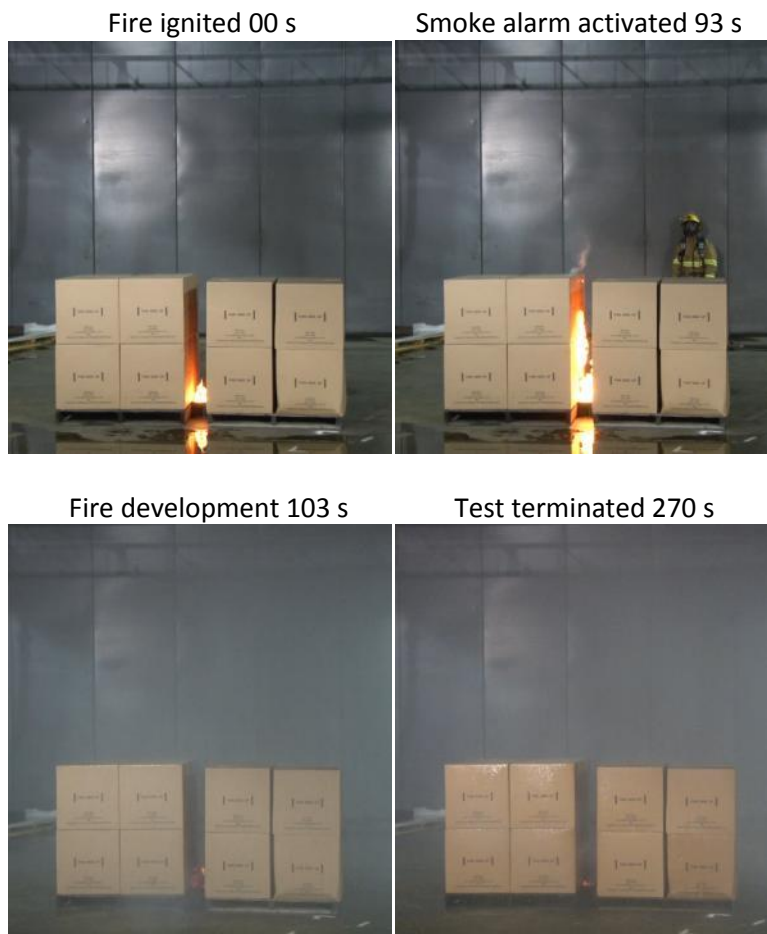


Figure 4-30: Fire development in Test 49 (K80 sprinkler, 15.3 mm/min).

Upon test termination, the fire appeared to be contained in the central flues of the fuel array as shown in the lower right panel in Figure 4-31. Considering that the fire was contained instead of suppressed, and the smoke generation was excessive, the temperature rise in the sprinkler activation condition was relaxed to 5 K in subsequent tests. Note that, in practice, the rate of rise of temperature can also be considered to replace the fixed temperature rise used in this work.

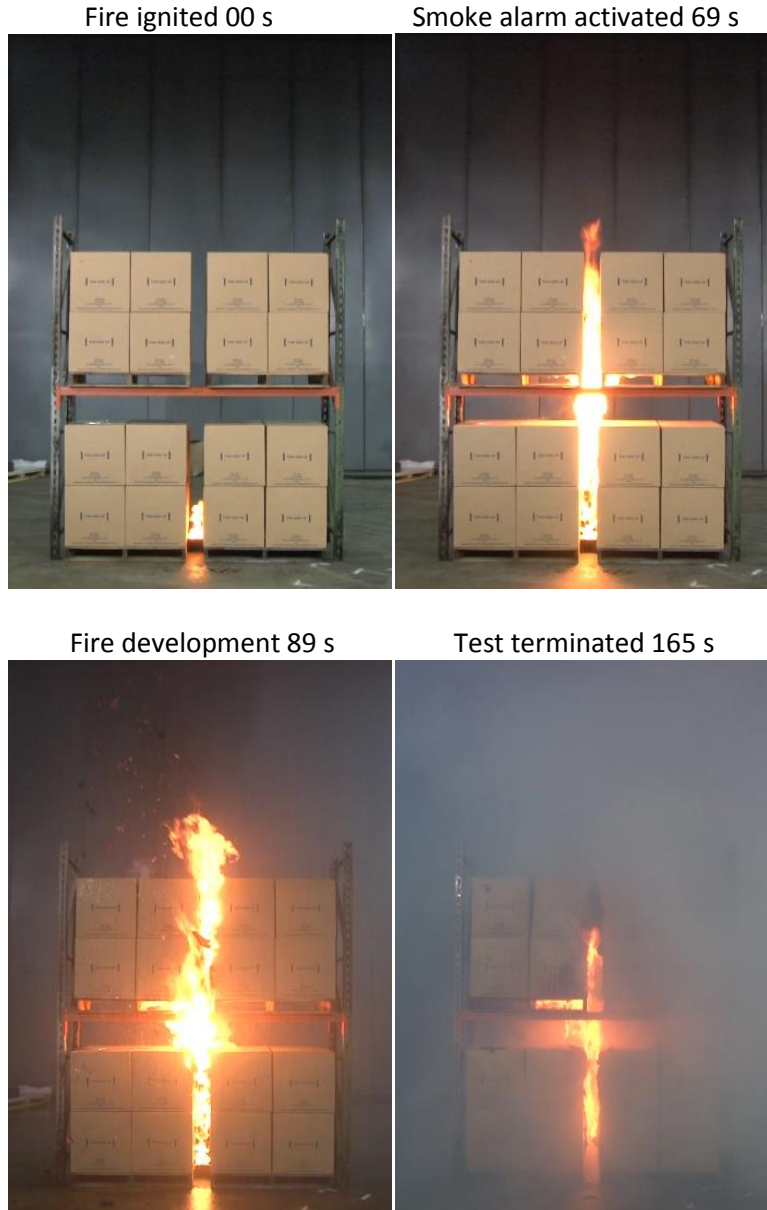


Figure 4-31: Fire development in Test 50 (K80 sprinkler, 15.3 mm/min).

#### 4.5.3 Development of CUP fires in 2x2, 3-tier rack storage

Based on the first four test results, the storage height was increased to 3-tiers in Tests 51-53. In Test 51, the sprinkler activation criteria were adjusted to include both a smoke alarm and a 5 K temperature rise above the ambient value. The adjustment of the  $\Delta T$  threshold from 10 K to 5 K was mainly due to observations in Test 50, where the fire was controlled, but not quite suppressed. Figure 4-32 shows the fire development in Test 51. The fire size upon sprinkler activation was about the same as those in the 1-tier tests,  $\sim 20$  kW. However, the fire size quickly increased to about 60 kW in 20 s after water application, suggesting continuous fire growth without control. Such continuous fire growth after water application was likely caused by the increased water transport time with higher storage, resulting in

delay of pre-wetting commodities adjacent to the burning zone. The fire test was terminated at 133 s after ignition because of excessive temperatures measured on the ceiling.

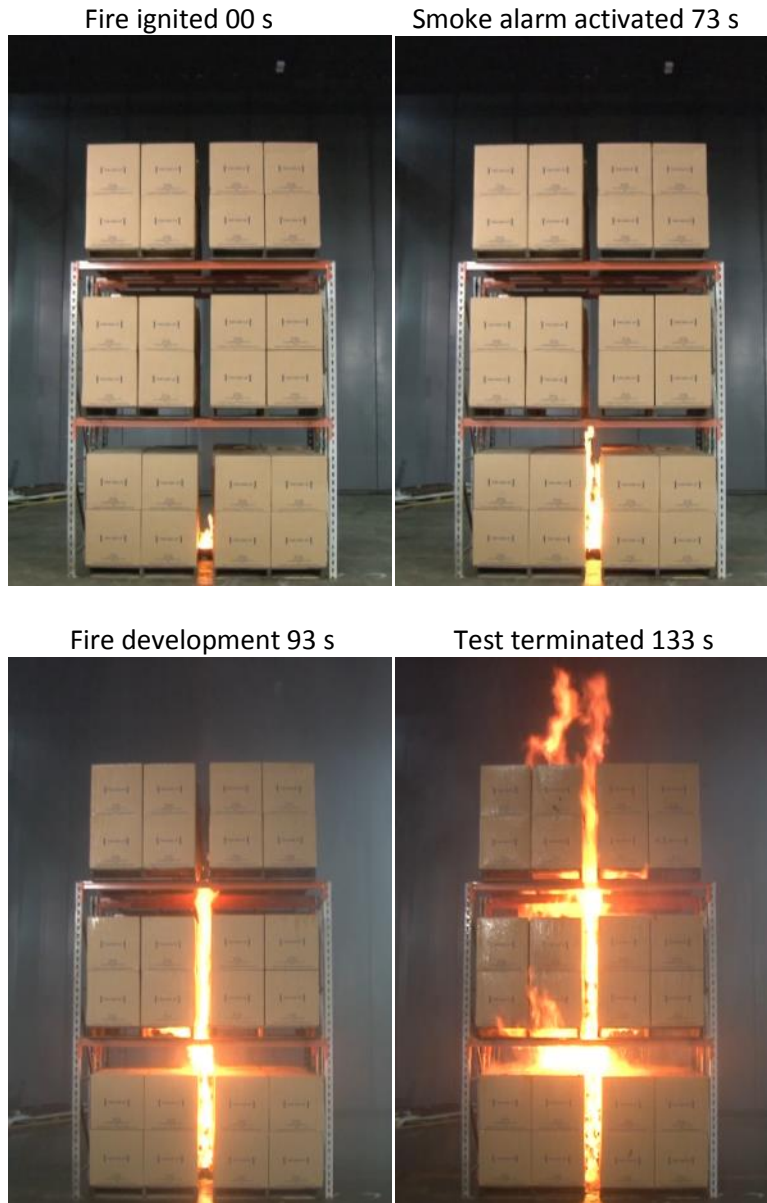


Figure 4-32: Fire development in Test 51 (K80 sprinkler, 15.3 mm/min).

Given the result in Test 51, the water density was increased to 26.9 mm/min (0.66 gpm/ft<sup>2</sup>) for Test 52. The sprinklers were also changed to a K200 lpm/bar<sup>1/2</sup> (K14 gpm/psi<sup>1/2</sup>) pendent type. Unfortunately, a technical error occurred in the first run of Test 52. An upstream water control valve was accidentally closed. As a result, no water was delivered to the open sprinklers (268 s) and the fire test was terminated shortly at 301 s after ignition when the water supply problem was confirmed. It should be pointed out that the relatively large variation in sprinkler activation time between Tests 51 and 52 was caused by the incipient fire growth, which was significantly affected by the contact conditions in each

test between the alcohol pan fire and the commodities. Although Test 52 failed due to the aforementioned technical error, the two panels on the right hand side in Figure 4-33 (t = 268 s and 301 s) approximately reflected the differences in fire size upon activation of SMART and traditional sprinklers as observed previously in commodity classification tests.

In Test 52, the water supply error was corrected. The fire development was similar to that in Figure 4-33 up to the time of sprinkler activation. Unfortunately, the wireless data transfer was frozen between ignition and sprinkler activation. Therefore, the central control unit had to be restarted when the smoke alarm was triggered. Even with such delay, the water density applied was apparently higher than the critical value, and the fire was suppressed rapidly after sprinkler activation.

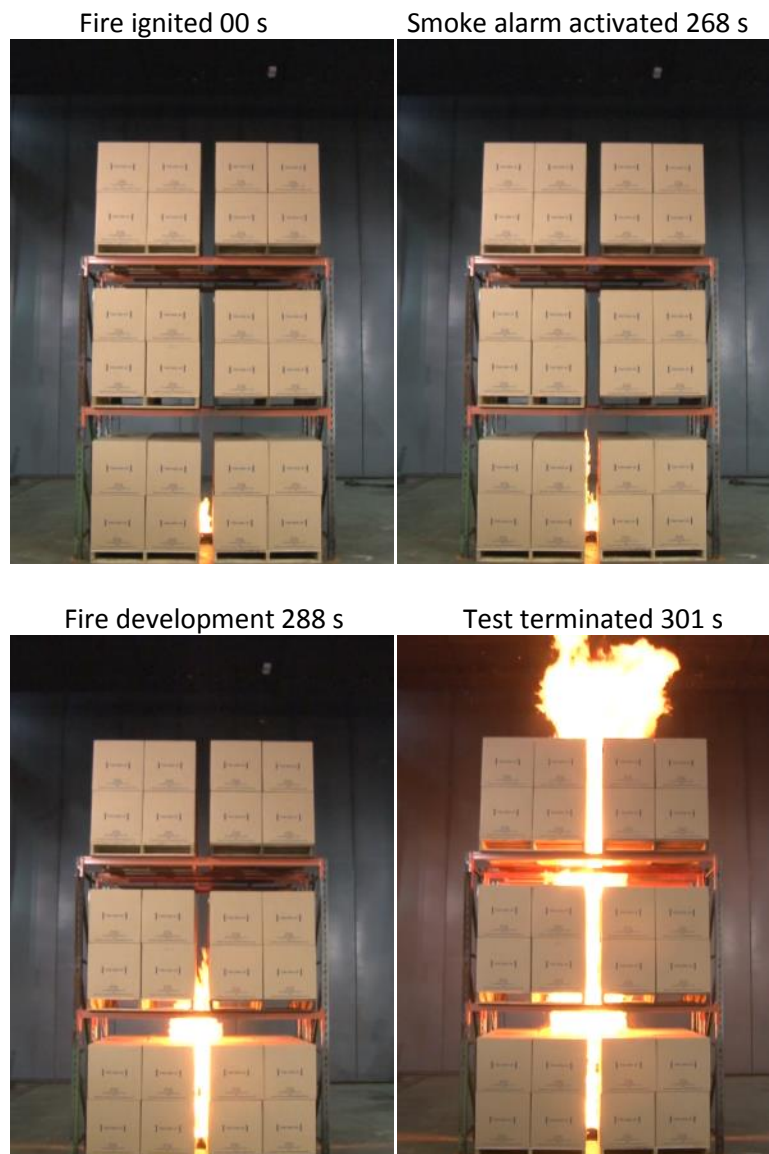


Figure 4-33: Fire development in Test 52 (no water delivered).

In Test 53, the same test setup and water density as Test 52 were used, except that the ignition location was moved to the between-2 condition. As shown in Figure 4-34, the fire grew to approximately 20 kW when the smoke alarm was triggered. The fire continued to grow for another 6 s before the maximum temperature rise of 5 K was reached. At this time, six sprinklers were activated simultaneously as shown in Figure 4-35. Under the applied water density of 26.9 mm/min (0.66 gpm/ft<sup>2</sup>), the fire was quickly suppressed. By the time of test termination (290 s), the flames were completely extinguished. For the same fire hazards, FM Global Loss Prevention Data Sheet 8-9 [15] requires protection design with 12 sprinkler activation and water density of 41 mm/min (1.0 gpm/ft<sup>2</sup>).

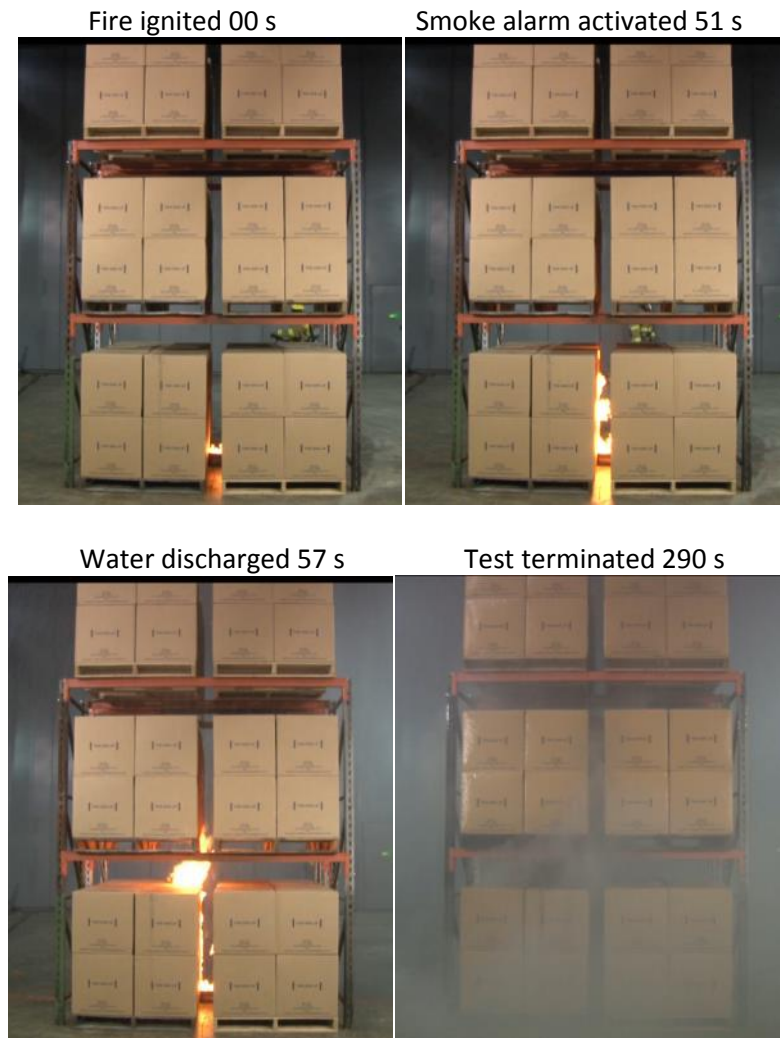


Figure 4-34: Fire development in Test 53 (K200 sprinkler, 26.9 mm/min).

		(South Up)		
	Node: 08e5 18.45	Node: 0a4c 18.97	Node: 0a48 18.19	
Node: 0a66 18.45	Node: 0741 21.68 SMOKE!	Node: 0a54 22.84 SMOKE!	Node: 0934 18.19	Node: 0a4a 17.55
	Node: 0a27 19.48	Node: 0730 19.87	Node: 0a50 19.23	
		Node: 6180 17.68		

Figure 4-35: Sprinkler activation with between-2 ignition in Test 53.

## 5. Conclusions and future work

---

### 5.1 Summary and conclusions of current work

The present work was initiated with emphasis on demonstrating a new sprinkler protection concept and its application to High Challenge Fires (HCFs). Based on a review of HCFs, a new sprinkler protection strategy was proposed. The new sprinkler protection utilizes Simultaneous Monitoring, Assessment and Response Technology, and is thus defined as SMART sprinkler protection. A prototype SMART sprinkler system was designed to achieve the key functions, namely fire detection, fire location calculation and dynamic sprinkler activation. In order to evaluate these system functions, dedicated experiments were designed and conducted. The results show that

- The use of multi-sensor technology, here a combination of smoke and temperature rise signals, can help balance fast fire detection and accurate fire location calculation.
- Fire location can be determined with reasonable accuracy based on thermal centroid calculations.
- Sprinkler activation can be achieved by the control unit through active triggering of each sprinkler unit locally and dynamically based on the results of fire detection and fire location.
- Fire suppression, even fire extinguishment, can be achieved with adequate water flux applied on top of a given commodity.

In summary, experimental results from fire detection, sprinkler activation and preliminary suppression tests have shown that the newly developed system meets design objectives in terms of system functions. The next step to further evaluate the effectiveness of the SMART sprinklers for fire protection purposes in full-scale fire tests is documented in a separate report [1].

### 5.2 Future work

Future work on the SMART sprinkler system evaluation will need to include full-scale tests using standard commodities within a rack storage configuration.

The full-scale tests using standard commodities in rack storage configurations are recommended because of a long history with these commodities and storage configurations, and the abundant data available to compare the SMART and traditional sprinklers. Testing should be conducted with 3-, 5- and 7-tier high rack storage tests using the CUP commodity, which is widely used in routine fire testing to represent a medium level of fire hazard.

The testing and analysis carried out for this project were intended as a proof-of-concept study of a new fire protection technology. In order to achieve this goal, hardware was assembled to produce the desired functionality. Even though such hardware was not intended for commercial implementation, experience with its use has pointed to areas of possible vulnerability, which will need to be addressed through proper testing and certification of any commercial units. In addition to the consideration of fire

protection effectiveness, there are other key issues that may affect the system performance. Some examples are:

- System reliability. In fire detection tests, the wireless communication occasionally became frozen without transmitting data between the sprinkler and the control unit. This issue clearly needs to be addressed.
- Variability in detector performance. Systematic investigation of detector response characteristics was not included in the present work, which can affect the overall system performance in fire suppression.
- Impact of ambient conditions on fire detection. Since ceiling temperatures can vary significantly, the use of rate of temperature rise may provide more reliable and consistent detection than the fixed temperature rise.
- System performance under non-flat ceilings. The fire location algorithm has been examined for conditions where the ceiling layer developed under a flat ceiling. The presence of obstructions and structural members in practical installations may present a challenge to the algorithm.

A plan needs to be developed to identify key issues that will likely affect the SMART sprinkler performance in engineering practice. Future work to address these issues, such as a reliability study, can certainly help setting a strong foundation for the commercialization of this new protection system.

## Nomenclature

---

$C$	Smoke concentration
$d_{ci}$	Thermal centroid deviation
$h_s$	Storage height
$\Delta h_c$	Heat of combustion
$\Delta l/l$	Smoke obscuration fraction
$l_{spc}$	Sprinkler spacing
$\dot{m}'_w$	Water flow rate per unit length
$\dot{m}$	Mass flow rate
$\dot{Q}$	Heat release rate
$R_{dl}$	Normalized thermal centroid deviation
$t$	Time
$\Delta T$	Temperature rise (K)
$u_w$	Velocity of surface water flow
$x$	X coordinate of fire location
$y$	Y coordinate of fire location
$y_s$	Soot yield
$z$	Vertical coordinate
$z_0$	Virtual original of fire plume

### Subscripts

$act$	activation
$chem$	chemical
$conv$	convective
$ctd$	centroid
$ent$	entrainment
$f$	fuel
$i$	index of temperature sensors
$ign$	ignition
$min$	minimum
$max$	maximum
$s$	storage
$smk$	smoke
$w$	water

### Superscripts

*	Normalized using max and min values
---	-------------------------------------

### Abbreviations

CDF	Critical delivered flux
HCF	Highly challenging fire
HRR	Heat release rate
SBL	Small Burn Lab

## References

---

1. Y. Xin, K. Burchesky, J. de Vries, H. Magistrale, X. Zhou, and S. D'Aniello, "Smart Sprinkler Protection for Highly Challenging Fires - Phase 2: Full-Scale Fire Tests in Rack Storage Configurations," FM Global Technical Report, February 2016.
2. FM Global, "Roll Paper Storage," FM Global Loss Prevention Data Sheets, 8-21, July 2014.
3. Y. Xin and J.M.A. Troup, "Advancements in Fire Hazard Classification of Roll Paper," in *The 5th International Seminar on Fire and Explosion Hazards*, Edinburgh, UK, April 23, 2007, pp. 532-540.
4. W.D. Moore, "Automatic Fire Detectors," in *Fire Protection Handbook*, 18th ed., A.E. Cote, Ed. Quincy, MA: National Fire Protection Association, 1997, ch. 5, pp. 5-1 - 5-23.
5. G. Heskestad and J.S. Newman, "Fire Detection Using Cross-Correlations of Sensor Signals," *Fire Safety Journal*, vol. 18, pp. 355-374, 1992. doi:10.1016/0379-7112(92)90024-7
6. J. de Vries, Y. Xin, and K.V. Meredith, "An Experimental Study of Fire Suppression Physics for Sprinkler Protection," *Fire Safety Science*, vol. 10, pp. 429-442, 2011. doi:10.3801/IAFSS.FSS.10-429
7. Y. Xin, "Storage Height Effects on Fire Growth Rates of Cartoned Commodities," in *The 7th International Seminar on Fire and Explosion Hazards*, Providence, RI, USA, May 5-10, 2013.
8. Y. Xin and F. Tamanini, "Assessment of Commodity Classification for Sprinkler Protection Using Representative Fuels," *Fire Safety Science*, vol. 9, pp. 527-538, 2008.
9. P. Croce, Y. Xin, and J. Hill, "An Investigation of the Causative Mechanism of Sprinkler Skipping," *Journal of Fire Protection Engineering*, vol. 15, pp. 107-136, 2005.
10. G. Heskestad, "Physical Modeling of Fire," *Journal of Fire and Flammability*, vol. 6, pp. 254-273, 1975.
11. G. Heskestad, "Scaling the Interaction of Water Sprays and Flames," *Fire Safety Journal*, vol. 37, pp. 535-548, 2002. doi:10.1016/S0379-7112(02)00012-7
12. A. Tewarson, "Generation of Heat and Chemical Compounds in Fires," in *The SFPE Handbook of Fire Protection Engineering*, 3rd ed., P.J. DiNenno, D. Drysdale, C.L. Beyler, W.D. Walton, R.L.P. Custer, J.R. Hall Jr., and J.M. Watts Jr., Eds. Quincy, MA: National Fire Protection Association, 2002, ch. 3-4.

13. G. Heskestad, "Fire Plumes, Flame Heights and Air Entrainment," in *The SFPE Handbook of Fire Protection Engineering*, 3rd ed., P.J. DiNenno, D. Drysdale, C.L. Beyler, W.D. Walton, R.L.P. Custer, J.R. Hall Jr., and J.M. Watts Jr., Eds. Quincy, MA: National Fire Protection Association, 2002, ch. 2-1.
14. Y. Xin, "Estimation of Chemical Heat Release Rate in Rack Storage Fires Based on Flame Volume," *Fire Safety Journal*, vol. 63, pp. 29-36, 2014.
15. FM Global, "Storage of Class 1, 2, 3, 4 and Plastic Commodities," FM Global Loss Prevention Data Sheets 8-9, July 2011.
16. FM Approvals LLC, "Approval Standard for Automatic Control Mode Sprinklers for Fire Protection, Class Number 2000," Norwood, MA 02062, USA , March 2006.

## Appendix A. Fire detection test data

### A.1 Test data with 0.76 m (2.5 ft) sprinkler spacing

The experimental results from Tests 2-23 are presented in this section including the temperature rise at the ceiling, the normalized thermal centroid deviation and the smoke detector response time. See Table 3-1 for detailed experimental conditions. The temperature rise plots are grouped based on the distance (R) between the TC and the ignition location. The normalized thermal centroid deviation (Distance/Spacing) is defined in Section 2.3. The smoke detector response time is also plotted with respect to the radial distance from the ignition location.

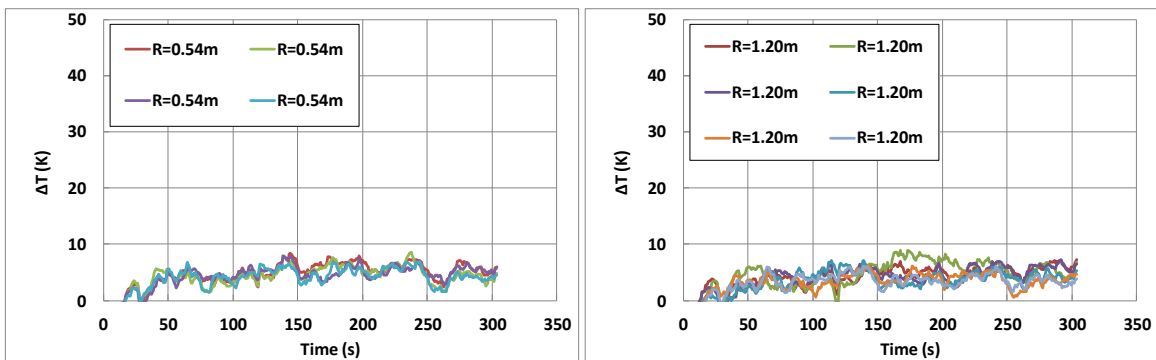


Figure A-1: Temperature rise at the ceiling in Test 2.

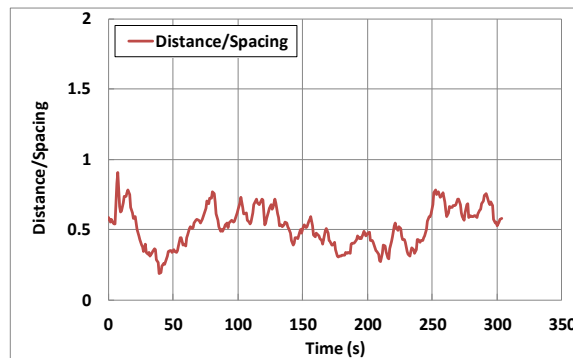


Figure A-2: Normalized thermal centroid deviations in Test 2 (no detector activated in 300 s).

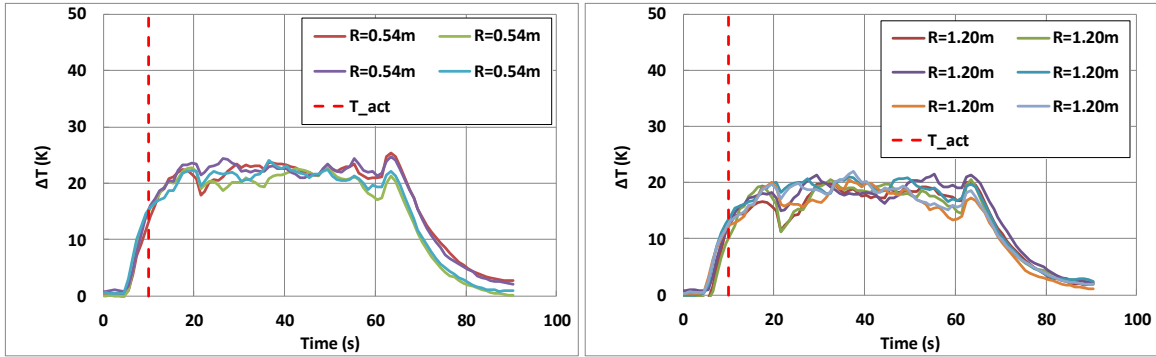


Figure A-3: Temperature rise at the ceiling in Test 3.

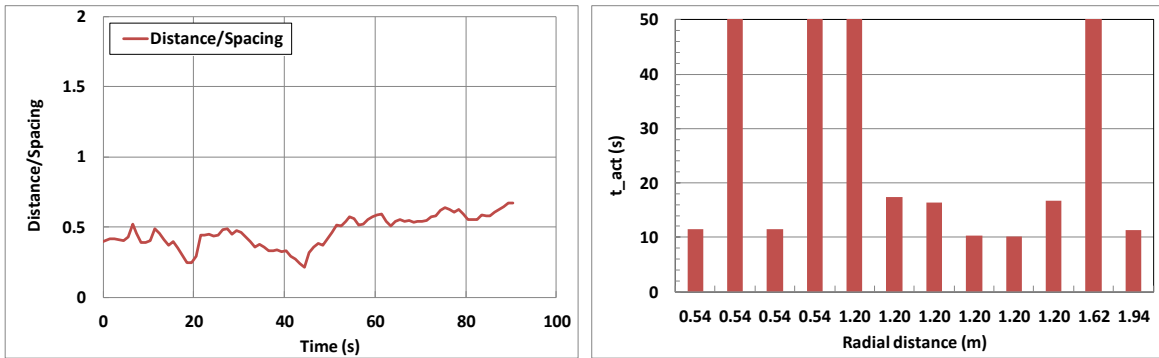


Figure A-4: Normalized thermal centroid deviations and smoke detector response times in Test 3.

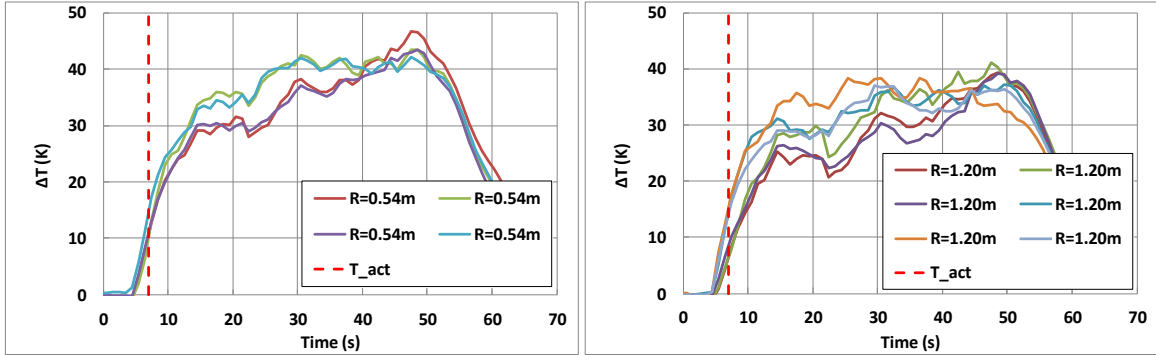


Figure A-5: Temperature rise at the ceiling in Test 4.

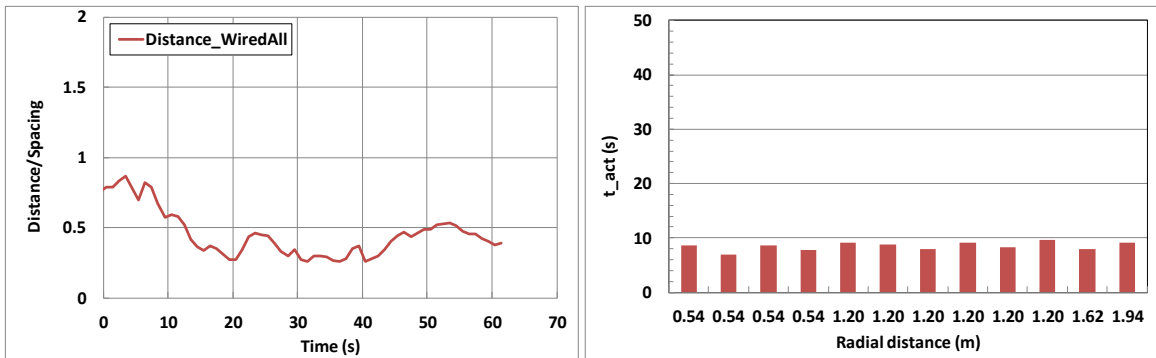


Figure A-6: Normalized thermal centroid deviations and smoke detector response times in Test 4.

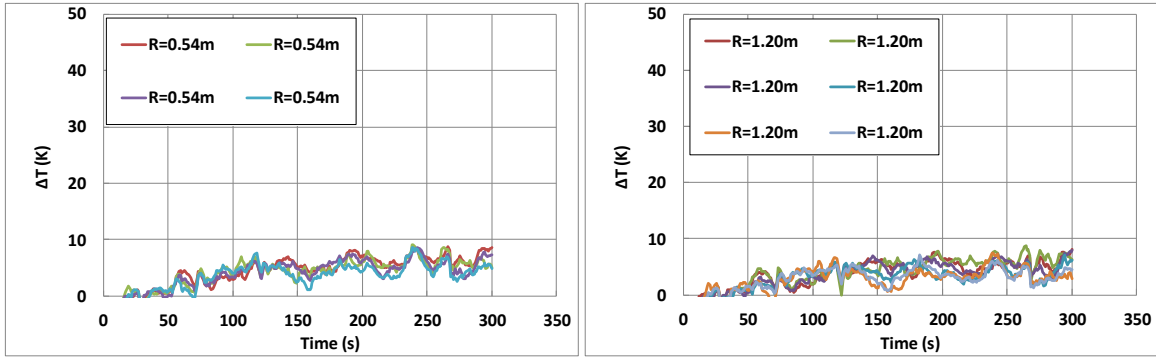


Figure A-7: Temperature rise at the ceiling in Test 5.

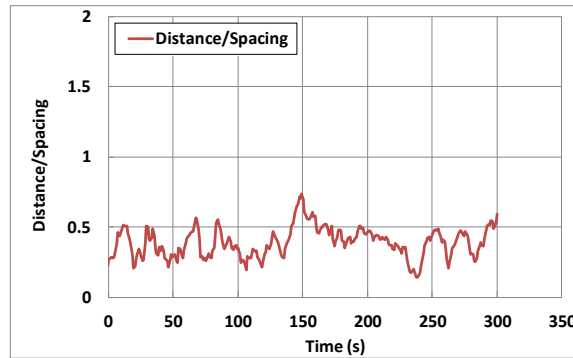


Figure A-8: Normalized thermal centroid deviations in Test 5 (no detector activated in 300 s).

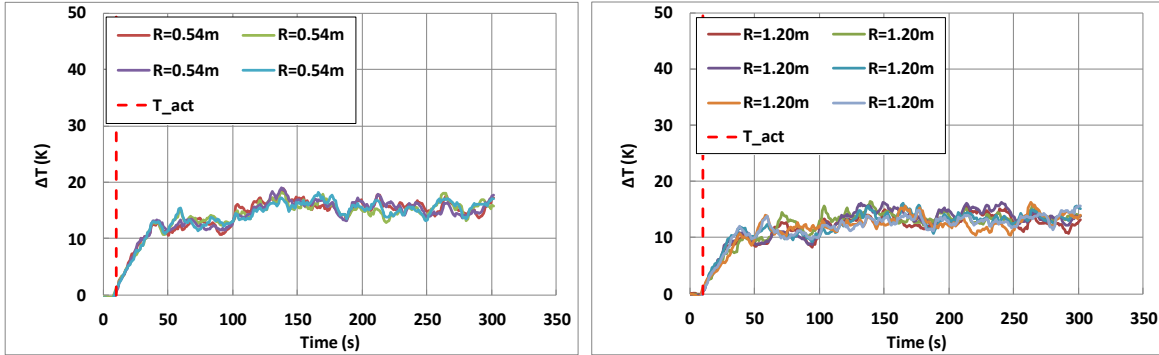


Figure A-9: Temperature rise at the ceiling in Test 6.

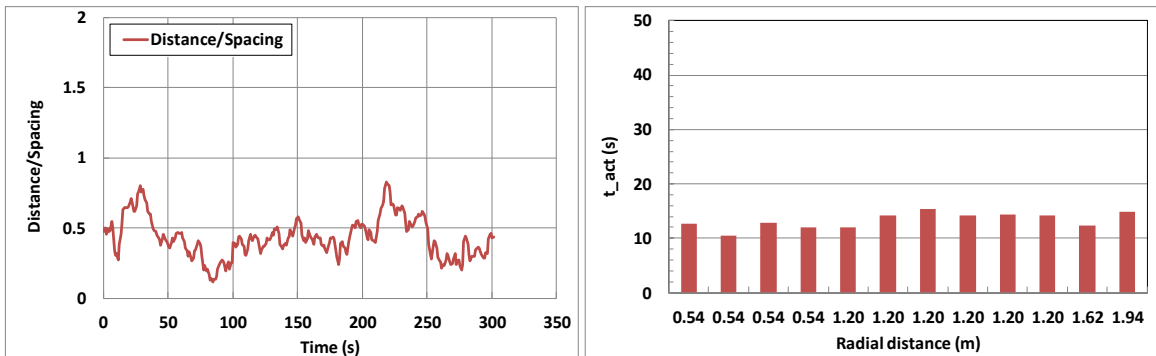


Figure A-10: Normalized thermal centroid deviations and smoke detector response times in Test 6.

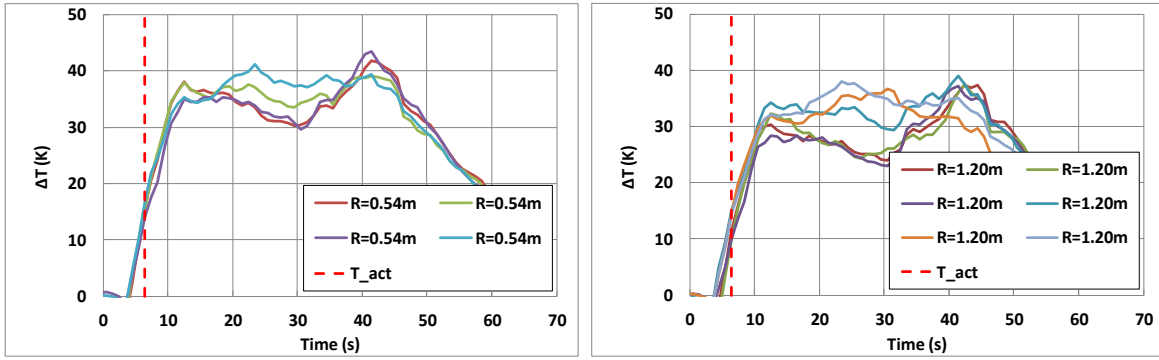


Figure A-11: Temperature rise at the ceiling in Test 7.

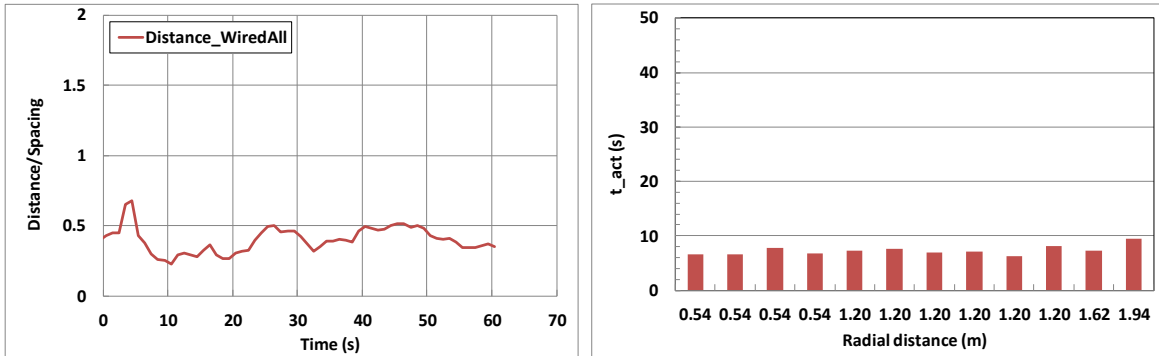


Figure A-12: Normalized thermal centroid deviations and smoke detector response times in Test 7.

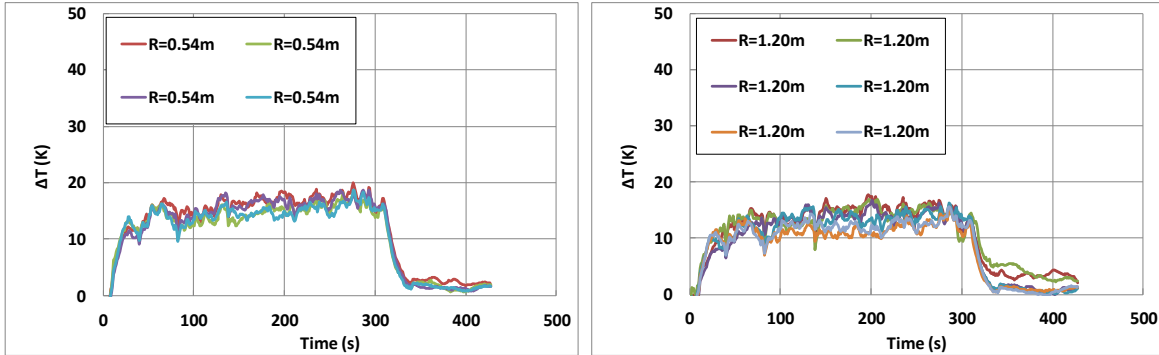


Figure A-13: Temperature rise at the ceiling in Test 8.

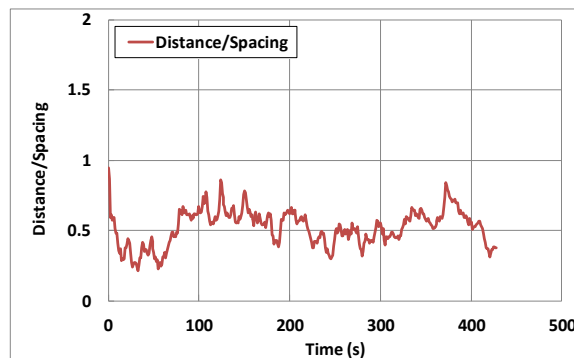


Figure A-14: Normalized thermal centroid deviations in Test 8 (no detector activated in 300 s).

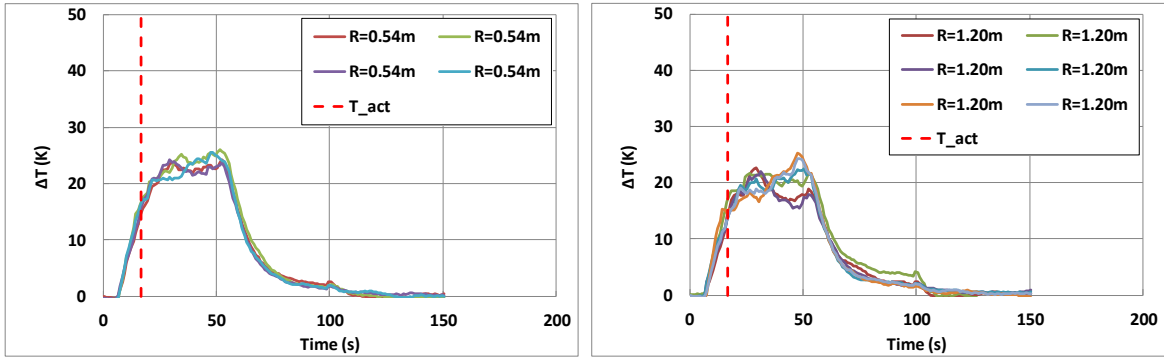


Figure A-15: Temperature rise at the ceiling in Test 9.

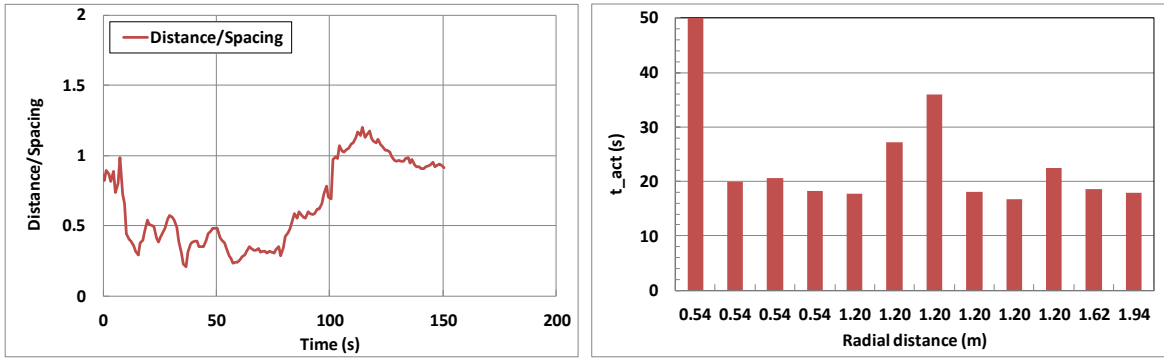


Figure A-16: Normalized thermal centroid deviations and smoke detector response times in Test 9.

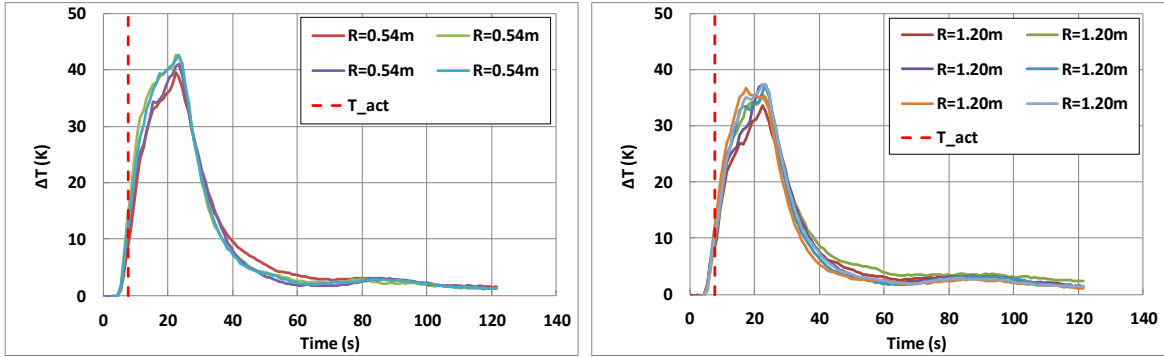


Figure A-17: Temperature rise at the ceiling in Test 10.

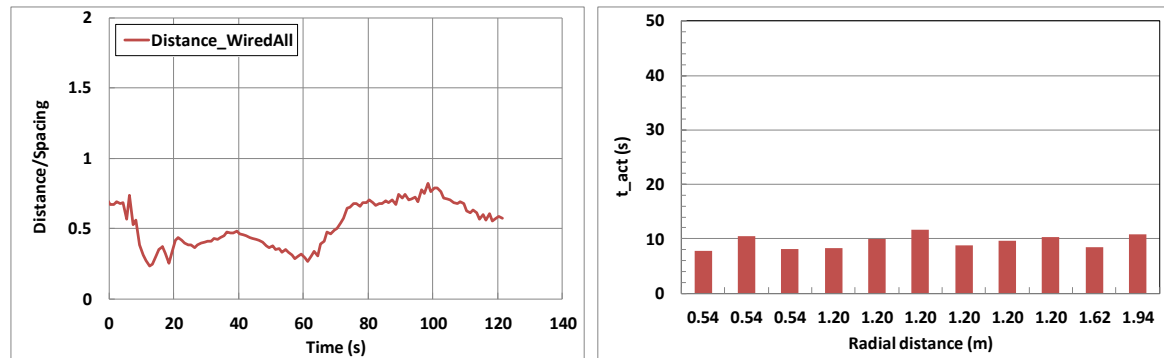


Figure A-18: Normalized thermal centroid deviations and smoke detector response times in Test 10.

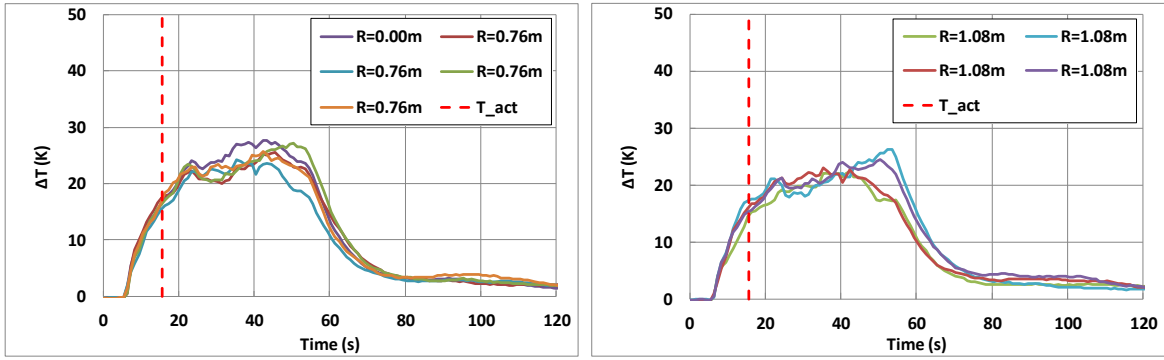


Figure A-19: Temperature rise at the ceiling in Test 11.

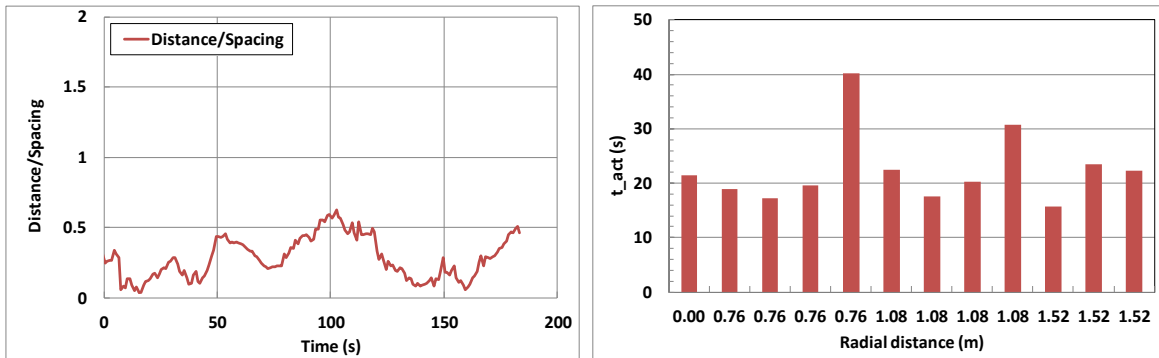


Figure A-20: Normalized thermal centroid deviations and smoke detector response times in Test 11.

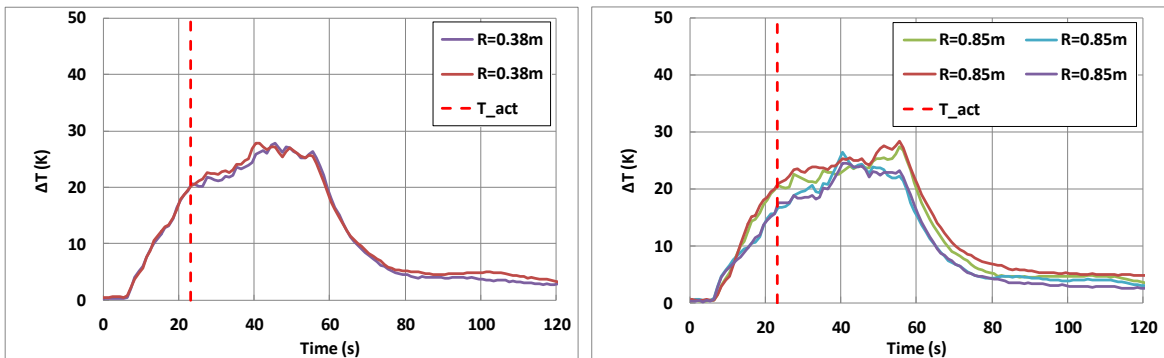


Figure A-21: Temperature rise at the ceiling in Test 12.

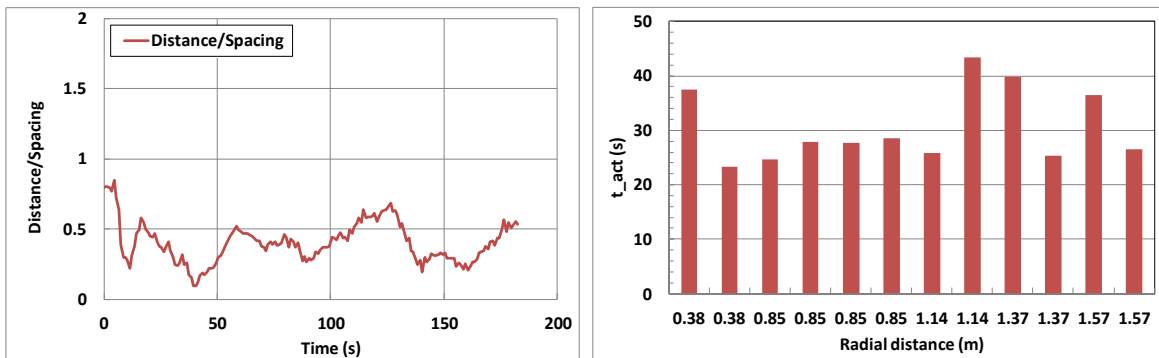


Figure A-22: Normalized thermal centroid deviations and smoke detector response times in Test 12.

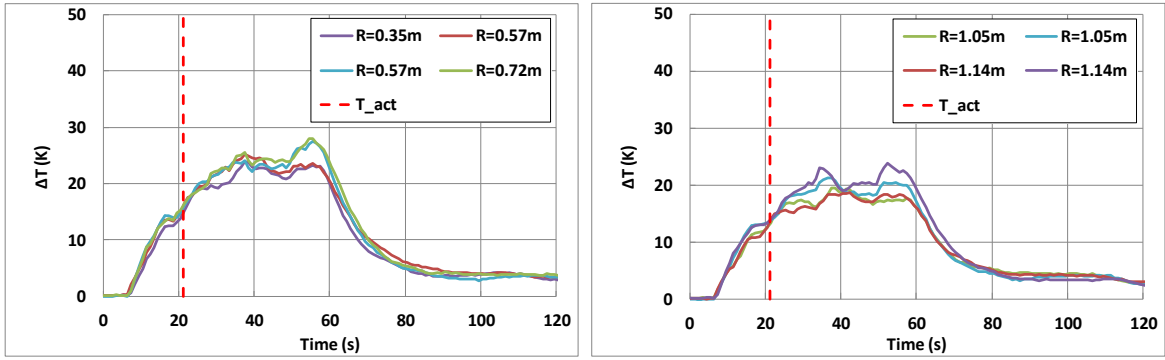


Figure A-23: Temperature rise at the ceiling in Test 13.

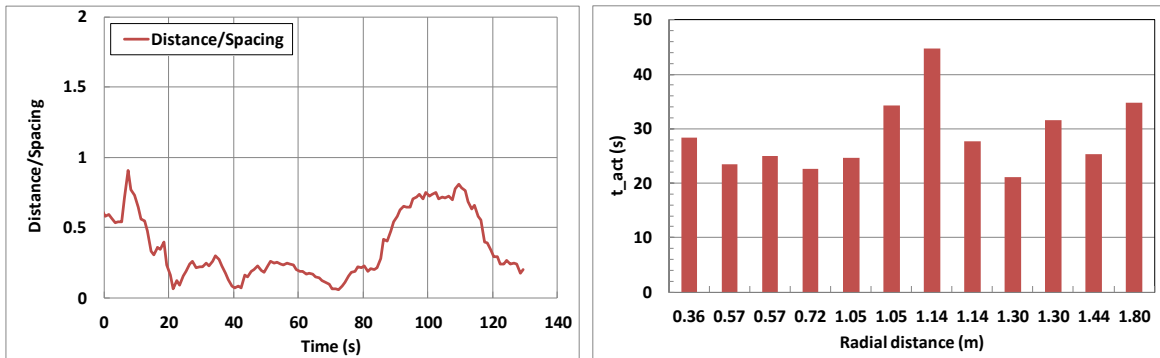


Figure A-24: Normalized thermal centroid deviations and smoke detector response times in Test 13.

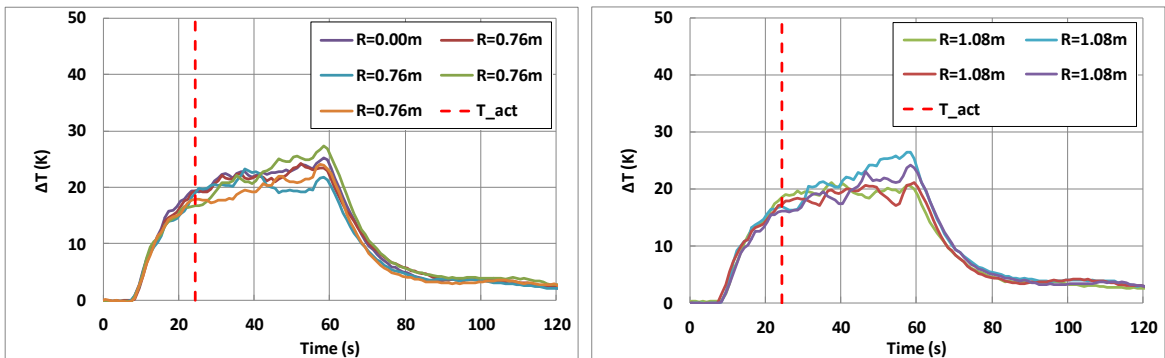


Figure A-25: Temperature rise at the ceiling in Test 14.

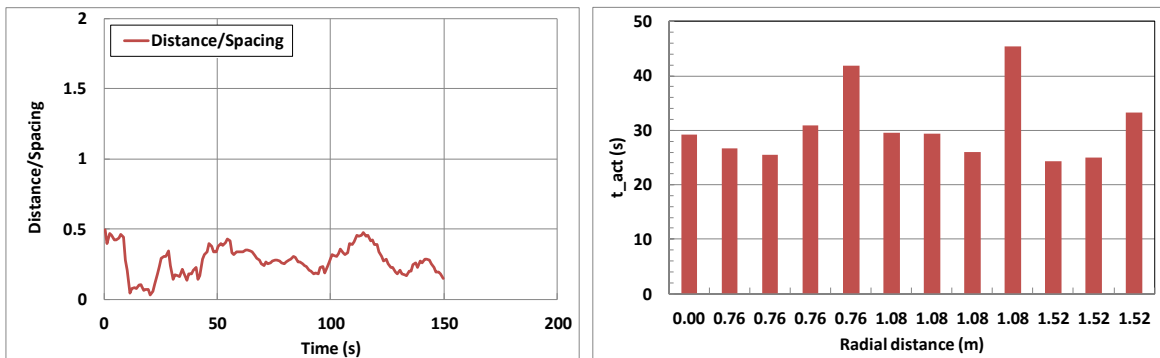


Figure A-26: Normalized thermal centroid deviations and smoke detector response times in Test 14.

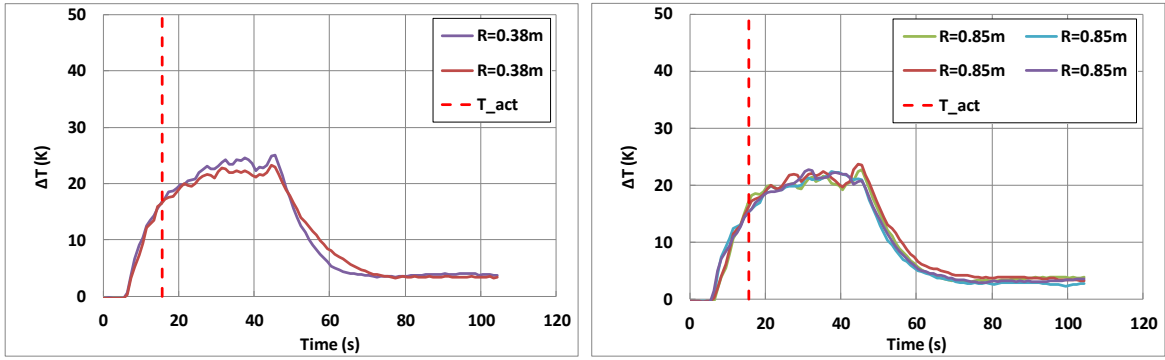


Figure A-27: Temperature rise at the ceiling in Test 15.

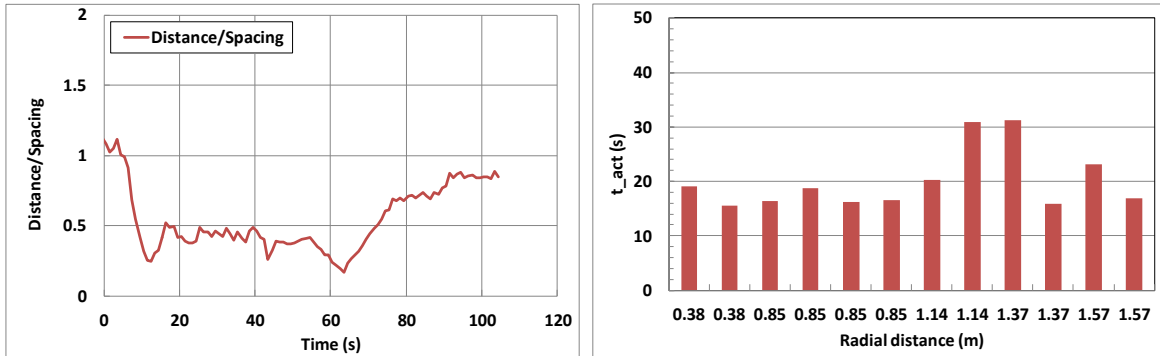


Figure A-28: Normalized thermal centroid deviations and smoke detector response times in Test 15.

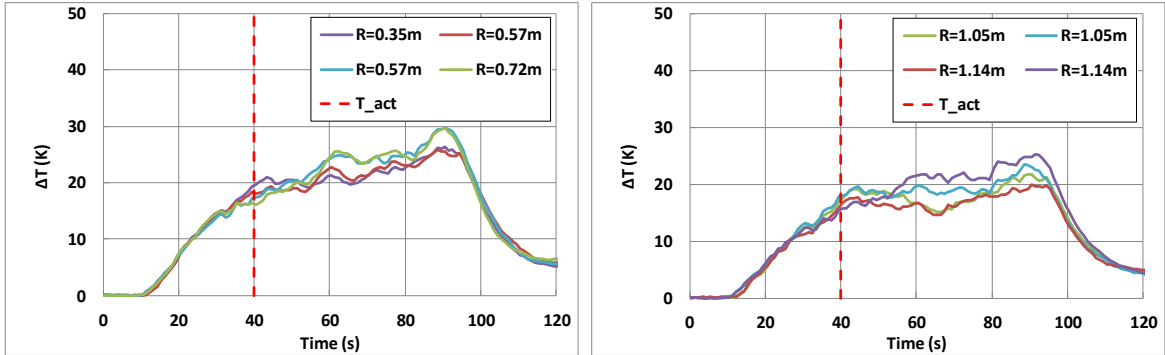


Figure A-29: Temperature rise at the ceiling in Test 16.

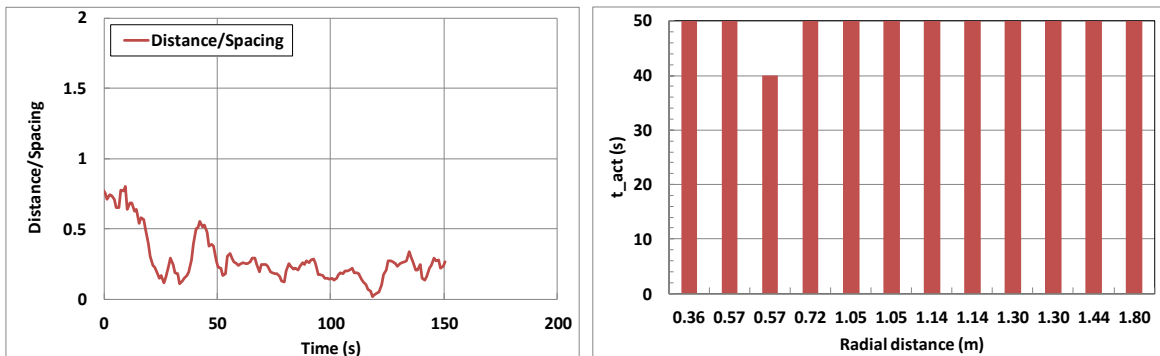


Figure A-30: Normalized thermal centroid deviations and smoke detector response times in Test 16.

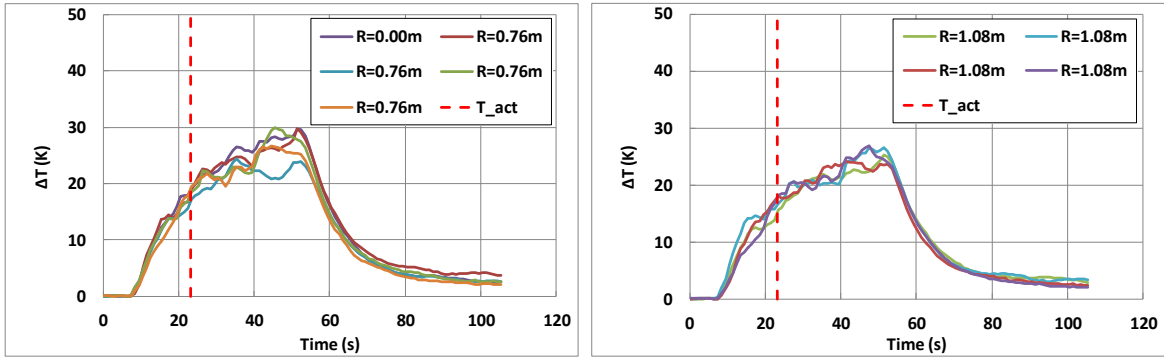


Figure A-31: Temperature rise at the ceiling in Test 17.

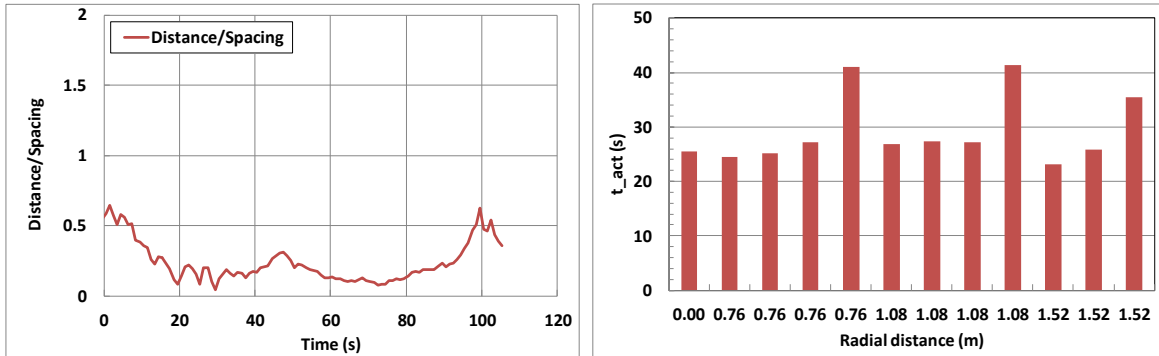


Figure A-32: Normalized thermal centroid deviations and smoke detector response times in Test 17.

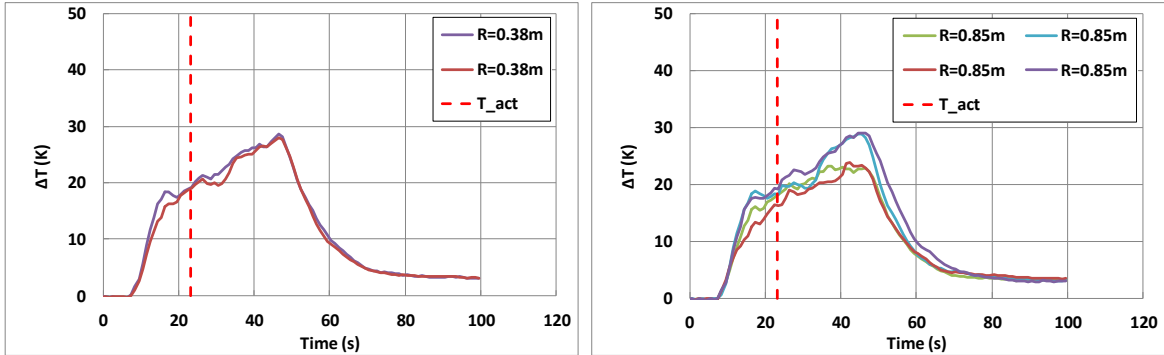


Figure A-33: Temperature rise at the ceiling in Test 18.

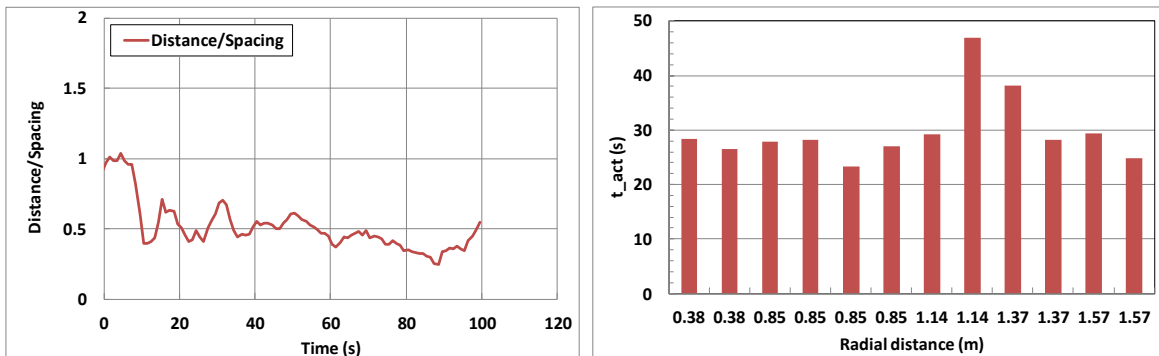


Figure A-34: Normalized thermal centroid deviations and smoke detector response times in Test 18.

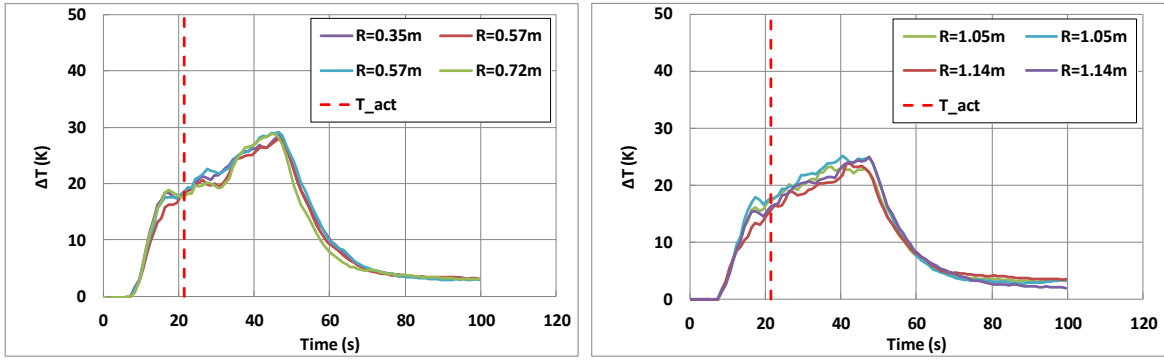


Figure A-35: Temperature rise at the ceiling in Test 19.

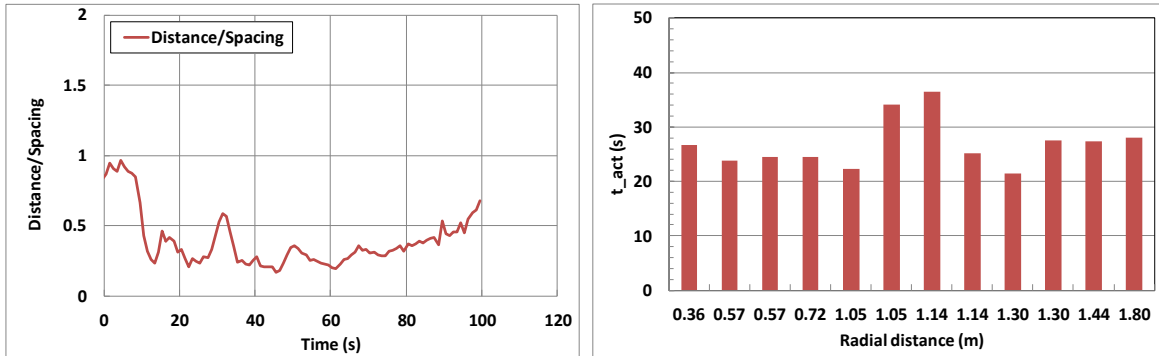


Figure A-36: Normalized thermal centroid deviations and smoke detector response times in Test 19.

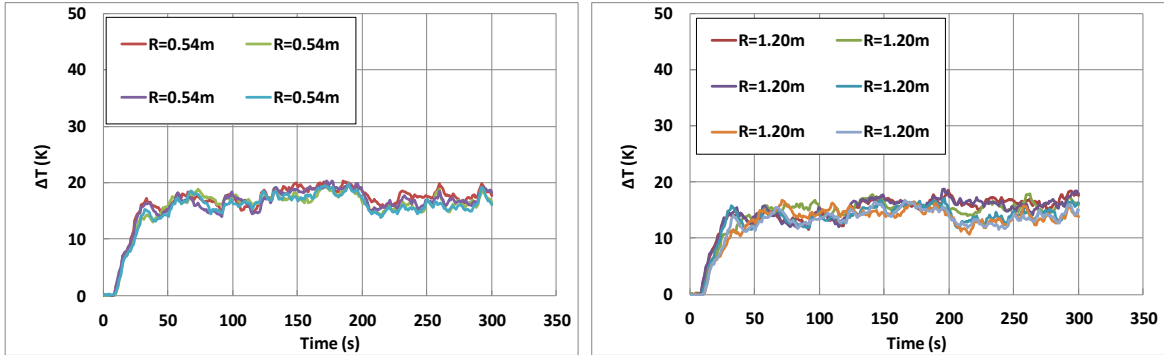


Figure A-37: Temperature rise at the ceiling in Test 20.

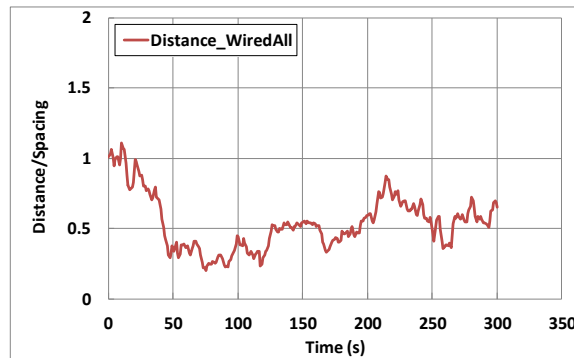


Figure A-38: Normalized thermal centroid deviation in Test 20 (no detector activated in 300 s).

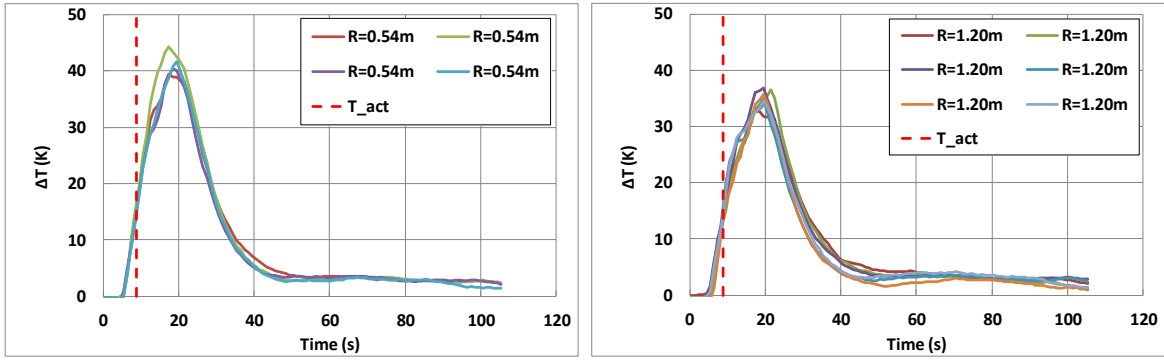


Figure A-39: Temperature rise at the ceiling in Test 21.

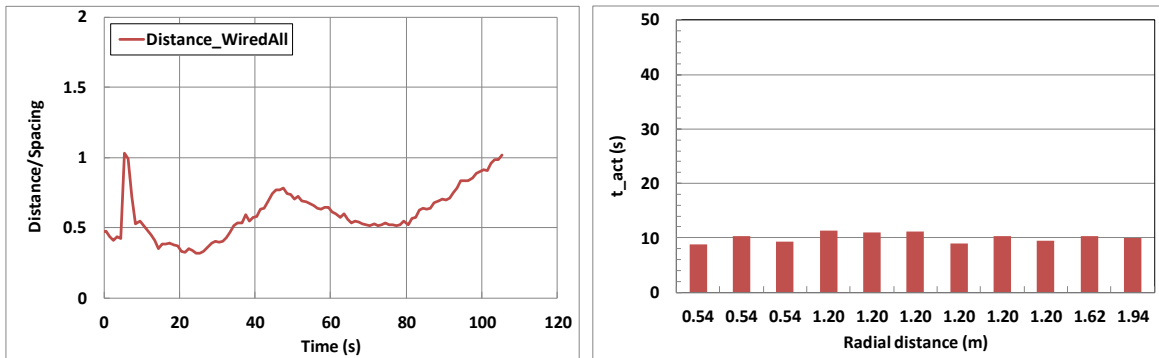


Figure A-40: Normalized thermal centroid deviations and smoke detector response times in Test 21.

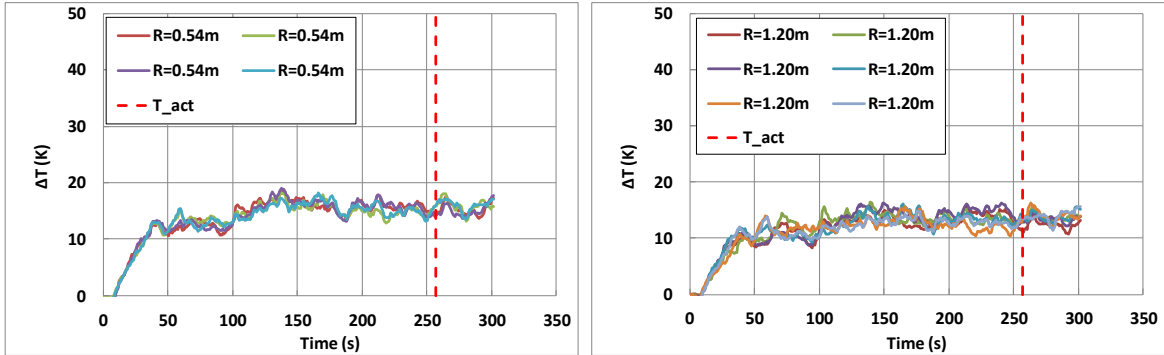


Figure A-41: Temperature rise at the ceiling in Test 22.

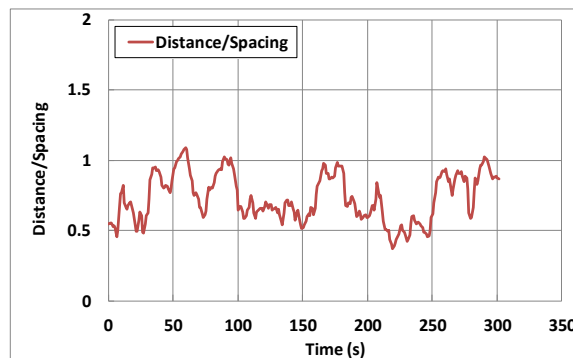


Figure A-42: Normalized thermal centroid deviations in Test 22 (no detector activated in 300 s).

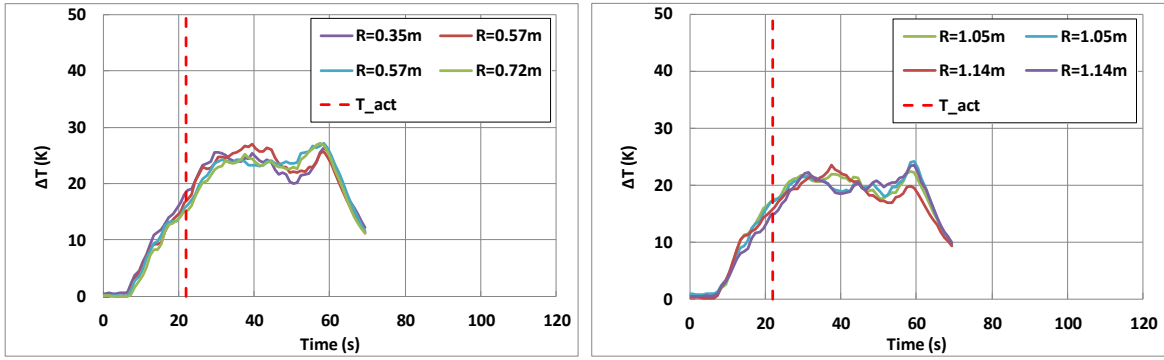


Figure A-43: Temperature rise at the ceiling in Test 23.

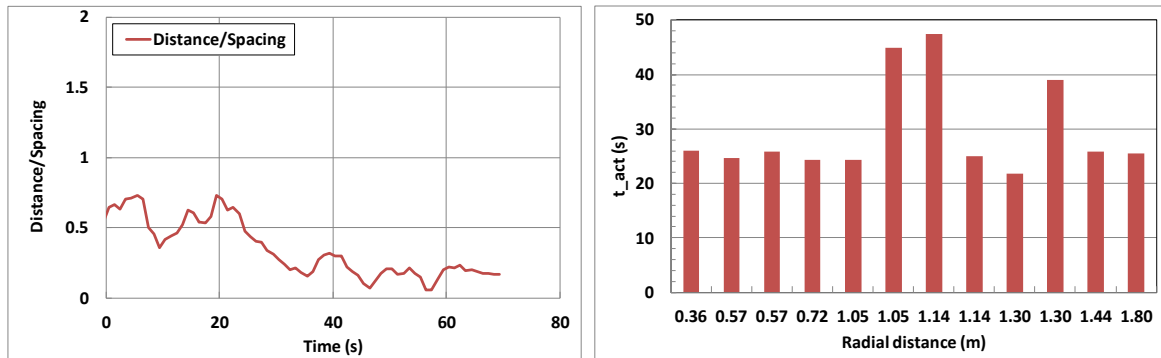


Figure A-44: Normalized thermal centroid deviations and smoke detector response times in Test 23.

## A.2 Fire detection tests with 2.44 m (8 ft) sprinkler spacing

The experimental results from Tests 24-38 are presented in this section including the thermal centroid deviation, the smoke detector response time and the temperature rise at the ceiling. See Table 3-2 for detailed experimental conditions. The thermal centroid deviation is defined in Section 2.3. The smoke detector response time and the temperature rise are plotted with respect to the radial distance from the ignition location.

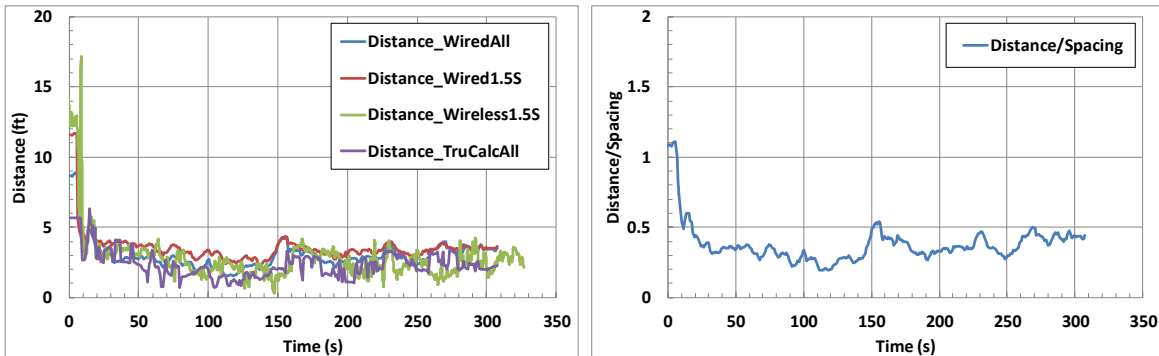


Figure A-45: Thermal centroid deviations in Test 24 (no detector activated in 300 s).

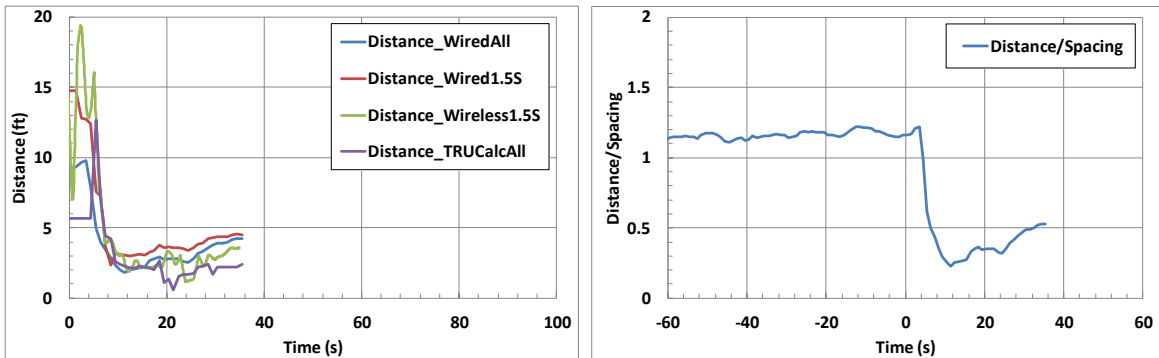


Figure A-46: Thermal centroid deviations in Test 25.

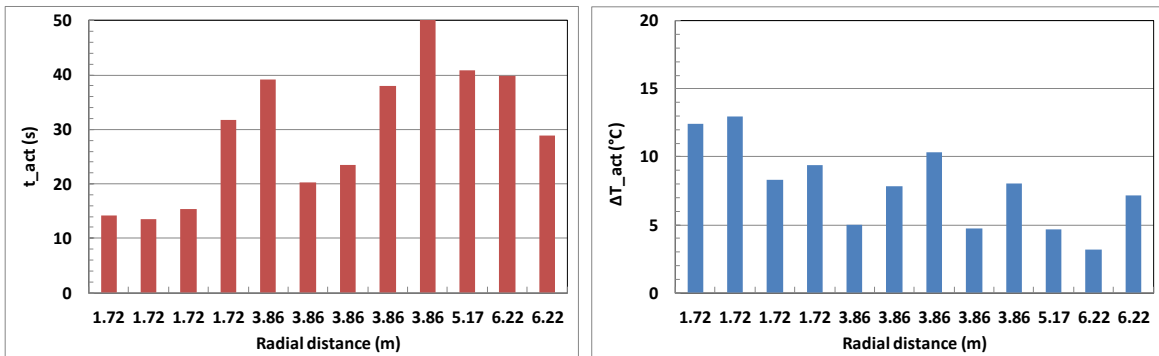


Figure A-47: Smoke detector response times and  $\Delta T_{act}$  at the ceiling in Test 25.

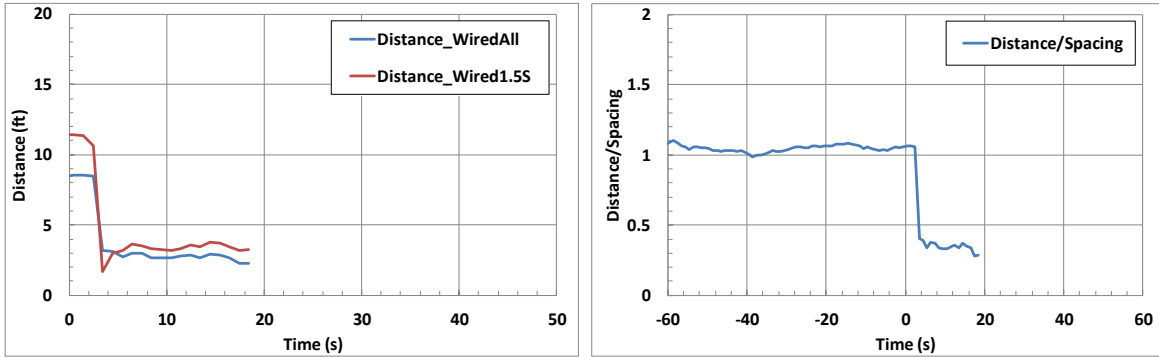


Figure A-48: Thermal centroid deviations in Test 26.

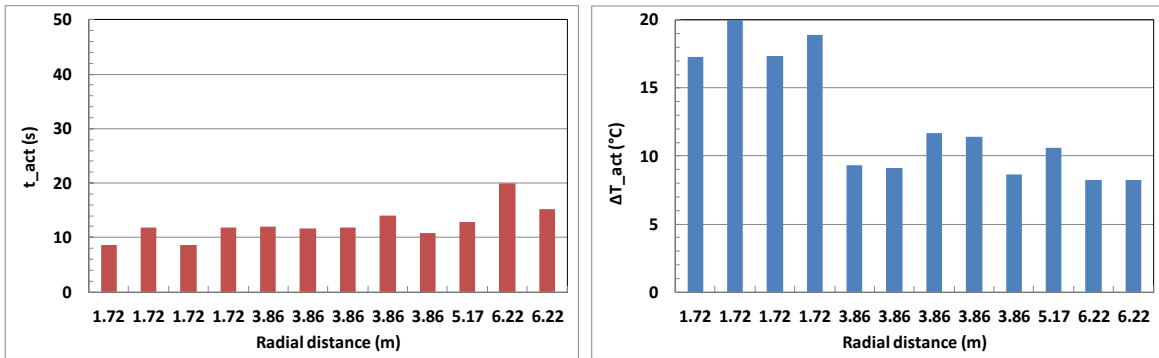


Figure A-49: Smoke detector response times and temperature rise at the ceiling in Test 26.

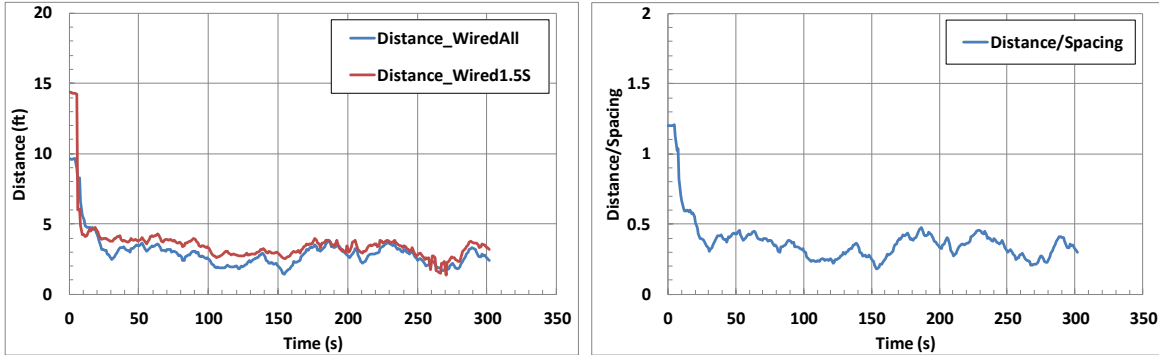


Figure A-50: Thermal centroid deviations in Test 27 (no detector activated in 300 s).

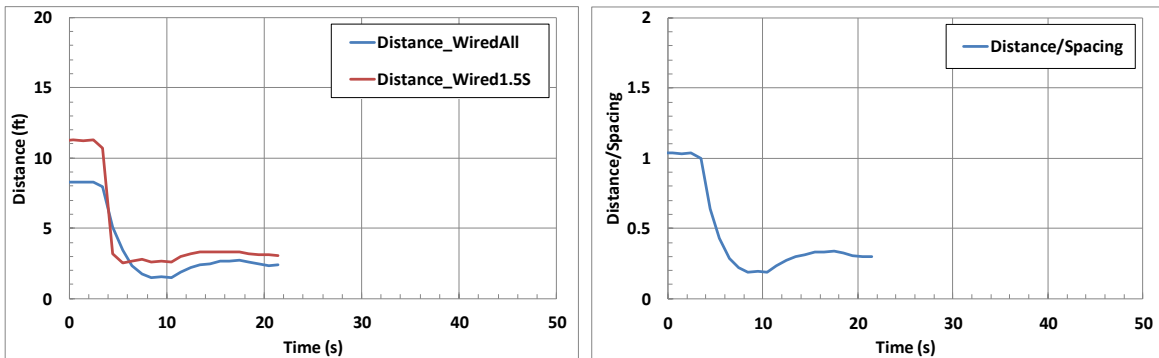


Figure A-51: Thermal centroid deviations in Test 28.

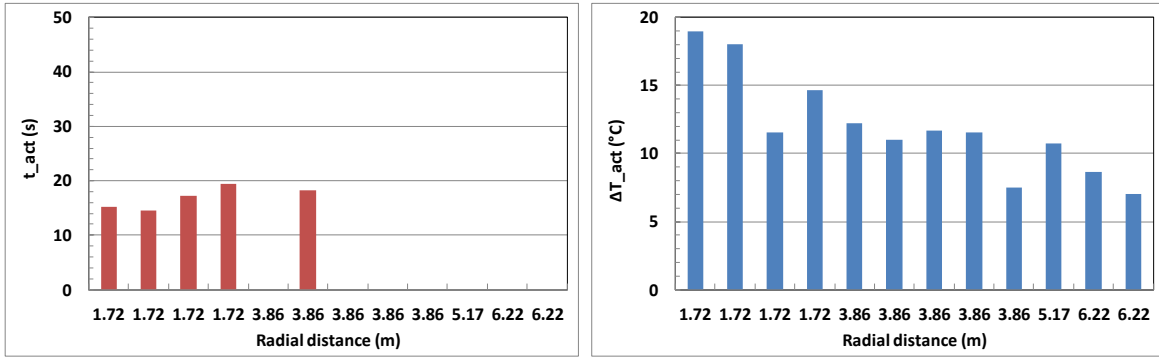


Figure A-52: Smoke detector response times and temperature rise at the ceiling in Test 28.

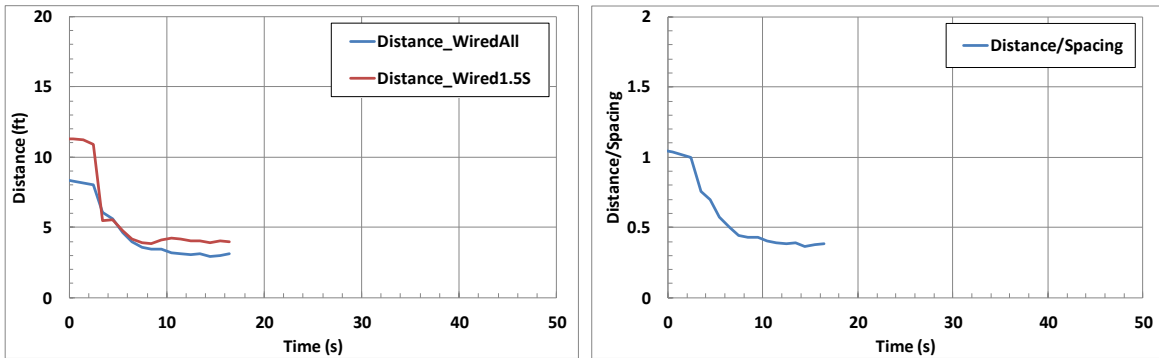


Figure A-53: Thermal centroid deviations in Test 29.

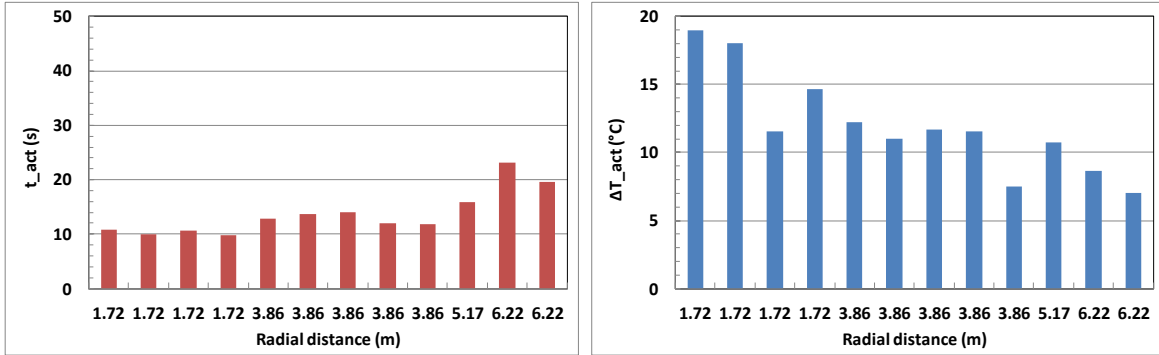


Figure A-54: Smoke detector response times and temperature rise at the ceiling in Test 29.

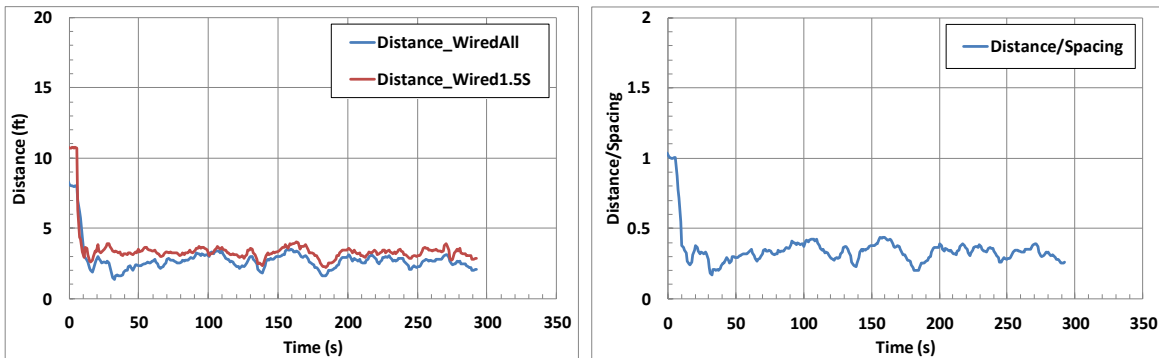


Figure A-55: Thermal centroid deviations in Test 30 (no detector activated in 300 s).

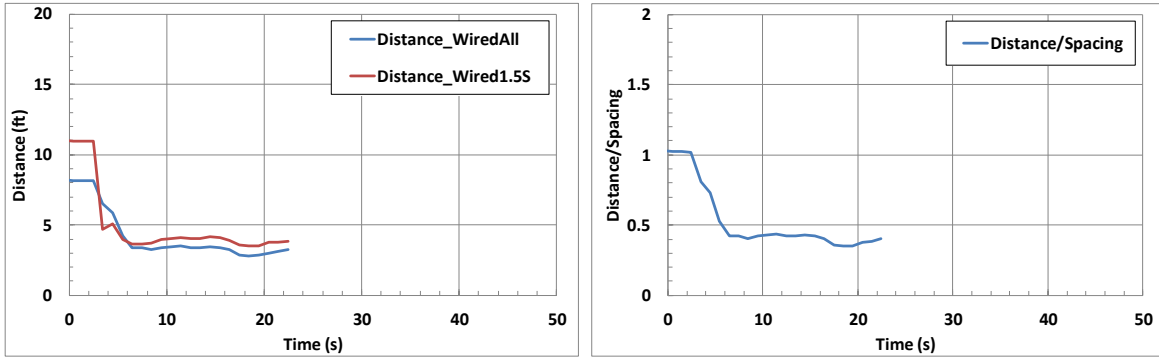


Figure A-56: Thermal centroid deviations in Test 31.

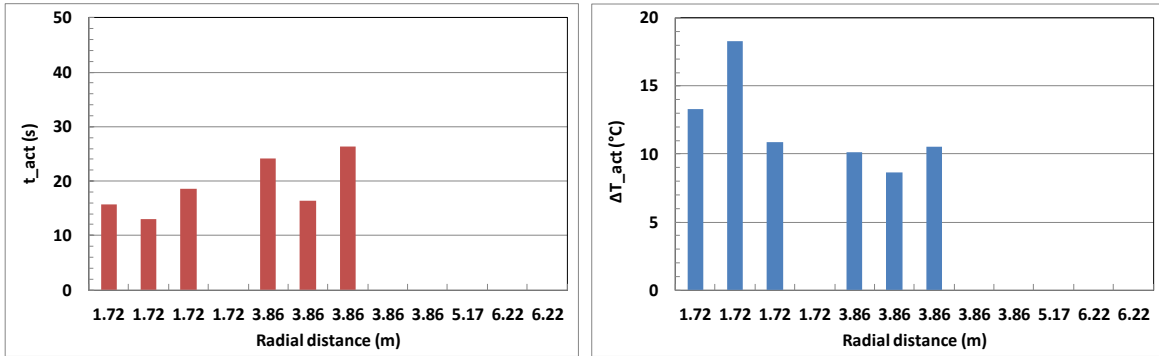


Figure A-57: Smoke detector response times and temperature rise at the ceiling in Test 31.

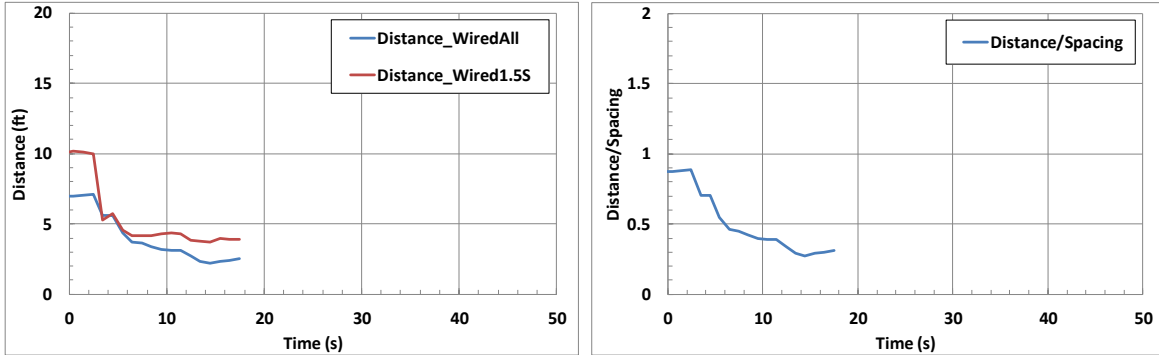


Figure A-58: Thermal centroid deviations in Test 32.

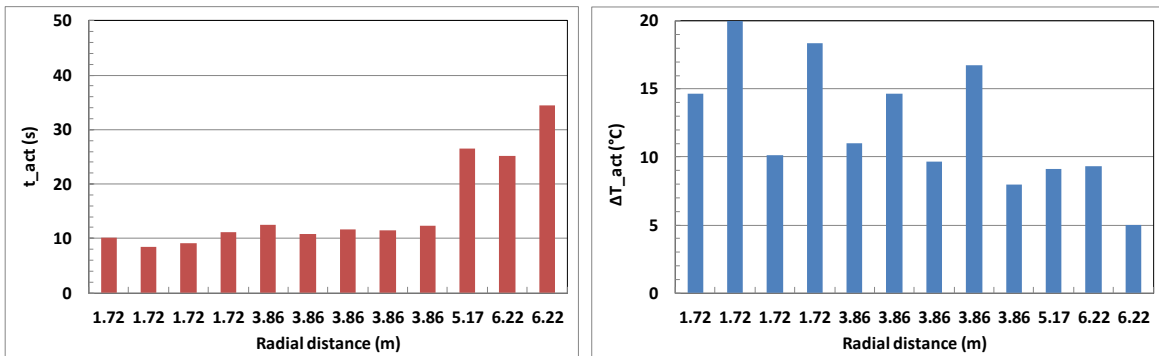


Figure A-59: Smoke detector response times and temperature rise at the ceiling in Test 32.

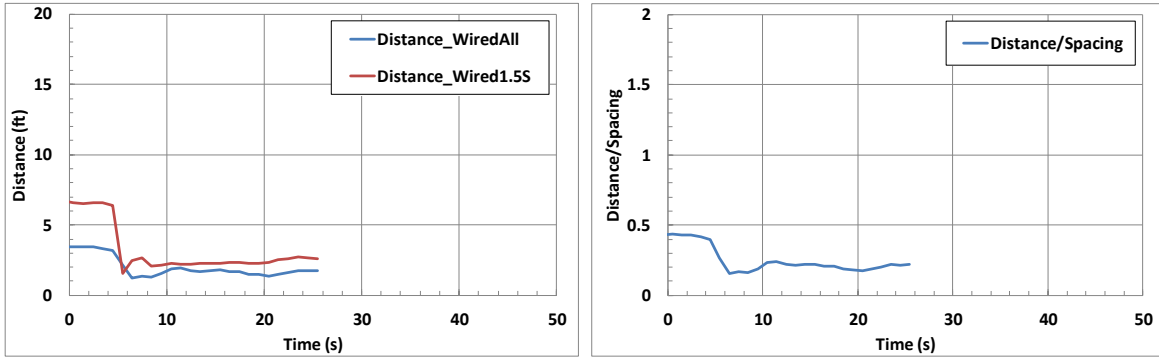


Figure A-60: Thermal centroid deviations in Test 33.

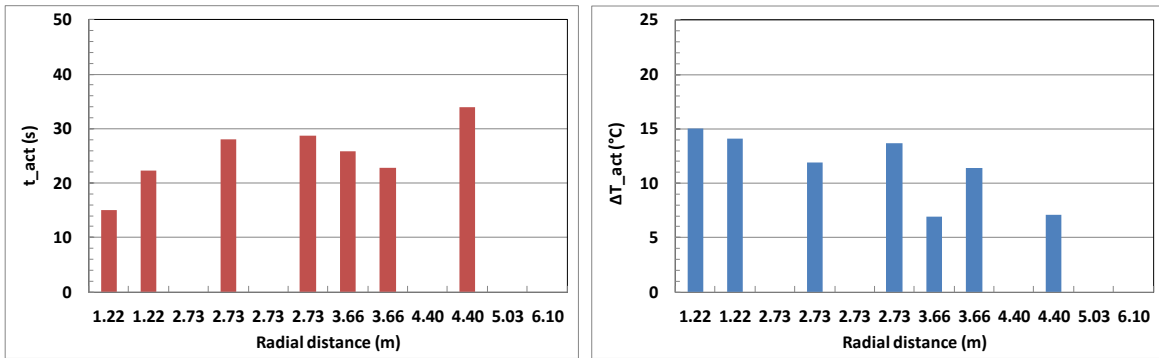


Figure A-61: Smoke detector response times and temperature rise at the ceiling in Test 33.

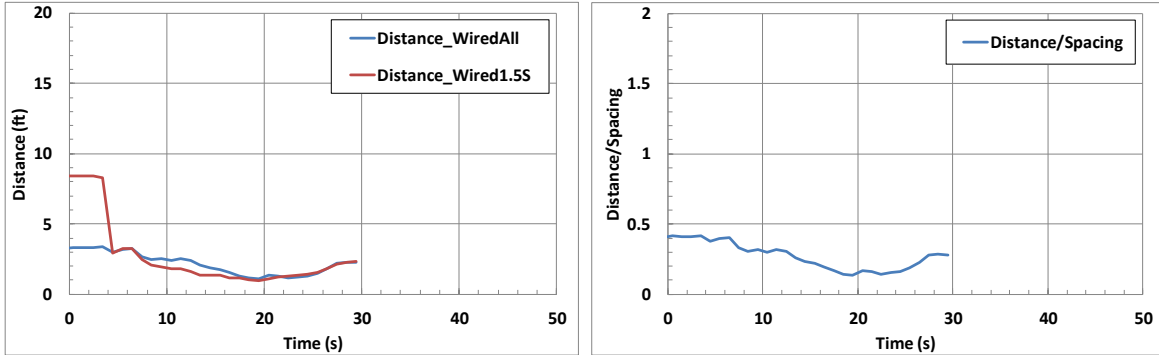


Figure A-62: Thermal centroid deviations in Test 34.

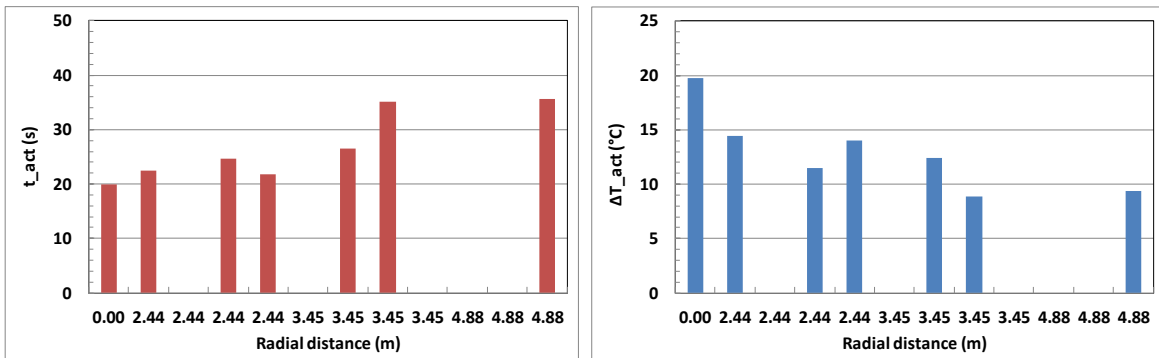


Figure A-63: Smoke detector response times and temperature rise at the ceiling in Test 34.

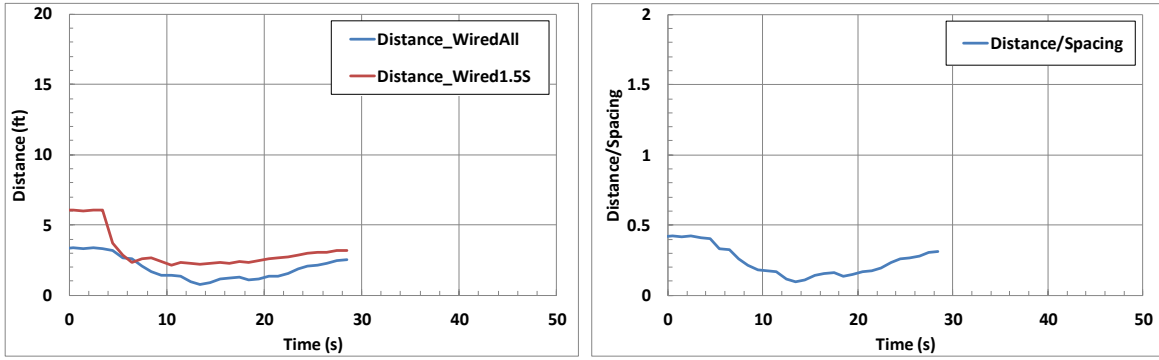


Figure A-64: Thermal centroid deviations in Test 35.

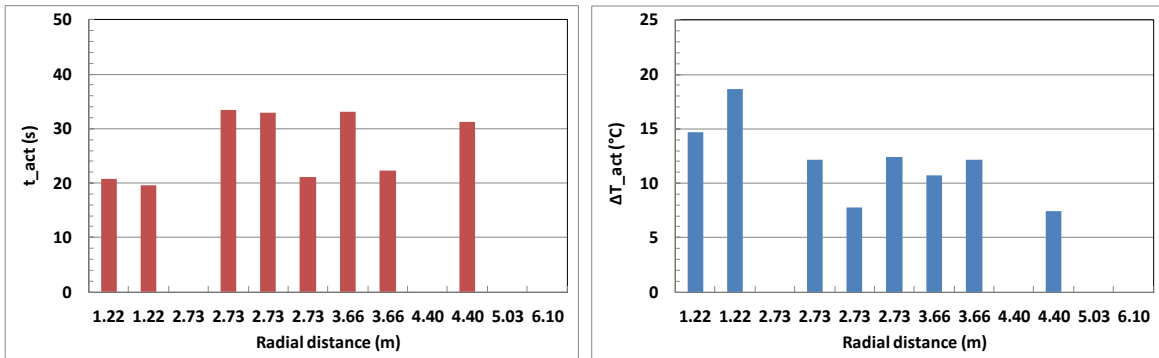


Figure A-65: Smoke detector response times and temperature rise at the ceiling in Test 35.

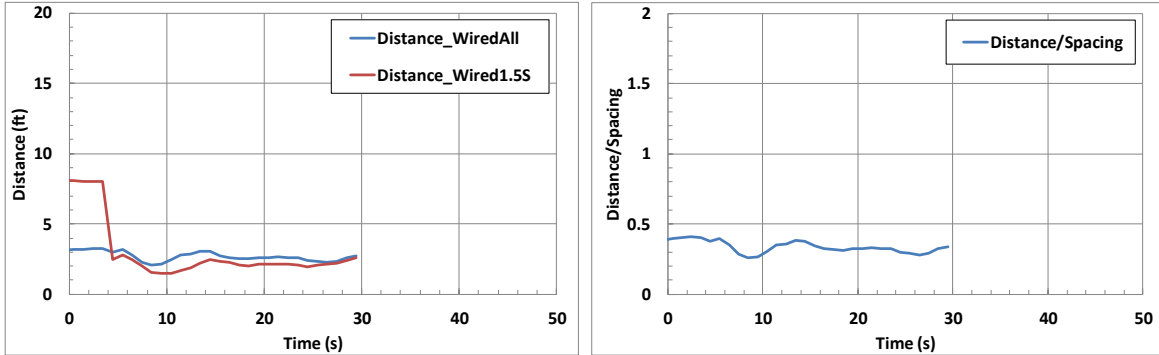


Figure A-66: Thermal centroid deviations in Test 36.

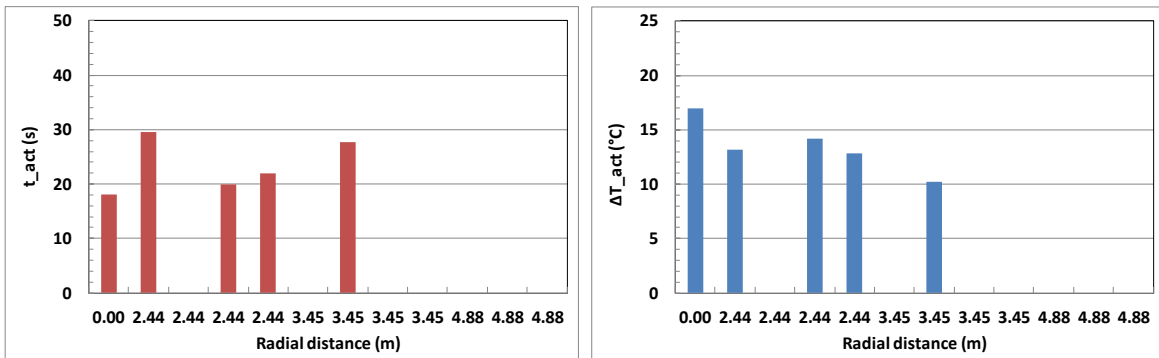


Figure A-67: Smoke detector response times and temperature rise at the ceiling in Test 36.

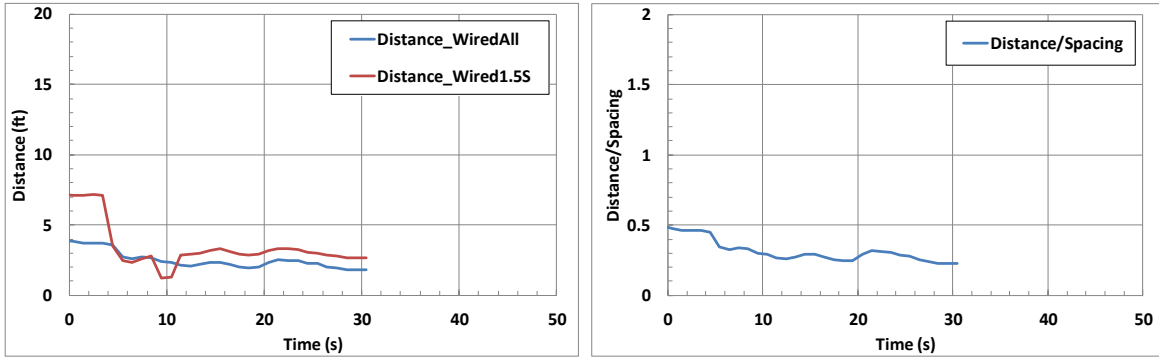


Figure A-68: Thermal centroid deviations in Test 37.

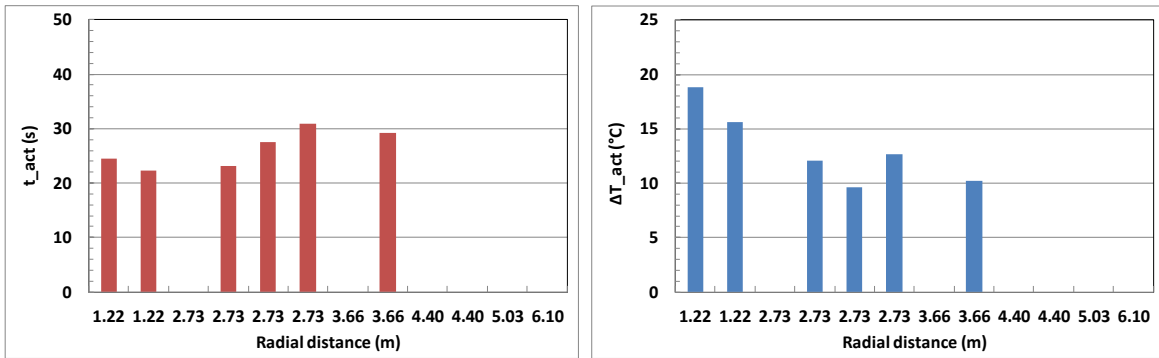


Figure A-69: Smoke detector response times and temperature rise at the ceiling in Test 37.

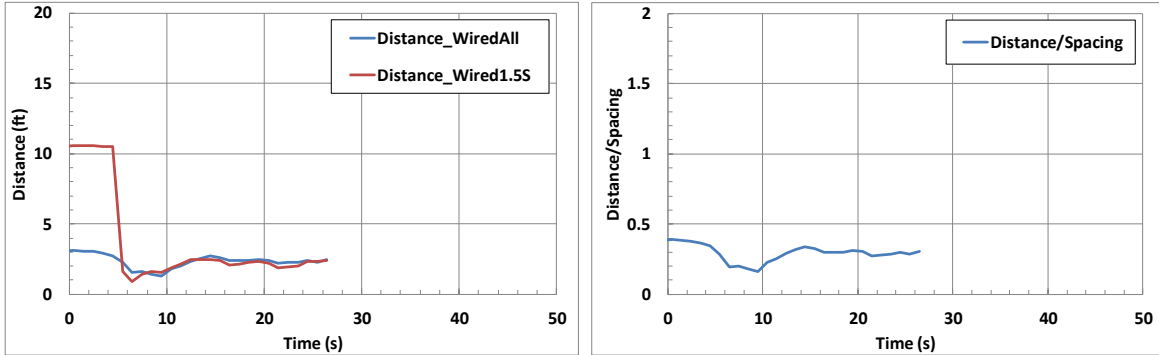


Figure A-70: Thermal centroid deviations in Test 38.

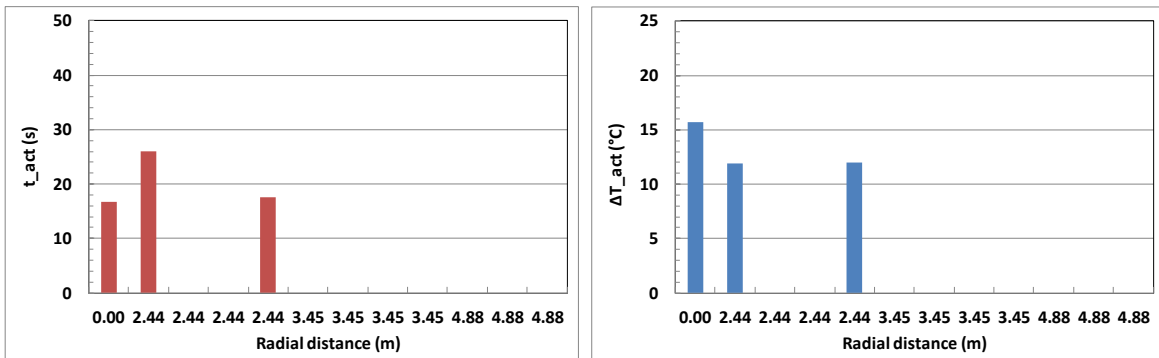


Figure A-71: Smoke detector response times and temperature rise at the ceiling in Test 38.

## Appendix B. Sprinkler activation test data

The experimental results from Tests 40-46 are presented in this section including the normalized thermal centroid deviation, the water operating pressure, the water flow rate, the smoke detector response time and the temperature rise at the ceiling. See Table 3-3 for detailed experimental conditions. The normalized thermal centroid deviation (Distance/Spacing) is defined in Section 2.3. The smoke detector response time and the temperature rise are plotted with respect to the radial distance from the ignition location.

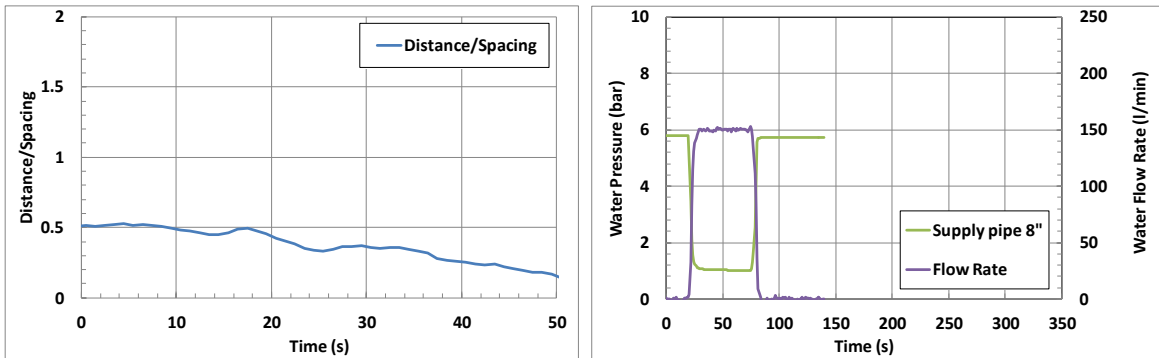


Figure B-1: Normalized thermal centroid deviations and water discharge rate in Test 40.

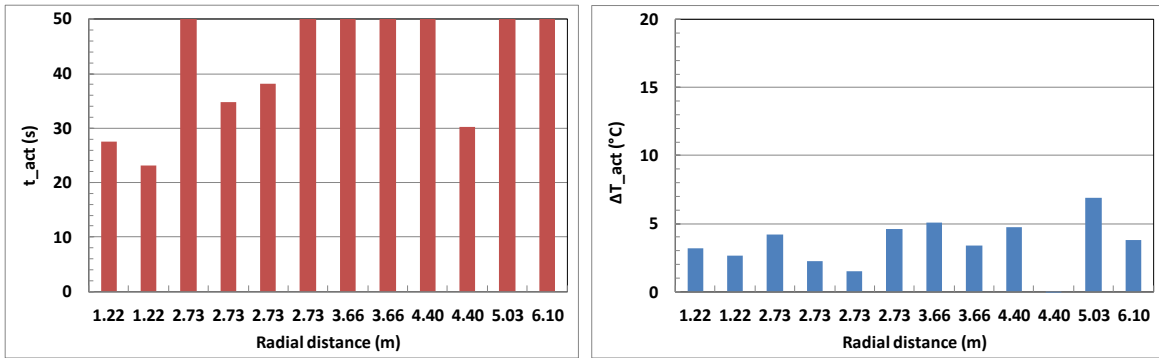


Figure B-2: Smoke detector response times and temperature rise at the ceiling in Test 40.

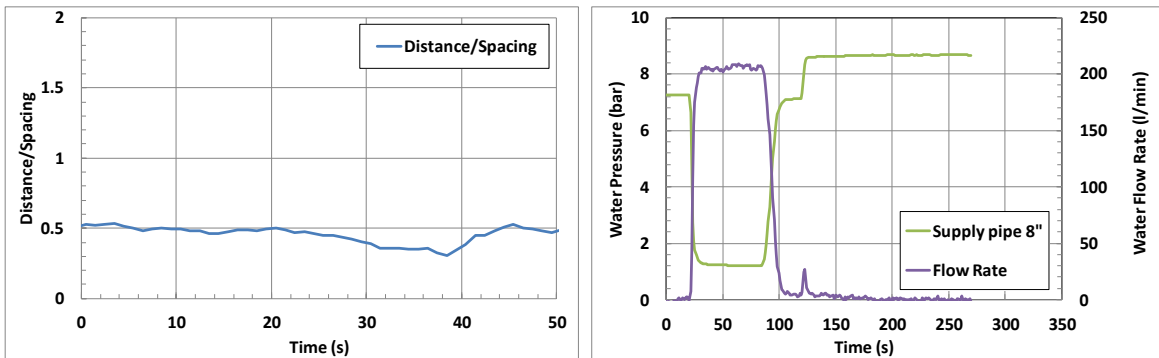


Figure B-3: Normalized thermal centroid deviations and water discharge rate in Test 41.

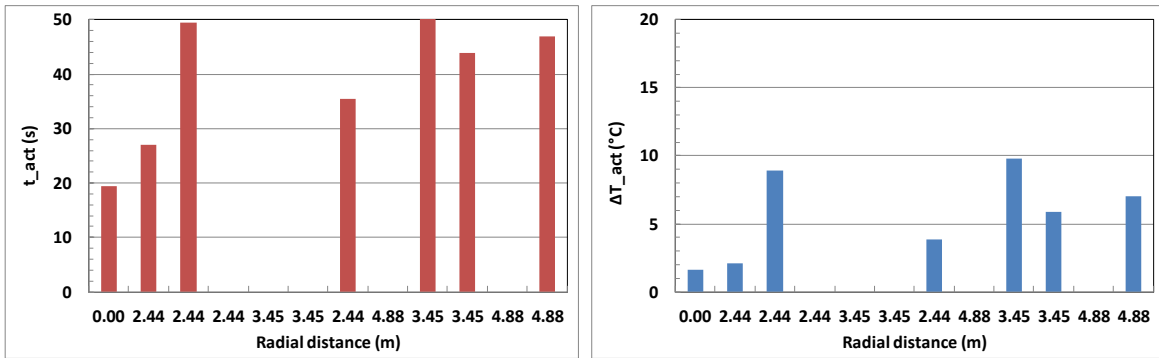


Figure B-4: Smoke detector response times and temperature rise at the ceiling in Test 41.

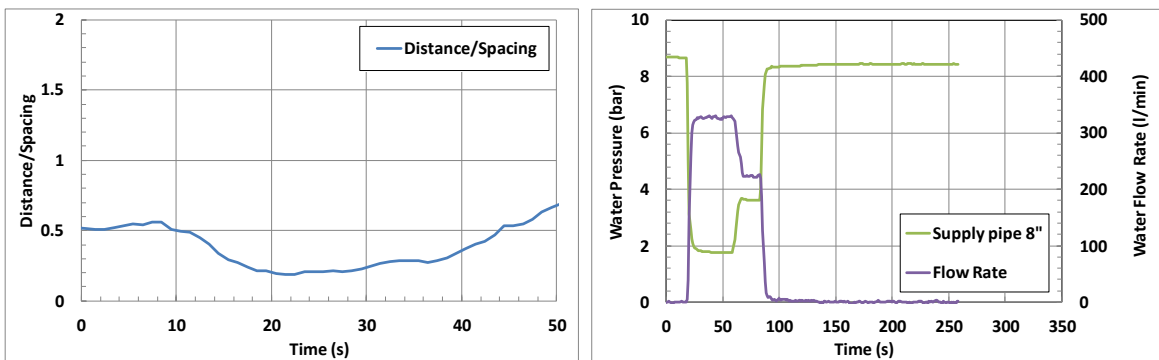


Figure B-5: Normalized thermal centroid deviations and water discharge rate in Test 42.

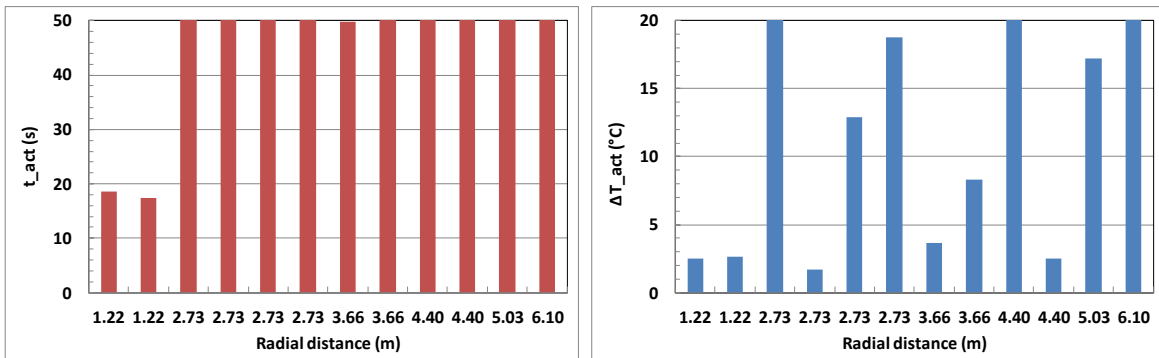


Figure B-6: Smoke detector response times and temperature rise at the ceiling in Test 42.

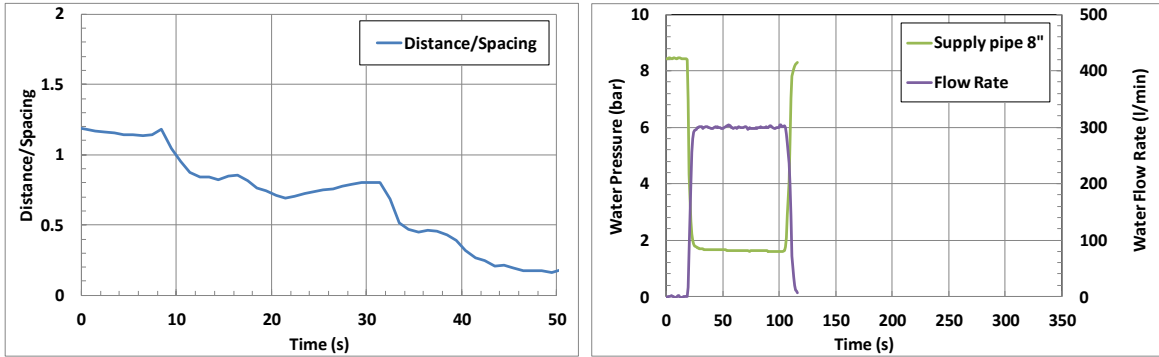


Figure B-7: Normalized thermal centroid deviations and water discharge rate in Test 43.

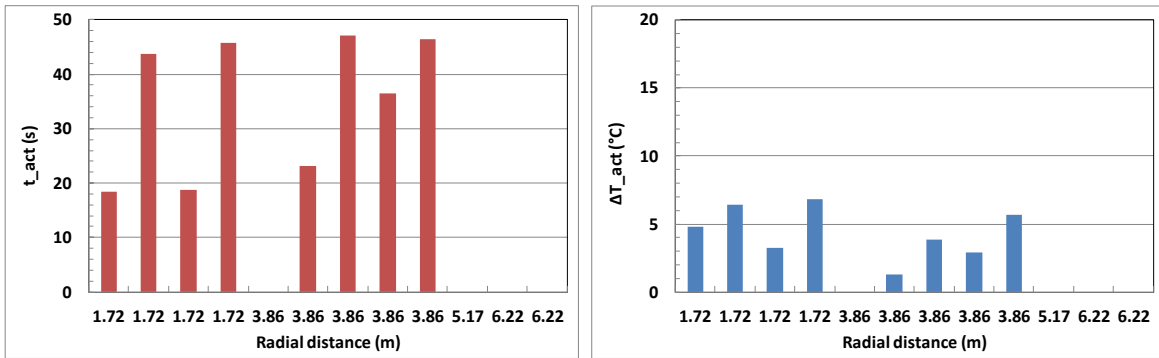


Figure B-8: Smoke detector response times and temperature rise at the ceiling in Test 43.

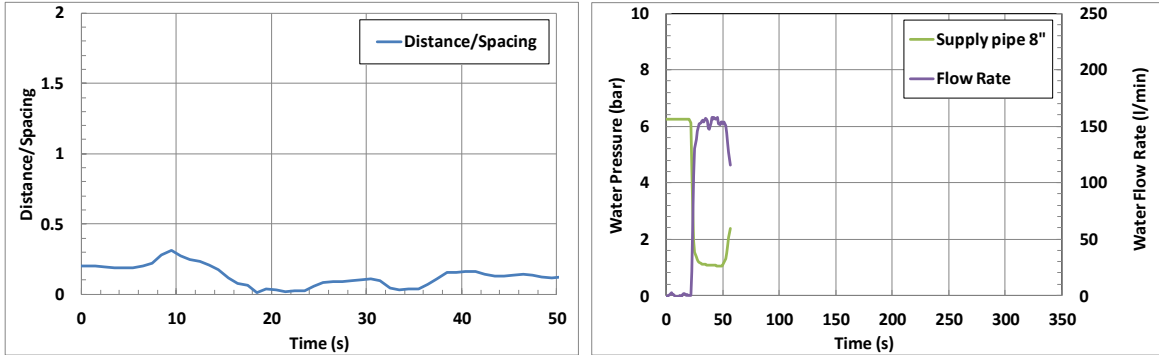


Figure B-9: Normalized thermal centroid deviations and water discharge rate in Test 44.

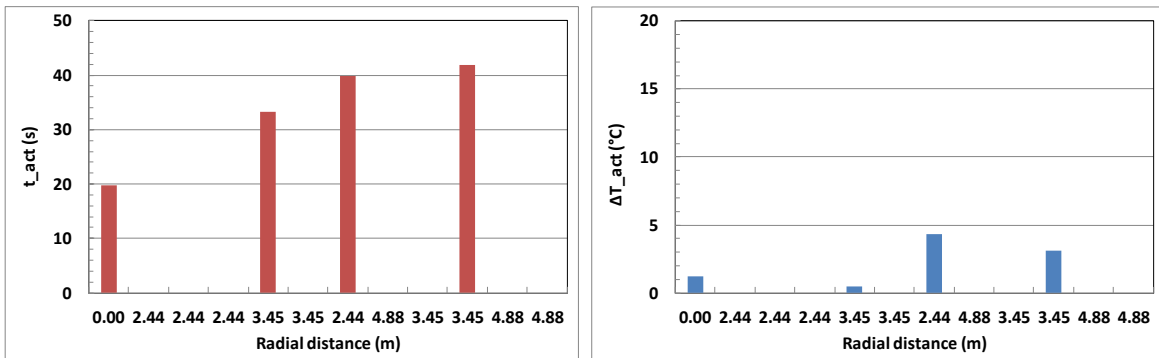


Figure B-10: Smoke detector response times and temperature rise at the ceiling in Test 44.

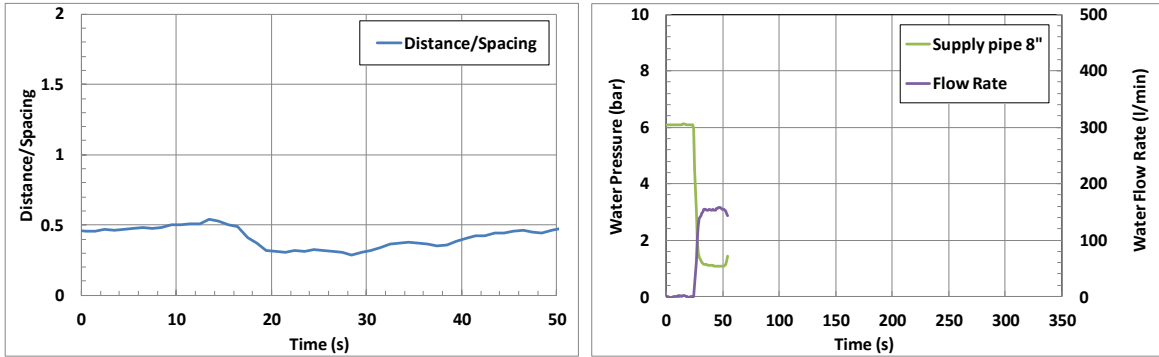


Figure B-11: Normalized thermal centroid deviations and water discharge rate in Test 45.

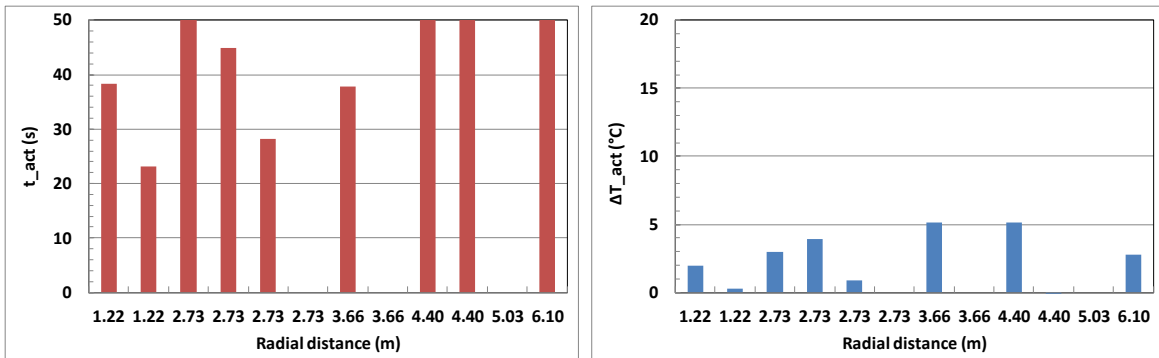


Figure B-12: Smoke detector response times and temperature rise at the ceiling in Test 45.

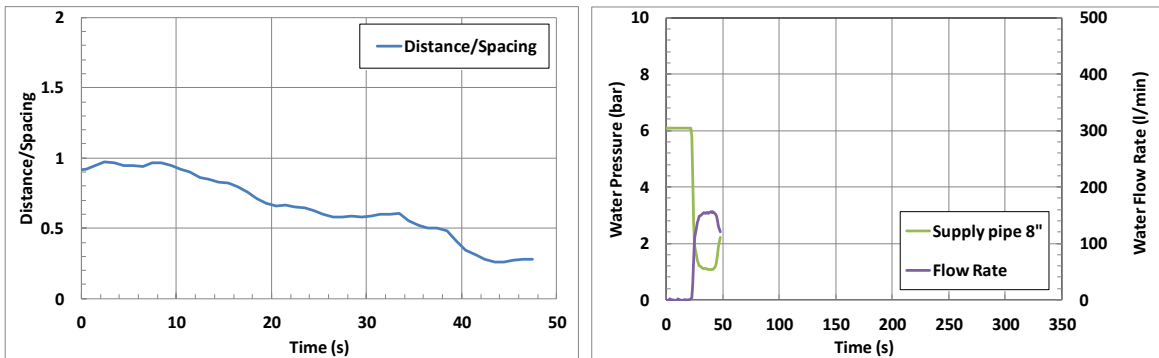


Figure B-13: Normalized thermal centroid deviations and water discharge rate in Test 46.

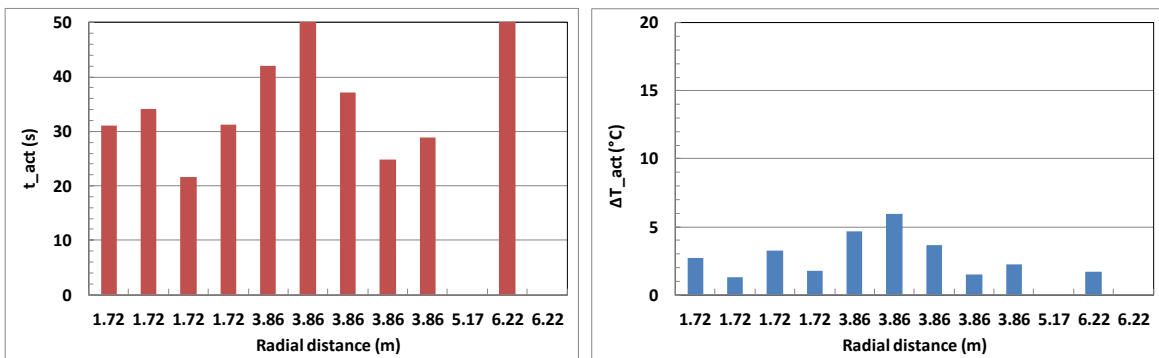


Figure B-14: Smoke detector response times and temperature rise at the ceiling in Test 46.

## Appendix C. Fire suppression test data

The experimental results from Tests 47-53 are presented in this section including the normalized thermal centroid deviation, the water operating pressure, the water flow rate, the smoke detector response time and the temperature rise at the ceiling. In addition, temperature rise near the ignition location are also plotted to show the effect of sprinkler suppression. Detailed experimental conditions are listed in Table 3-4. The normalized thermal centroid deviation (Distance/Spacing) is defined in Section 2.3. The smoke detector response time and the corresponding temperature rise are plotted with respect to the radial distance from the ignition location.

### C.1 Test 47

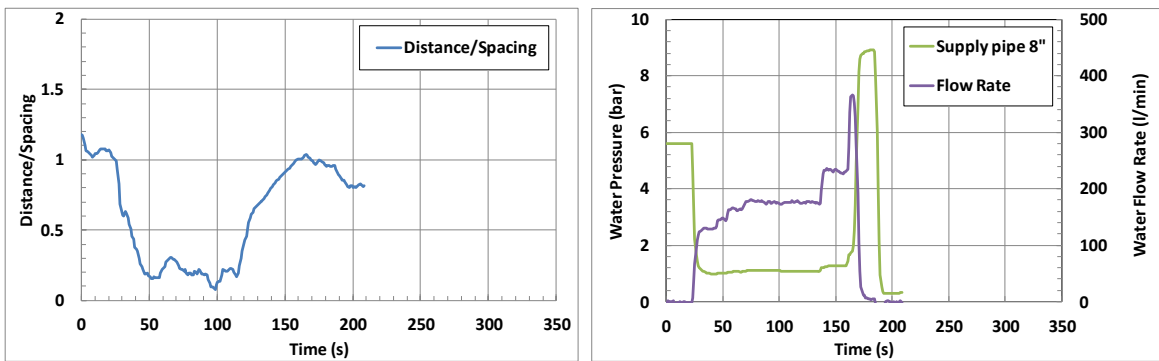


Figure C-1: Normalized thermal centroid deviations and water discharge rate in Test 47.

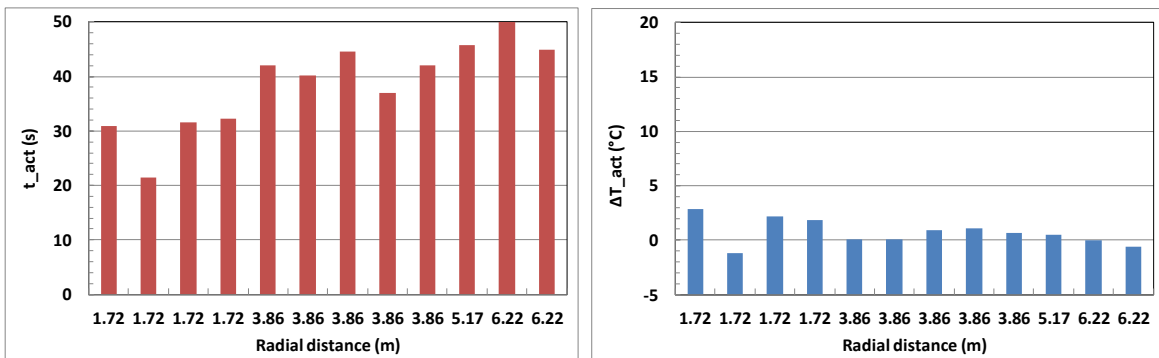


Figure C-2: Smoke detector response times and temperature rise at the ceiling in Test 47.

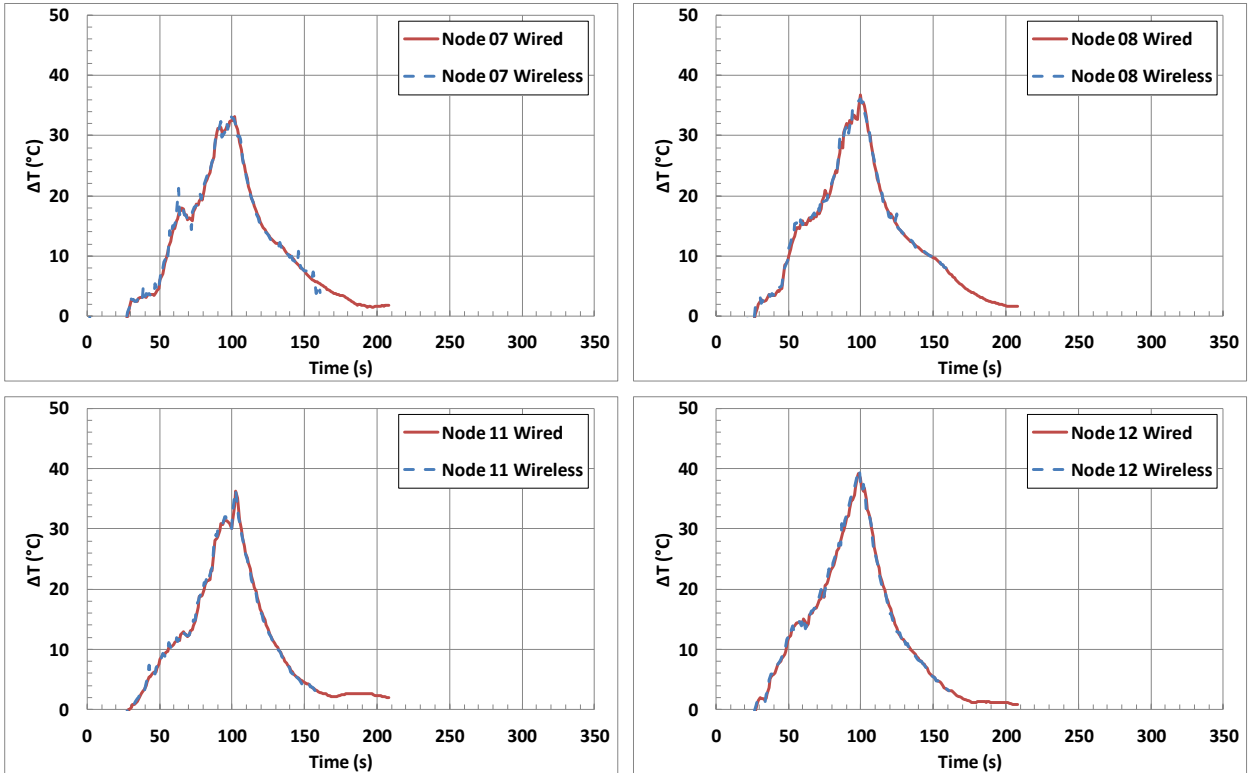


Figure C-3: Temperature rise at the ceiling near ignition location ( $R = 1.72$  m) in Test 47.

## C.2 Test 48

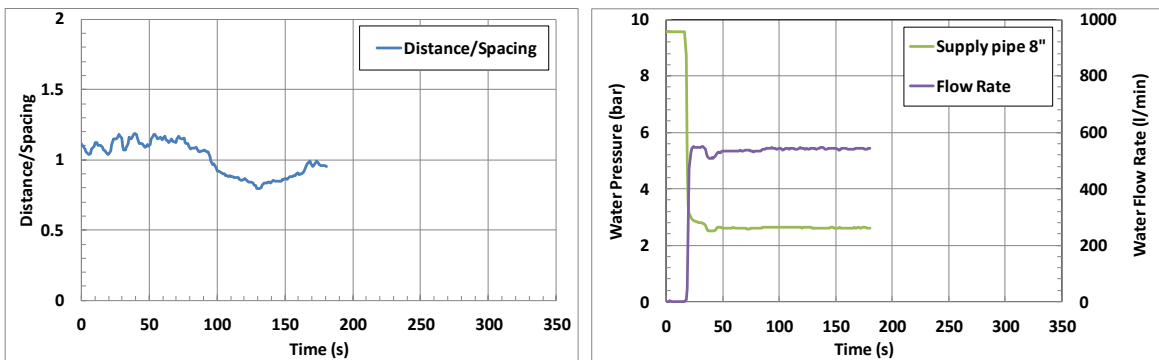


Figure C-4: Normalized thermal centroid deviations and water discharge rate in Test 48.

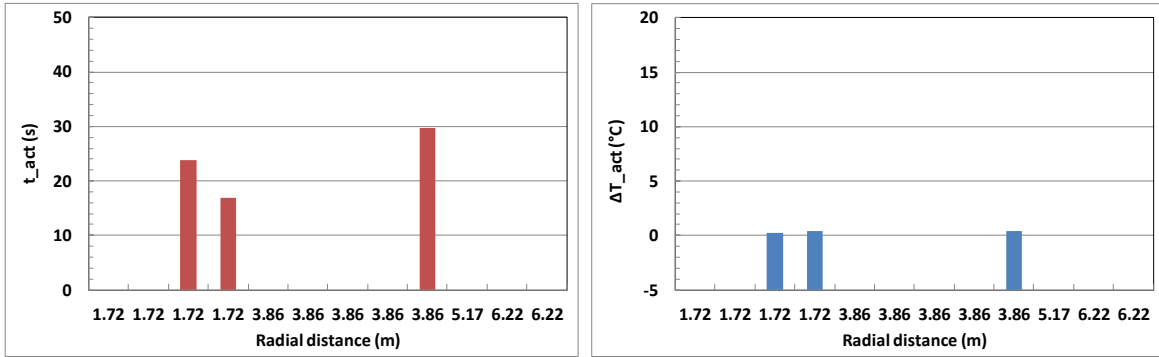


Figure C-5: Smoke detector response times and temperature rise at the ceiling in Test 48.

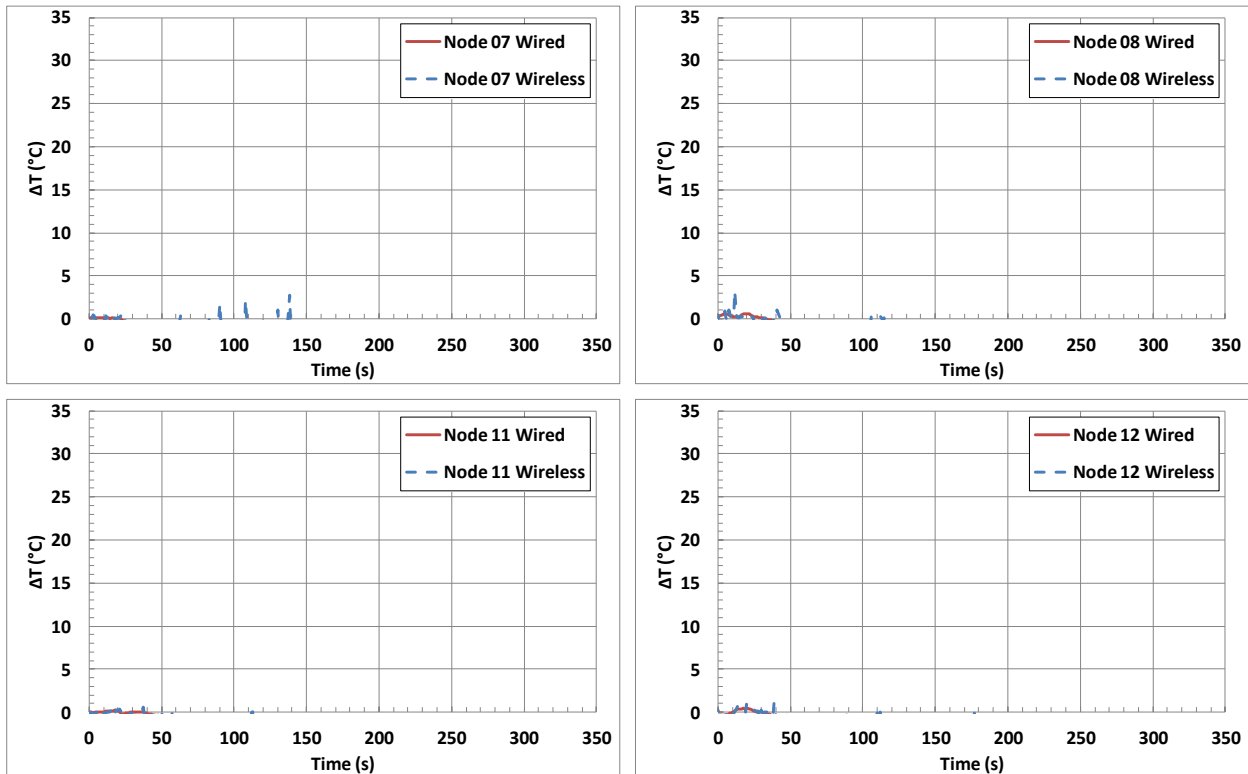


Figure C-6: Temperature rise at the ceiling near ignition location ( $R = 1.72$  m) in Test 48.

### C.3 Test 49

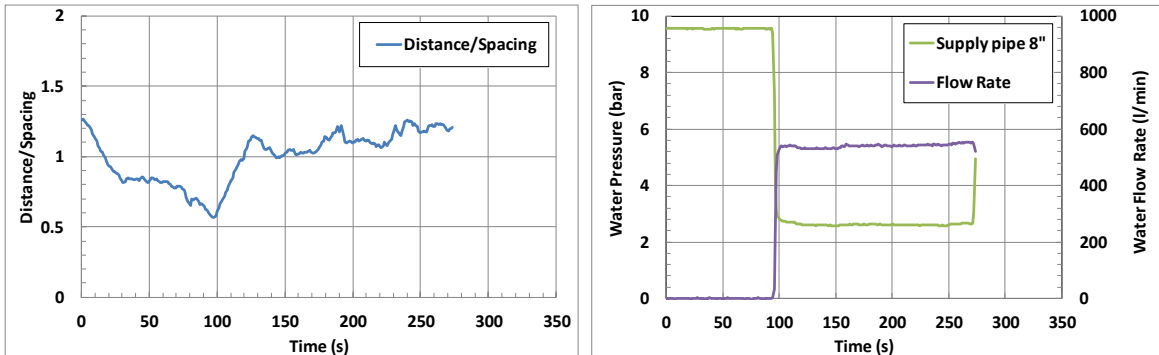


Figure C-7: Normalized thermal centroid deviations and water discharge rate in Test 49.

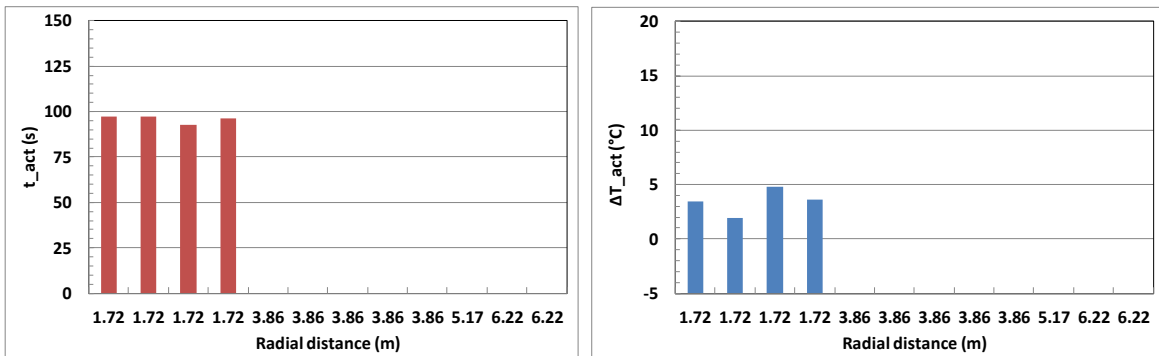


Figure C-8: Smoke detector response times and temperature rise in Test 49.

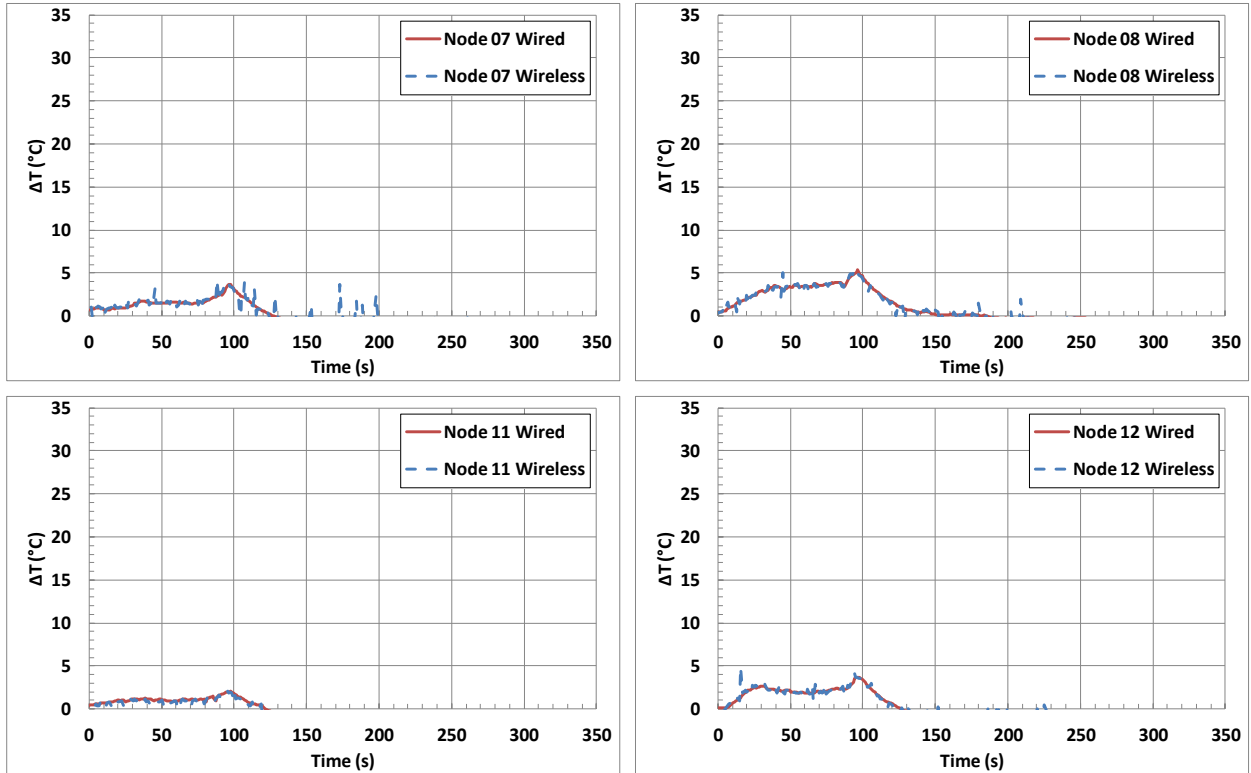


Figure C-9: Temperature rise at the ceiling near ignition location ( $R = 1.72$  m) in Test 49.

## C.4 Test 50

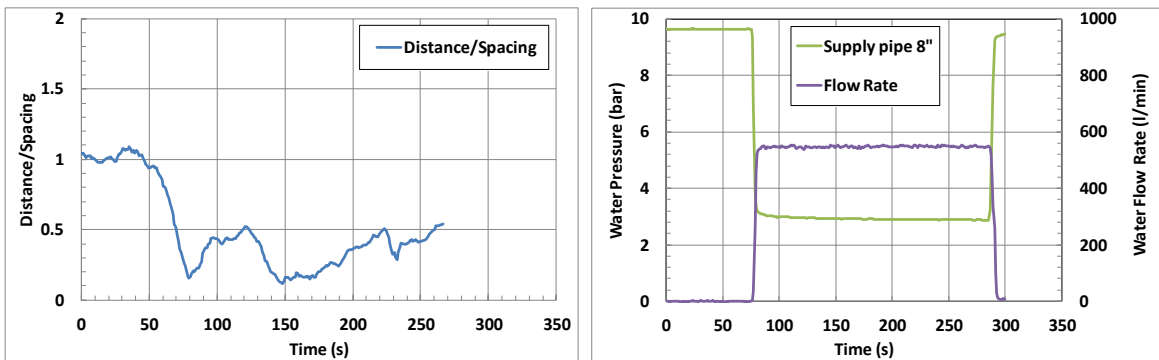


Figure C-10: Normalized thermal centroid deviations and water discharge rate in Test 50.

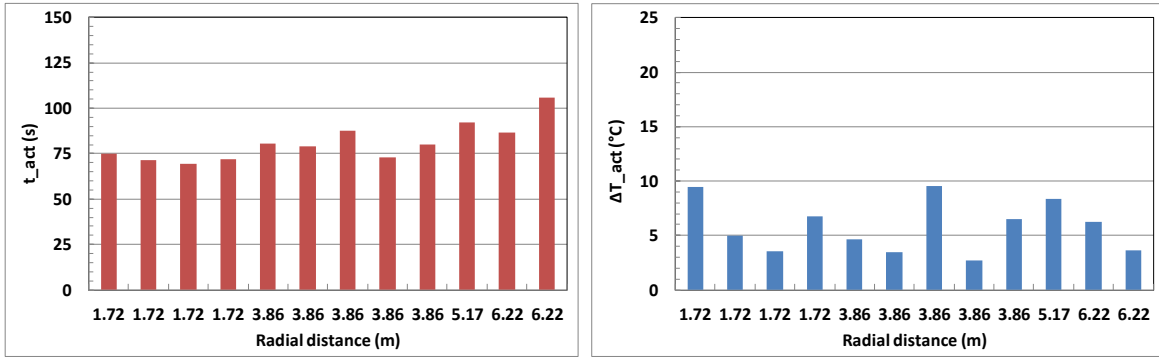


Figure C-11: Smoke detector response times and temperature rise at the ceiling in Test 50.

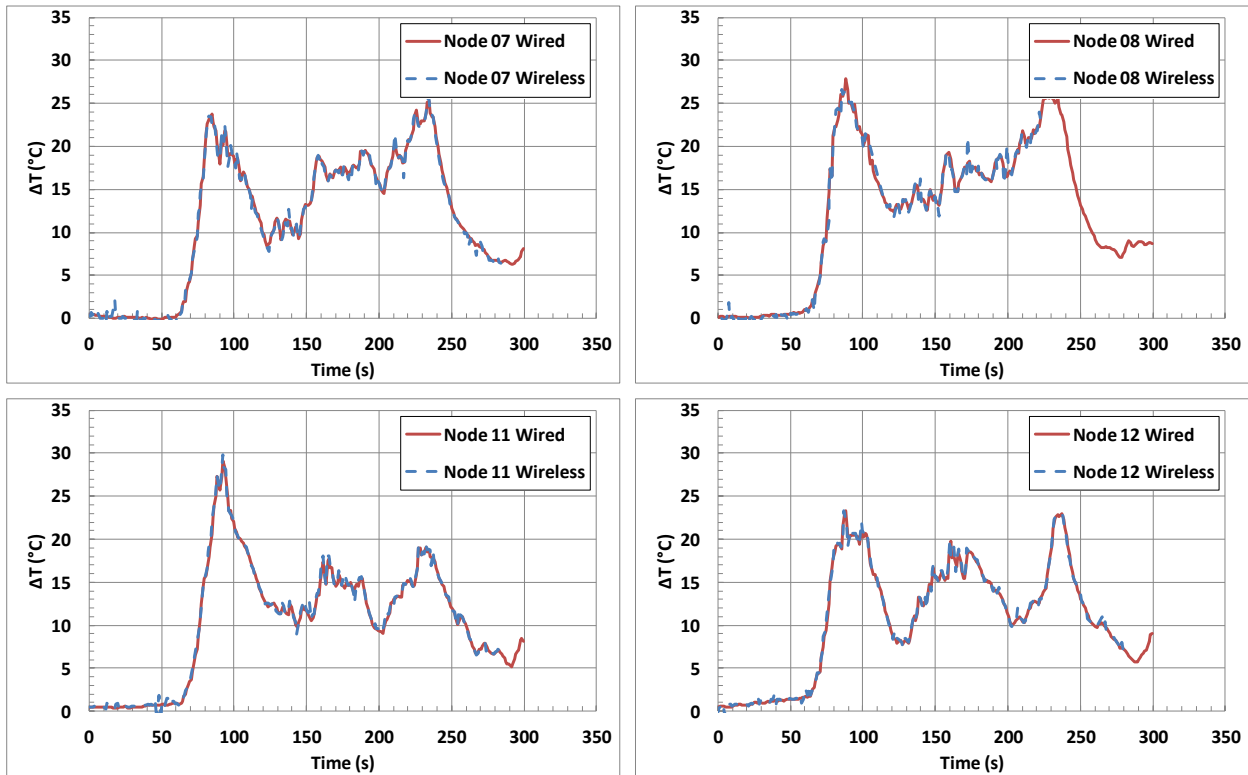


Figure C-12: Temperature rise at the ceiling near ignition location (R = 1.72 m) in Test 50.

## C.5 Test 51

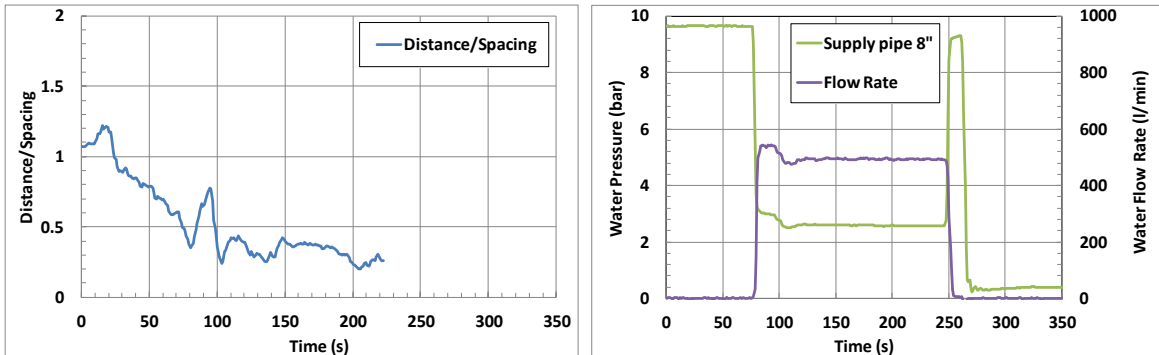


Figure C-13: Normalized thermal centroid deviations and water discharge rate in Test 51.

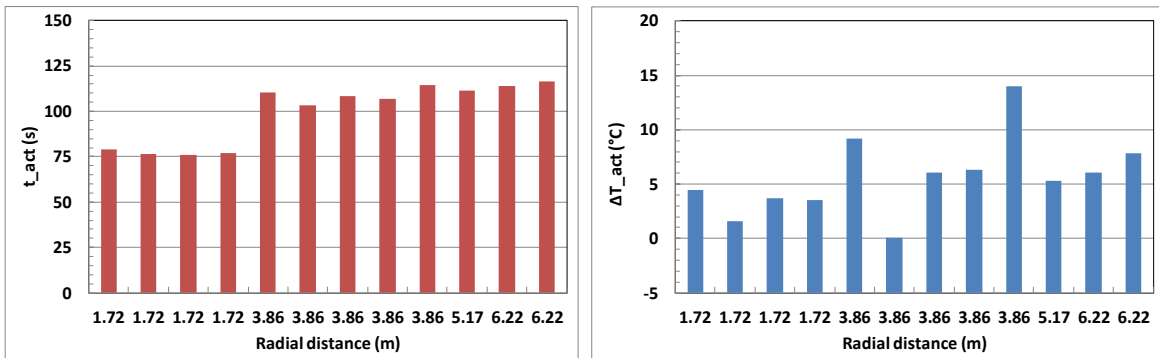


Figure C-14: Smoke detector response times and temperature rise at the ceiling in Test 51.

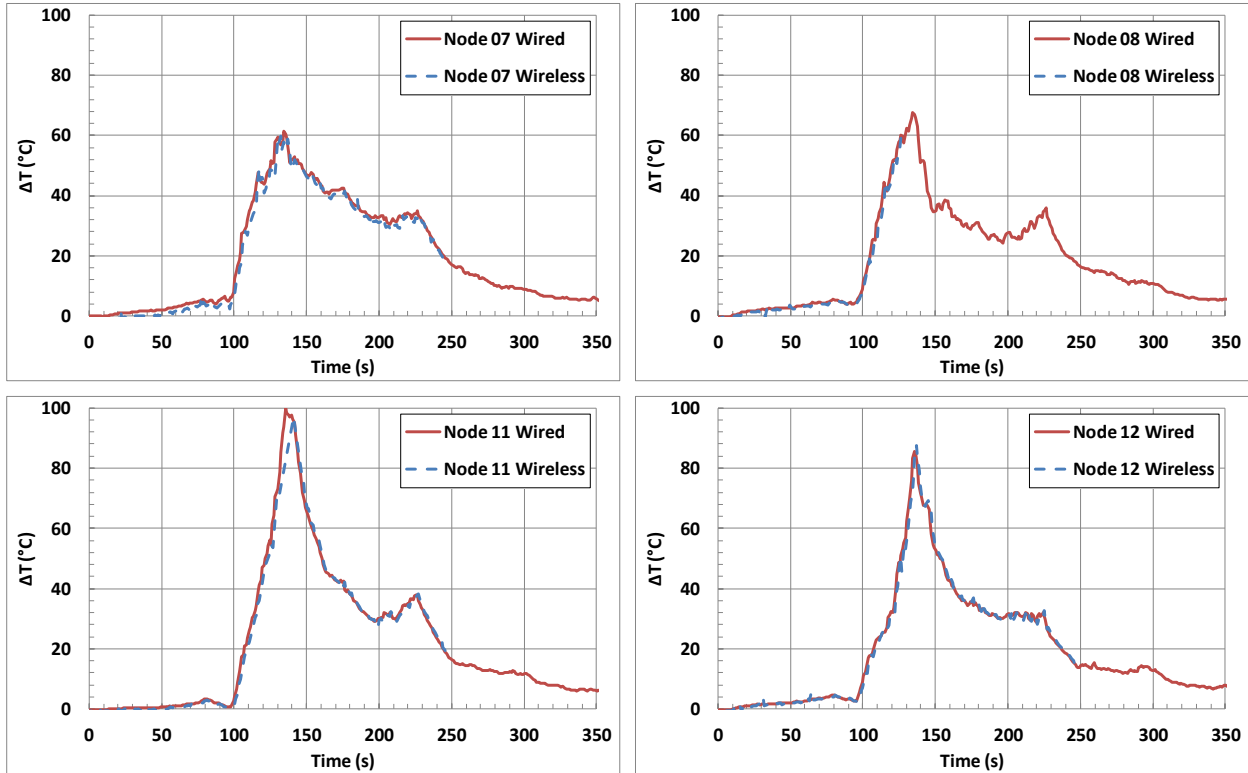


Figure C-15: Temperature rise at the ceiling near ignition location ( $R = 1.72$  m) in Test 51.

## C.6 Test 52

### C.6.1 First run

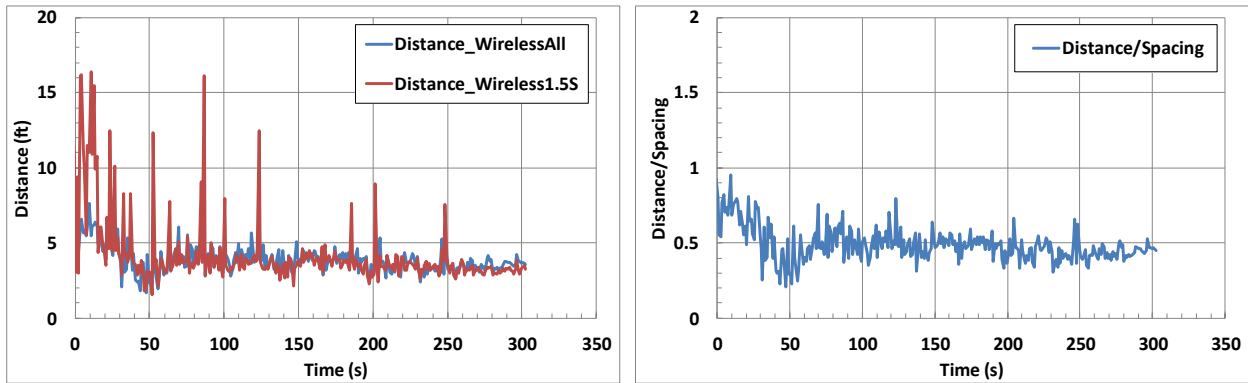


Figure C-16: Thermal centroid deviations in Test 52-1.

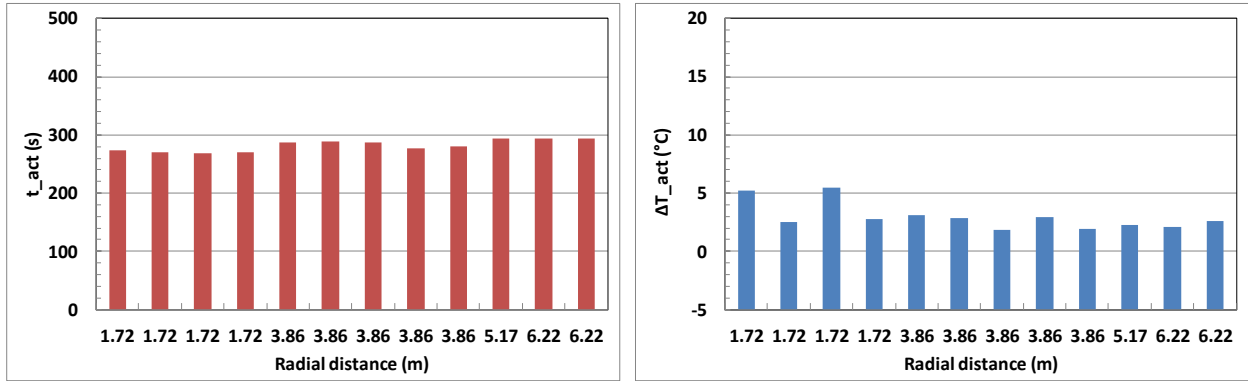


Figure C-17: Smoke detector response times and temperature rise at the ceiling in Test 52-1.

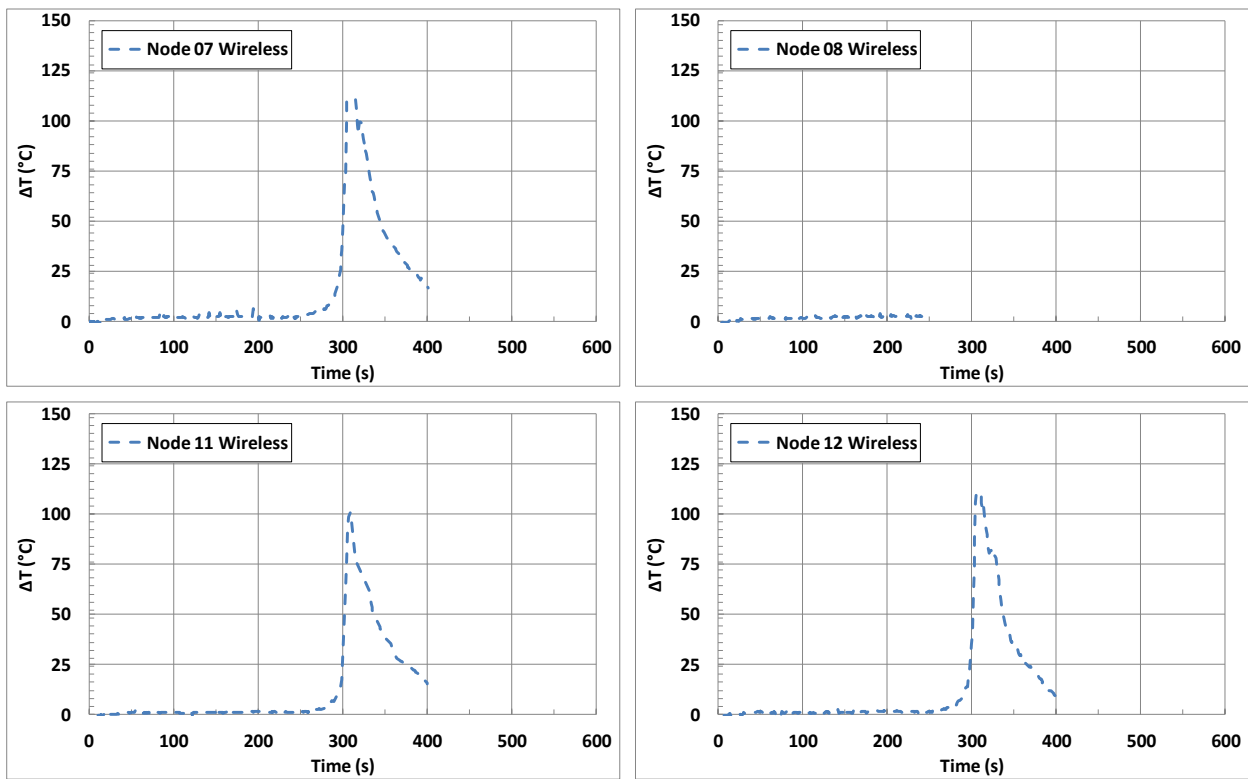


Figure C-18: Temperature rise at the ceiling near ignition location (R = 1.72 m) in Test 52-1.

C.6.2 Second run

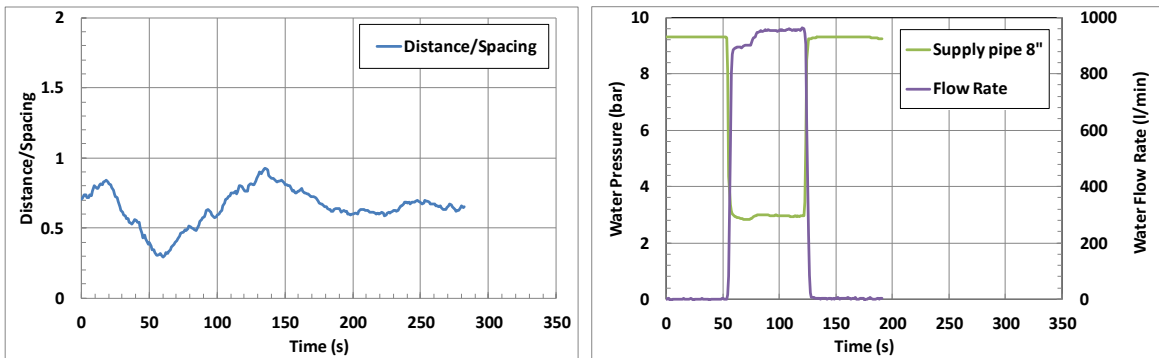


Figure C-19: Normalized thermal centroid deviations and water discharge rate in Test 52-2.

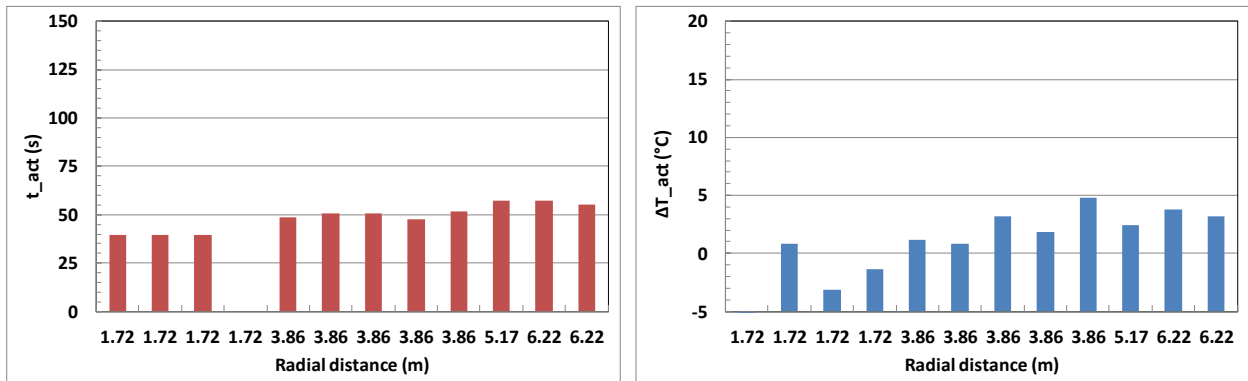


Figure C-20: Smoke detector response times and temperature rise at the ceiling in Test 52-2.

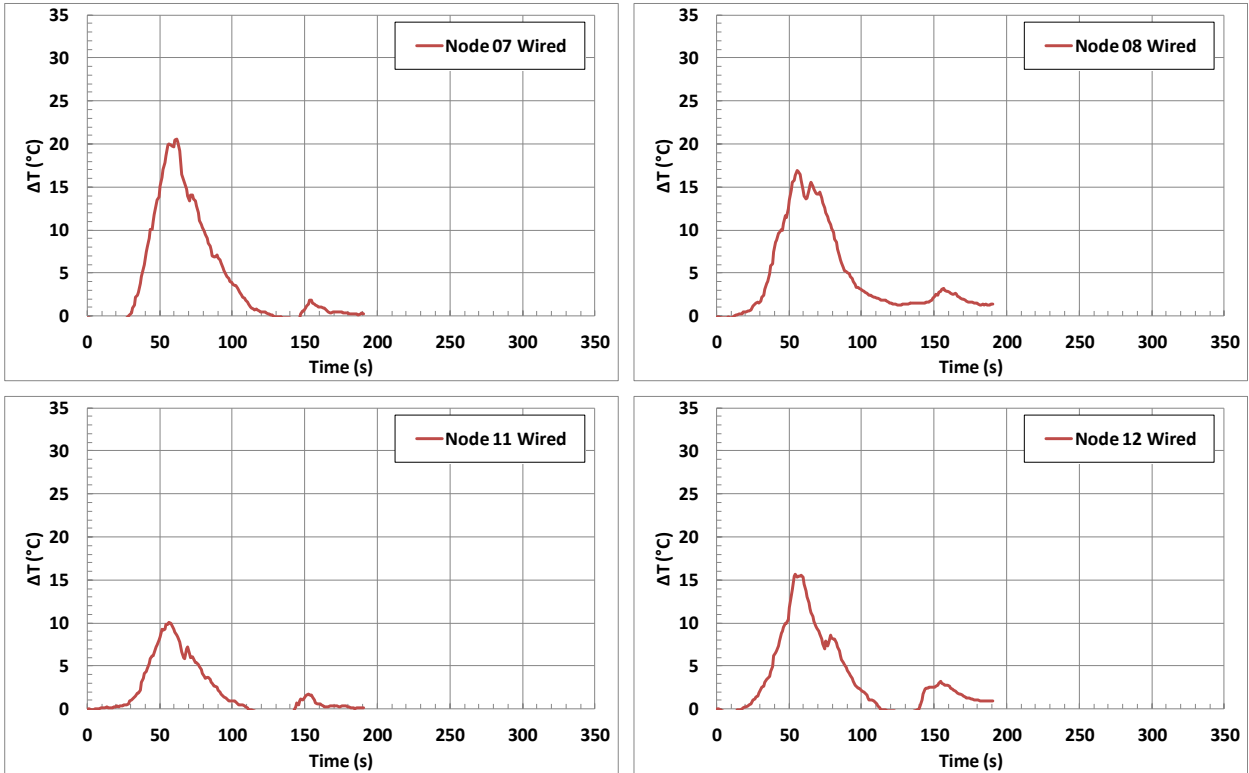


Figure C-21: Temperature rise at the ceiling near ignition location ( $R = 1.72$  m) in Test 52-2.

## C.7 Test 53

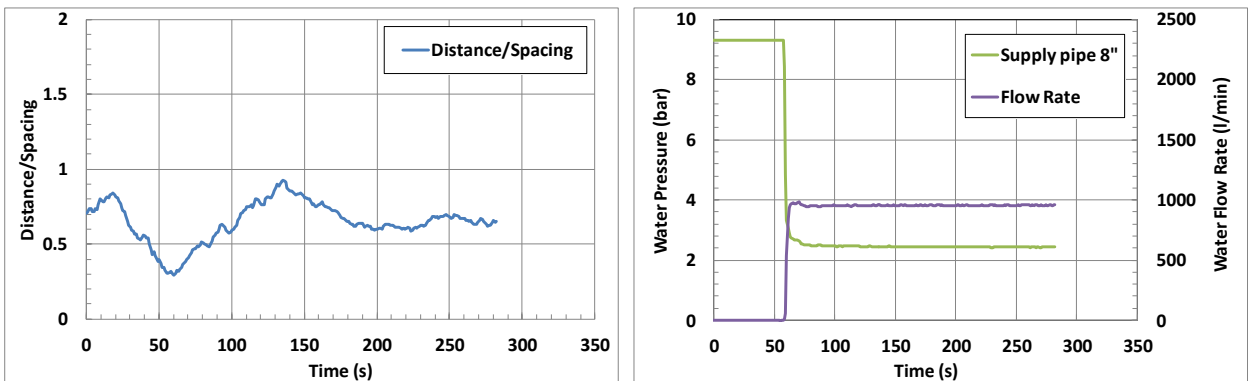


Figure C-22: Normalized thermal centroid deviations and water discharge rate in Test 53.

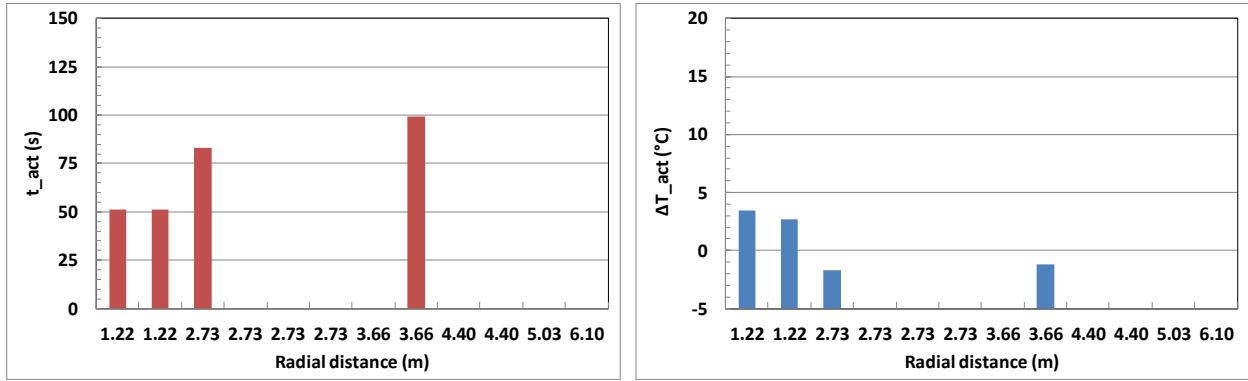


Figure C-23: Smoke detector response times and temperature rise at the ceiling in Test 53.

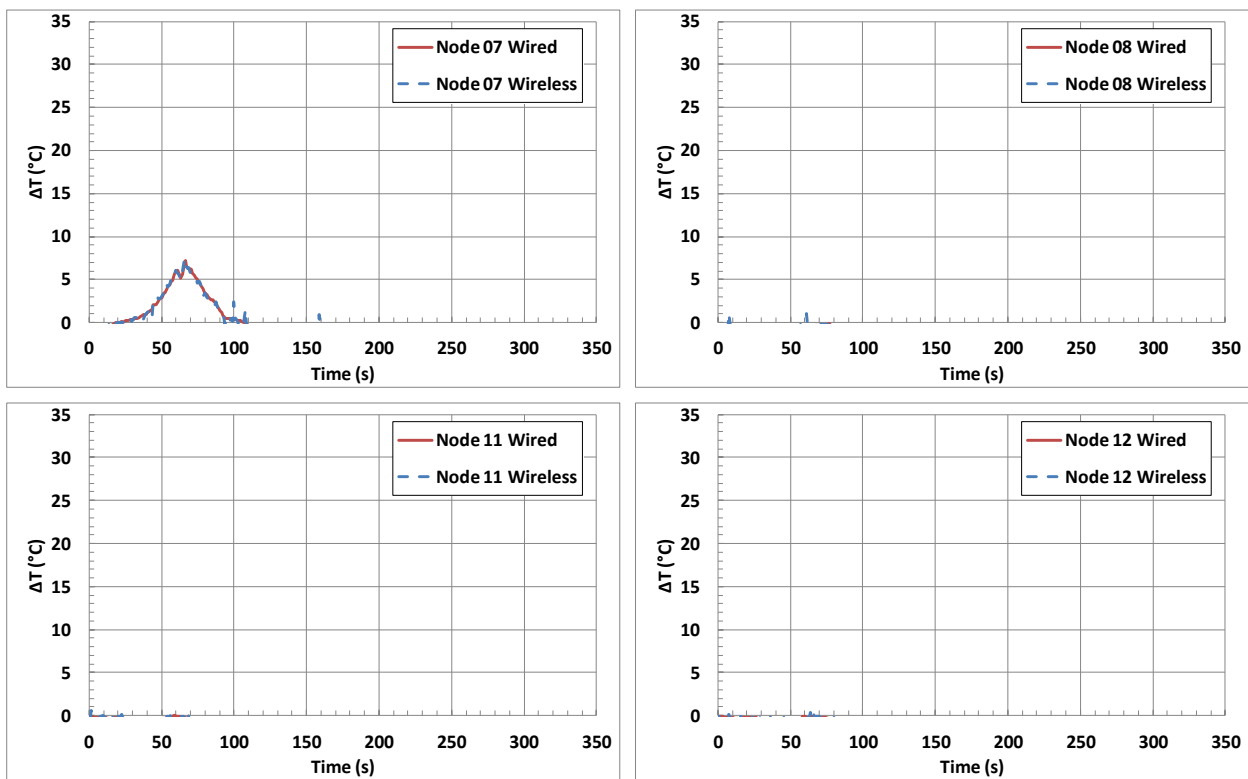


Figure C-24: Temperature rise at the ceiling near ignition location ( $R = 1.72$  m) in Test 53.







Printed in USA © 2016 FM Global  
All rights reserved.  
[fmglobal.com/researchreports](http://fmglobal.com/researchreports)

FM Insurance Company Limited  
1 Windsor Dials, Windsor, Berkshire, SL4 1RS  
Authorized by the Prudential Regulation Authority and regulated by the Financial Conduct  
Authority and the Prudential Regulation Authority.